VILNIUS UNIVERSITY
STATE RESEARCH INSTITUTE CENTER FOR PHYSICAL SCIENCES AND TECHNOLOGY

SIMONAS KECORIUS

APPLICATION OF AEROSOL SPECTROMETRY TO DEFINE PROCESSES WHICH CHANGE ATMOSPHERIC AEROSOL PARTICLE PROPERTIES

Doctoral dissertation, Physical Sciences, Physics (02P)

Vilnius, 2014

The dissertation was prepared at the State Research Institute Center for Physical Sciences and Technology in 2010 –2014.

Scientific supervisor:

Dr. Vidmantas Ulevičius (State Research Institute Center for Physical Sciences and Technology, Physical Sciences, Physics – 02P).

VILNIAUS UNIVERSITETAS
VALSTYBINIS MOKSLINIŲ TYRIMŲ INSTITUTAS
FIZINIŲ IR TECHNOLOGIJOS MOKSLŲ CENTRAS

SIMONAS KECORIUS

AEROZOLIO SPEKTROMETRIJOS METODO TAIKYMAS ATMOSFERINIŲ AEROZOLIO DALELIŲ SAVYBES KEIČIANČIŲ VYKSMŲ TYRIMAMS

Daktaro disertacija, Fiziniai mokslai, fizika (02P)

Vilnius, 2014

Disertacija rengta 2010 – 2014 metais Valstybiniame mokslinių tyrimų institute Fizinių ir technologijos mokslų centre.

Mokslinis vadovas:

Dr. Vidmantas Ulevičius (VMTI Fizinių ir technologijos mokslų centras, fiziniai mokslai, fizika – 02P).

dedicated to my parents Gražina and Gaudentas

thank you for leaving me a choice

CONTENTS

SUMMARY

In this dissertation the aerosol spectrometry method was used to define the processes which change the physical properties of atmospheric aerosol particles. It presents the results from both, long term and field campaign measurements. The state of art instrumentation was used to determine sub-micron aerosol particle number size distribution (Neutral cluster and Air Ion Spectrometer, NAIS, and Scanning Mobility Particle Sizer, SMPS) volatility (Volatility Tandem Differential Mobility Analyzer, V-TDMA), and hygroscopicity (Hygroscopicity Tandem Differential Mobility Analyzer, H-TDMA) properties of an aerosol. In this work volatility and hygroscopicity techniques, which link aerosol size to chemical composition, were combined to determine aerosol particle mixing state and to understand factors favouring nocturnal new particle formation.

Long term measurements at the Preila Environmental Research Station (Lithuania) indicated periodic, exclusively high aerosol particle number and black carbon (BC) mass concentration episodes. The processes altering physical properties of the background environment aerosol particles were found to be biomass burning and emissions from the ships. It was shown that high levels of black carbon and high accumulation mode particle number concentration are related to the transport of air masses rich in biomass burning products arriving from Kaliningrad region, Ukraine and south western part of Russia. One hour aerosol particle number and BC mass concentrations during such episodes exceed 40000 ± 4000 cm^{-3} and 11000 ± 550 ng/m^3, respectively. The background concentration values are known to be around 3800 ± 380 cm^{-3} and 340 ± 20 ng/m^3. Ångström exponent of light absorption coefficient was 2.4. Moreover, during the situation of connected atmospheric flow between three atmospheric observation stations along the Baltic Sea coast: Vavihill (upwind, Sweden), Utö (upwind, Finland), and Preila (downwind, Lithuania) a clear increase in particle number concentration (diameter interval 50 – 400 nm) by a factor of 2.1 from Utö ($N_{Utö}$ = 870 ± 90 cm^{-3}) to Preila, and by a factor of

1.7 from Vavihill (N_{Vavihill} = 870 ± 90 cm^{-3}) to Preila, was found. Likewise, the aerosol particle light absorption coefficient (λ = 530 nm) was 2.7 times greater at Preila than at Vavihill ($b_{\text{abs, Vavihill}}$ = 0.9 ± 0.05 Mm^{-1}) and 1.7 times greater than at Utö ($b_{\text{abs, Utö}}$ = 2.2 ± 0.1 Mm^{-1}). During the periods of connected flow, the absorption Ångström exponent at Preila was found to be near unity, further supporting the conclusion that ship-emitted particulate matter contributed to the background aerosol properties in Lithuania.

A one month long field campaign was carried out in Xianghe, China, as a part of "Campaign of Air Quality Research in Beijing and Surrounding Region 2013" (CARE-Beijing 2013) project. The results indicate that during the observation period, 19 of 32 nights experienced rapid bursts of ultra-fine particle, which were attributed to a new particle formation with a condensation sink (for particles in the range of 2 – 750 nm) of CS = 0.055 s^{-1}. The lower limit of nocturnal new particle formation rate was 45 ± 5 $cm^{-3}s^{-1}$, which is 1.25 times higher than a daytime value. Several factors were found to favour a new particle formation including relative humidity, wind speed and most important – wind direction. The upwind life-stock lofts were found to be the main source of possibly high concentrations of NH_3 and condensable organics (amines), all contributing to a nocturnal new particle formation and rapid growth. It was also concluded that such nocturnal events intensify particle aging and effectively change the mixing state of aerosol particles.

List of Abbreviations:

AQI	Air Quality Index
ATN	Optical Attenuation
BC	Black Carbon
CCN	Cloud Condensation Nuclei
cgs	centimeter–gram–second system
CPC	Condensation Particle Counter
CS	Condensation Sink
DF	Total Deposition Fraction
DMA	Differential Mobility Analyzer
DMPS	Differential Mobility Particle Sizer
DPS	Differential Pressure Sensor
EC	Elemental Carbon
FRP	Fire Radiative Power
GDAS	Global Data Assimilation System
GF	Growth Factor
GF-PDF	Growth Factor – Probability Density Function
HELCOM	Helsinki Commission
H-TDMA	Hygroscopicity Tandem Differential Mobility Analyzer
HV	High Voltage
HYSPLIT	HYbrid Single-Particle Lagrangian Integrated Trajectory
IPCC	Intergovernmental Panel on Climate Change
LV	Low Volatility
MAE	Mass Absorption Efficiency
MDF	Measurement Distribution Function
MODIS	Moderate-resolution Imaging Spectroradiometer
NAIS	Neutral Cluster and Air Ion Spectrometer
NF	Number Fraction
NH	Nearly Hydrophobic
NPF	New Particle Formation

PM_{10}	Particles (< 10 μm (geometric) diameter)
$PM_{2.5}$	Particles (< 2.5 μm (geometric) diameter)
PNSD	Particle Number Size Distribution
PSAP	Particle Soot Absorption Photometer
PSL	Polystyrene Latex
PVSD	Particle Volume Size Distribution
RH	Relative Humidity
R-MDF	Retrieved-Measurement Distribution Function
SF	Shrinking Factor
SMPS	Scanning Mobility Particle Sizer
STP	Standard Temperature and Pressure
T-DMA	Twin-Differential Mobility Analyzer
T-DMPS	Twin Differential Mobility Particle Sizer
TPF	Total Particle Filter
VOC	Volatile Organic Compound
V-TDMA	Volatility Tandem Differential Mobility Analyzer
WD	Wind Direction
WS	Wind Speed

INTRODUCTION

Scientific problem

Because of the unique location of the Preila Environmental Pollution Research station, representing East Baltic region, biomass burning (wildfire) and ship related emissions have a profound influence onto background aerosol properties. Due to high sorption capacity and optical properties, black carbon originated from biomass burning is of a great importance to the atmosphere processes. Black carbon alters chemical and physical properties of the atmosphere and snow albedo. The long-range transport of atmospheric particulate matter is a trans-boundary problem that can have significant impacts on PM_{10} and $PM_{2.5}$ levels in the background environments.

Moreover, ship emissions are one of the largest and least regulated sources of a various atmospheric pollutants. On a global scale, more than 60000 cardiopulmonary and lung cancer related deaths, and a change in radiative balance over a marine environment is associated with particulate matter from ships. Increasing traffic in the Baltic Sea necessitates the evaluation of the impact how ship emissions affect the background environment. However, despite these processes relevance, no attempts were made to identify how regional biomass burning and shipping in the Baltic Sea influences the background aerosol particle physical properties.

In parallel to the direct aerosol sources, atmospheric new particle formation by a nucleation from gaseous precursors has become a subject of intense experimental and modeling studies. A better understanding about this phenomenon and how it changes the aerosol particle mixing state is needed. The exact molecular mechanisms and participating vapors causing atmospheric nucleation events are still open to discuss.

Aim of the work

The aim of this work is to investigate the processes which alter the atmospheric aerosol particle physical properties using the aerosol spectrometry method as well as to develop the new methods.

The following tasks were set:

1. To conduct a long term aerosol particle physical properties measurement using the aerosol spectrometry method at the Preila Environmental pollution research station.
2. To identify and evaluate the processes which alter the particle properties in the background environment during the air mass transport.

Following task for a new method development was set:

1. To combine the newest aerosol particle volatility and hygroscopicity spectrometry methods to investigate how nocturnal new particle formation alters the mixing state of aerosol particles.

Novelty of the work

1. Regarding the long term measurements, the regional biomass burning impact onto aerosol particle physical properties during the long range air mass transport to Preila Environmental Research station was assessed.
2. The Baltic Sea shipping influence onto background aerosol particle physical properties was evaluated.
3. Two different (volatility and hygroscopicity) tandem differential mobility analyzers were combined to investigate a rare nocturnal new particle formation and the favoring conditions for this process.

4. The influence of a nocturnal new particle formation onto particle mixing state was evaluated.

Work relevance

1. The derived aerosol particle physical properties, which are influenced by wildfire and shipping in the Baltic Sea, can be directly implemented in air quality models.
2. The results of a nocturnal new particle formation augment the knowledge about this process leading to reduced uncertainties in nucleation models.
3. The assessed factors altering aerosol particle volatility and hygroscopicity augment the knowledge about the mixing state of aerosol particles.

Author input

The author applied the aerosol spectrometry methods to define the processes changing atmospheric aerosol particle physical properties, participated in the field measurements, was processing and evaluating the data and presenting the results. The input covers:

1. Conducting the long-term measurements, being responsible for instrument calibration, diagnostics and repair as well as measurement quality.
2. Data evaluation, visualization, interpretation and preparation for publication.
3. Writing publications, presenting the results at conferences and seminars.

Statements to defend

1. During the long range air mass transport regional scale biomass burning influences the background environment aerosol particle physical properties. The aerosol particle number and black carbon mass concentrations increase up to 10 and 33 times, respectively.
2. The intensive shipping in the Baltic Sea contributes up to 60% of aerosol particle number and black carbon mass concentrations in the background environment.
3. Nocturnal new particle formation under 0.055 s^{-1} condensation sink is favored by a high (> 98%) relative humidity, volatile organics and condensable vapor concentration.
4. Nocturnal new particle formation up to 3 times increases the internally mixed particle fraction by changing particle volatility and hygroscopicity properties.

List of publications included into this thesis:

1. Ulevicius, V., Bycenkiene, S., Remeikis, V., Garbaras, A., **Kecorius, S**., Andriejauskiene, J., Jasineviciene, D., Mocnik, G. 2010. Characterization of pollution events in the East Baltic region affected by regional biomass fire emissions. *Atmos. Res*., **2**, 190-200.
2. Ulevicius, V., Bycenkiene, S., Špirkauskaitė N., and **Kecorius, S**. 2010. Biomass burning impact on black carbon aerosol mass concentration at a coastal site: case studies. *Lith. Journ. of Phys*., 50, 3, 335 – 344.
3. Bycenkiene, S., Ulevicius, V., **Kecorius, S**. 2011. Characteristics of black carbon aerosol mass concentration over the East Baltic region from two-year measurements. *J. Environ. Monit*., 13, 1027-1038.

4. **Kecorius, S**., Zhang, S.L., Wang, Z., Gröβ, J., Ma, N., Wu, Z., Ran, L., Hu, M., Wang, P.C., Ulevicius V., and Wiedensohler A. 2015. Nocturnal nucleation of aerosol particles in the North China Plain. *Lith. Journ. of Phys.*
5. **Kecorius S**., Kivekäs N., Kristensson A., Tuch T., Covert D., Birmili B., Lihavainen H., Hyvärinen A. P., Martinsson J., Sporre M., Swietlicki E., Wiedensohler A., and Ulevicius V. 2015. Significant increase in Aerosol concentrations in air masses crossing a densely trafficked sea area. *Aerosol and Air Quality Research.*

Proceedings:

1. Kivekäs, N., **Kecorius, S**., Massling, A., Grythe, H., Tuch, T., Ulevicius, V. and Kristensson, A. Land-based studies of ship emissions at the Baltic and North Sea, *CRAICC Conference*, 1-4, 2014, Stockholm, Sweden.

Results concerning this thesis were presented in the following conferences:

1. **Kecorius, S.**, Tuch, T., Birmili, W., Wiedensohler, A., Lihavainen, H., Hyvärinen, A. P., Kristensson, A., Martinsson, J., Kivekäs, N., Sporre, M., Ulevicius, V. Towards understanding Baltic Sea traffic influence on coastal aerosol properties. NOSA Aerosol Symposium, Stockholm, Sweden, 30th – 31th, January, 2014.
2. **Kecorius, S**., Plauškaitė, K., Byčenkienė, S., Ulevicius, V. Observations of elevated aerosol particle number and mass concentration events in Vilnius city. The 2012 European Aerosol Conference. Spain, Granada, 2nd - 7th September, 2012.
3. Plauškaitė, K., Špirkauskaitė, N., **Kecorius, S**., Petelski, T., Zielinski, T. and Ulevicius, V. Aerosol particle distribution in the Baltic Sea marine boundary layer with the enlarged continental outflows and ship exhaust

emissions. The 2012 European Aerosol Conference. Spain, Granada, 2nd - 7th September, 2012.

4. Ulevicius, V., **Kecorius, S**. Aerosol spectrometry: parameterization of sub-micrometer aerosol particle size distribution during nucleation episodes in Preila. 54th Scientific Conference for Young Students of Physical and Natural Sciences, Lithuania, Vilnius, 17th – 19th, March, 2011.
5. Kilpys, J., Ulevicius, V., **Kecorius, S**., Andriejauskiene, J., Remeikis, V., Garbaras, A. High aerosol concentration in Lithuania caused by long range transport: episode on March 31 – April 3, 2008. 53rd Scientific Conference for Young Students of Physical and Natural Sciences, Lithuania, Vilnius, 24th – 27th March, 2010.
6. Ulevicius, V., Byčenkienė, S., **Kecorius, S**., Remeikis, V., Garbaras, A., Andriejauskienė, J., Jasinevičienė, D., Mocnik, G. Characterization of pollution events in east Baltic region affected by regional biomass fire emissions. International Aerosol Conference, Helsinki, Finland, August 29th – September 3th, 2010.

1. REVIEW OF THE LITERATURE

1.1. Atmospheric aerosol particles

An aerosol is defined as a system of solid, liquid or intermediate state particles suspended in air or other gaseous environments, meaning that basically the whole atmosphere can be seen as an aerosol (Hinds, 1982). The most evident example of aerosol particles in the atmosphere are cloud droplets with a particle diameter of approximately 10 μm. Earth's atmosphere is constantly enriched with aerosol particles from natural sources such as windblown dust, sea spray, volcanic eruptions, forest fires etc., as well as from anthropogenic sources, such as human driven fuel combustion and industrial processes. Chemical components of air particulate matter are mostly sulfate, nitrate, ammonium, sea salt, mineral dust, organic compounds, and soot carbon, each of which typically contributes to 10 – 30% of the overall mass load (Heintzenberg, 1994). The life time of an aerosol particle depends on meteorological conditions and particle size, lasting from a few days in the atmospheric boundary layer to several weeks in the free troposphere, thus allowing the distribution of particles around the planet. Particle number concentrations vary with time and space and can reach as high as 10^6 particles per cubic centimeter (cm^{-3}) in polluted urban areas, while a clean marine environment would accommodate as low as 100 particles per cubic centimeter (Junge, 1963). The main sink of atmospheric aerosol particles is wet deposition or so called in-cloud scavenging. Dry particle deposition by a convective transport, diffusion and adhesion to the Earth's surface is less important on a global scale. However, it is highly relevant with the respect to local air quality, health effects, soiling of cultural monuments.

Depending on the origin, aerosol particles can be classified as primary, directly emitted in the condensed phase, or secondary, formed by chemical reactions and gas to particle conversion of volatile organic compounds (VOCs) in the atmosphere. VOCs are emitted into the atmosphere from both,

anthropogenic and biogenic sources (Aschmann et al., 2002). Anthropogenic VOC sources include organics such as alkanes, alkenes, aromatics and carbonyls. Biogenic VOCs, for example, are isoprenes and monoterpenes. In urban environments aromatics as well as monoterpenes are identified as secondary organic aerosol precursors (Griffin et al., 2003).

The main sources of primary organic aerosol particles are natural and anthropogenic biomass burning, fossil-fuel combustion, biological materials, sea spray etc.

1.1.1. Aerosol particle size distribution

Aerosol particle size distribution ranges from exceedingly mono-disperse laboratory aerosols to multimodal atmospheric aerosols where sizes are spread more than five orders of magnitude. The climate forcing and human health effects of aerosols depend on both, diameter and concentration of the particles (Willeke and Baron, 1993). The evolution of aerosol particle size distribution reflects the physical and/or chemical processes in the atmosphere. The second moment of the atmospheric particle size distributions can be related to a global climate modification through the effects on the radiation balance. The chemical composition of the aerosol particles is found to be size-dependent. Moreover, human respiratory system is size-selective. Different tracts absorb different size ranges of the aerosol particles. Therefore, an aerosol particle size distribution is the most important physical parameters of particles.

The well-known normal distribution is the earliest mathematical formula used to approximate the measured particle size distributions. However, the works of Kottler (1950a, 1950b) show that most of the particle size distributions are skewed. Lognormal distribution was firstly applied to fit silver halide grain, dust particle, silica and granite/calcite powder measurements. Kottler has summarized the previous studies and proved that lognormal distribution fits the atmospheric aerosol surface or volume size distributions the best. However, the nature of processes which modify

atmospheric aerosol particle size distribution to a form of lognormal distribution was never fully understood. Back in 1978, Whitby showed that most of the atmospheric environment physical entity size distribution can be characterized by a tri-modal model consisting of a three additive lognormal distributions:

$$\frac{dN}{d\log d_p} = \frac{N_t}{\sqrt{2\pi}\log\sigma_g} exp\left(-\frac{\left(\log d_p - \log d_g\right)^2}{2\left(\log\sigma_g\right)^2}\right), \quad (1.1)$$

where N_t - total number concentration of the mode, d_g - number-mean diameter, σ_g – geometric mean standard deviation of the distribution, d_p – particle diameter, and log - representation of $\log_{10}$. Note that eq. (1.1) is used to describe aerosol particle number size distribution.

The modal size distribution structure greatly depends on the aerosol sources, physical and chemical processes. Characteristic modes and relevant processes shaping the particle size distribution are shown in Fig 1-1. Referring to a particle size, four distinct aerosol size distribution modes can be separated (Whitby and McMurry, 1997). Firstly, there is a clear separation between the fine mode (particle diameter < ~ 2 μm) and the coarse mode (> ~ 2 μm) particles. The fine mode further is separated to a nucleation mode (2 to 20 nm), which describes freshly nucleated particles, the following Aitken mode with the particles of 20 to 100 nm and the accumulation mode of particles between 100 and 1000 nm. After a new particle formation, the nucleation mode particles coagulate into Aitken and accumulation modes.

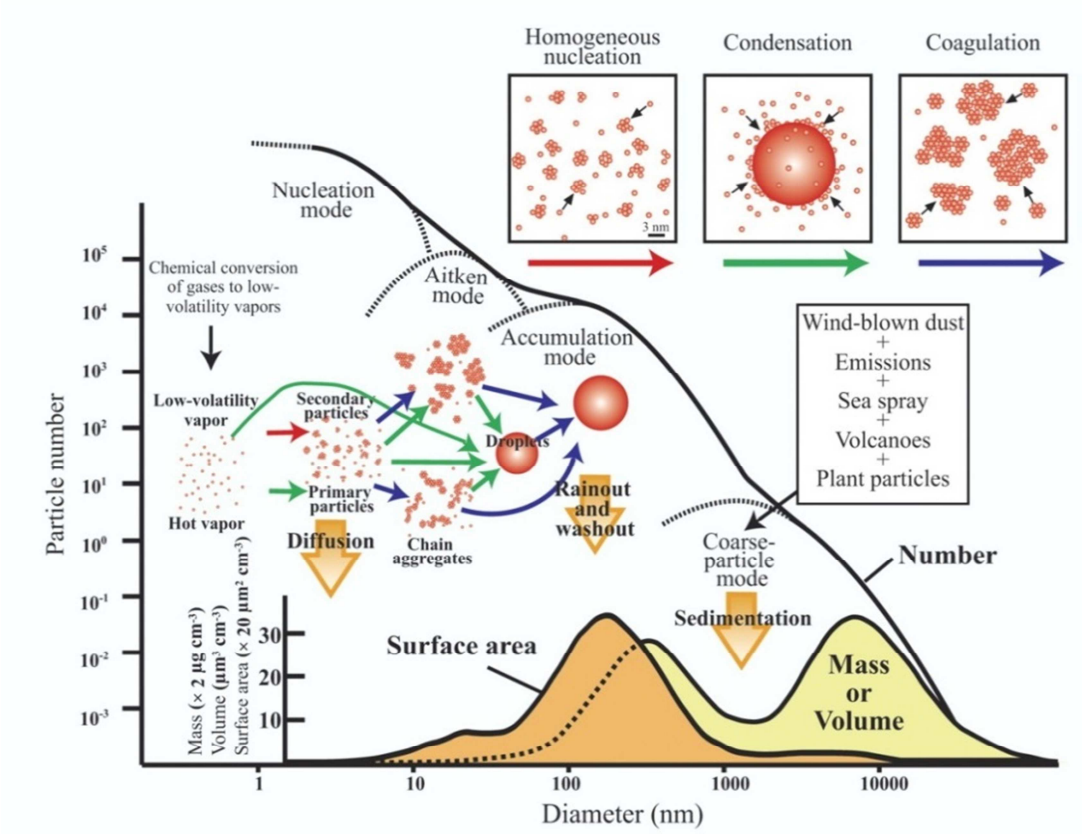

Fig. 1-1. Schematic of the atmospheric aerosol size distributions, different sources and removal mechanisms (sinks) leading to different modes (picture from http://elements.geoscienceworld.org).

Particles grow either by coagulation or condensation processes. The accumulation mode name derives from the observation that aerosol particles growing into this range tend to remain there maintaining the longest life time of any particle size. If the physico-chemical properties of the particles are right, accumulation mode particles can grow further to a coarse mode by condensation. Coarse mode particles are mainly removed by sedimentation. As an accumulation mode particles are less sufficient to be removed via rain-out or washout - typical three mode particle size distribution is found in the atmosphere. As can be seen in Fig. 1-1, ultrafine particles are dominant in the nucleation and Aitken number concentration modes.

Size, position and total number of the sub-micrometer modes are controlled by the strengths of the related gas-to-particle sources combined with the effects of aerosol dynamics. Boundaries between the modes differ depending on the aerosol particle origin. Modal aerosol particles size

distribution structure can give insights about possible aerosol sources, their transformation and evolution in the atmosphere (Seinfeld and Pandis, 2006). For example, the urban aerosol number size distribution has a strong nucleation mode in a 10 to 20 nm size range. This mode resembles traffic aerosol particles and corresponds to a vehicle exhaust particulate matter. Biomass burning aerosols contain a strong mode at 120 nm and a weak mode at 2.2 μm with a characteristic mode standard deviation of 2.0. Particle number size distribution (PNSD) measured in the exhaust duct of the coal fired heating plant can be represented with a strong Aitken and accumulation mode with a mean diameter of 45 to 100 nm. A sub-micrometer part of the fly ash mode is at 400 nm. Natural gas burning produces a bimodal shape number size distribution with mean diameters of 4 and 100 nm. Gasoline and diesel engines produce particles which can be characterized by two modes with the geometric mean diameters of 10 and 80 nm. Despite the similar modal structure, total particle number concentration is considerably higher for a diesel than a gasoline engines. The presence of several modes in the marine aerosol PNSD show the existence of different aerosol types in the environment. The mode at 600 – 1200 nm is representative for a sea salt component of a marine aerosol. Different marine aerosol/chamber measurements also confirmed a presence of 200 nm mode at a marine aerosol PNSD. The number size distribution of a suburban background aerosol has two predominant modes at 25 and 900 nm. These modes are very similar to those of the traffic-influenced aerosols (Morawska, 1999c; Kumar et al., 2013).

1.1.2. Aerosol – climate interactions

Global climate change describes the increase in average Earth's surface temperature. The radiative forcing (in Wm^{-2}) is a measure of incoming and outgoing radiative energy balance. It is defined as the stratospherically adjusted radiative flux change evaluated at the tropopause level (IPCC, 2007). The radiative forcing is linearly related to the mean surface temperature.

Positive forcing tends to increase the surface temperature while negative forcing contributes to cooling. Intergovernmental Panel on Climate Change (IPCC, 2007) states the importance of the anthropogenic radiative forcing, which is believed to have greater importance for the current climate change than the natural existing radiative forcing components. Parameters controlling the aerosol forcing are combined together in the following equation (Haywood and Shine, 1995):

$$\Delta F \approx -DS_0T_{at}^2(1-A_c)(1-R_s)^2\omega_0\bar{\beta}\delta \cdot A. \qquad (1.2)$$

Where ΔF – average aerosol forcing at the top of the atmosphere, D – daylight fraction, S_0 – solar constant, T_{at} – atmospheric transmission, A_c – cloud fraction, R_s – surface albedo, ω_0 – aerosol single scattering albedo, $\bar{\beta}$ – average aerosol up-scatter function, δ – aerosol optical depth,

$A = 1 - \frac{2R_S}{(1-R_S)^2}\left(\frac{1-\omega_0}{\omega_0\bar{\beta}}\right)$.

Eq. (1.2) represents annual mean forcing at the top of the atmosphere. Surface forcing can be much larger. The algebraic sign of the radiative forcing determines whether forcing is negative (cooling) or positive (warming). The key parameter controlling the amount of cooling versus heating is the single scattering albedo. When aerosol particles interact with light, two different types of processes occur: received energy might be scattered or absorbed. Scattering takes place in all directions but with different intensities. The absorbed radiation energy might also be transformed into other forms of energy, such as heat and/or energy of chemical reaction. Carbonaceous aerosol particles are known to attenuate the visible light mainly by absorption. Scattering is dominant for water droplets (Friedlander, 2000). The amount of incoming solar radiation that is scattered by aerosols depends strongly on the particle size distribution, where the accumulation mode is the most efficient size range. Light extinction is dependent on the refractive index of the particles. The refractive index depends on the chemical particle composition

and their water uptake ability at different relative humidity (RH). Ångström exponent and single scattering albedo is defined as:

$$\alpha = -\frac{\log\left(\sigma_{scatt}^{\lambda_1}/\sigma_{scatt}^{\lambda_2}\right)}{\log(\lambda_1/\lambda_2)},\ \omega_0 = \frac{\sigma_{scatt}}{\sigma_{ext}}, \quad (1.3)$$

where α - Ångström exponent, σ_{scatt}^{λ} – light scattering coefficient at the wavelength λ, ω_0 – single scattering albedo, σ_{ext} – light extinction coefficient.

Radiative forcing caused by gases is considered to be well understood (relatively small error bars in Fig. 1-2). The dominant uncertainty in the radiative forcing is caused by the lack of knowledge in aerosol effects. The greenhouse gases such as carbon dioxide, methane, nitrous oxide, water vapor and halocarbons alter the incoming solar radiation, thus having a warming effect. In contrast, the direct aerosol effect is estimated to cool the atmosphere by a 0.27 Wm^{-2} (IPCC, 2007). However, the indirect aerosol effect, or aerosol particle ability to act as cloud condensation nuclei, is much less understood (Lohmann and Feichter, 2005). Under atmospheric conditions, pure water vapor concentration is not enough to initiate homogeneous nucleation. The needed supersaturation to form a cloud, however, is reduced if pre-existing particles are present, because those particles can act as potential cloud condensation nuclei (CCN) (Twomey effect, or so called first indirect radiative forcing effect of an aerosol). This leads to a higher concentration of cloud droplets which greatly reduce the amount of present water vapor being condensed onto particles (Twomey, 1974). Such change in cloud structure has implications on the radiative properties (albedo) of clouds – it reflects much greater portion of the incident solar radiation back to space. The decrease in cloud droplet size decreases the precipitation efficiency and hence, prolongs a lifetime of the cloud. This effect is called the second indirect effect or Albrecht effect (Albrecht, 1989). The changes in aerosol particle physical and chemical properties influence the processes in the clouds (Levin and Cotton, 2009). The

assessment of the radiative forcing is still associated with high uncertainties due to the limited knowledge of the temporal and spatial global distribution of aerosols and their related physico-chemical and optical properties. Global modeling studies require extensive long-term field measurements to completely characterize aerosols with respect to their concentration, size distribution, size-dependent chemical composition, state of mixture and morphology, as well as information about aerosol-related formation and transformation processes which are still poorly understood (Heintzenberg et al., 1997).

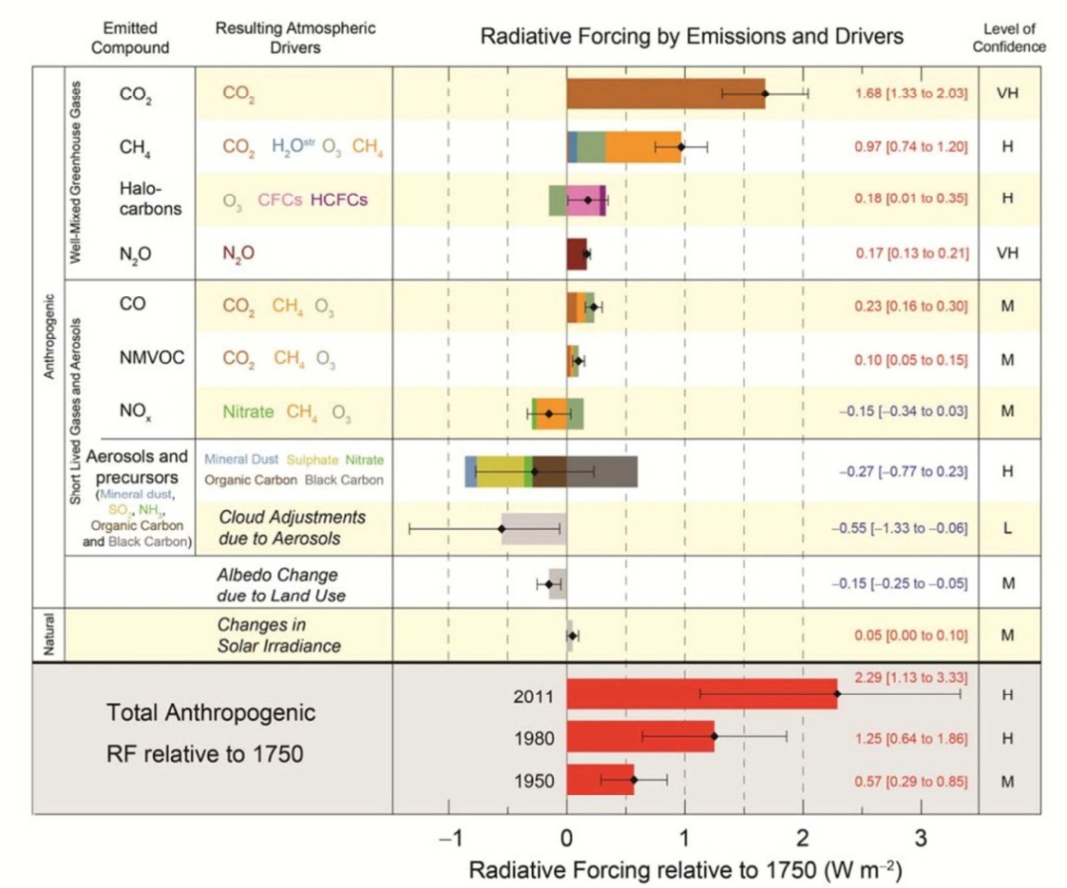

Fig. 1-2: Global average radiative forcing for the year 2005 relative to the start of the industrialization (1750). Error bars indicate the uncertainty of the respective forcing (IPCC, 2007).

1.1.3. Aerosol particles and health effects

Numerous cardiovascular, respiratory, allergic diseases, severe health effects, even enhanced mortality are related to the fine particulate matter and traffic-related air pollutants (Rissler et al., 2012). One of the most severe air pollution incidents, related to aerosol particles, was recorded in London, 1952. Under certain meteorological conditions, the pollutants were trapped within the city causing thick fog and the death of 4000 citizens.

The scale of a damage which aerosol particles cause to human respiratory system highly depends on the physical and chemical particle properties. The particle size is one of the most important characteristics, which defines particle permittivity, the depth which particle will penetrate after the inhalation (Scanlan et al., 2003). As it goes deeper in the respiratory system, the diameter and the length of airways decrease while the number of branching increases. In the head and lung airways, the surface is covered with a layer of mucus. This layer is slowly propelled by ciliary action to the pharynx and is then subconsciously swallowed to the gastrointestinal tract. This mucociliary transport can get the deposited particles out of the respiratory system in a matter of hours. The alveolar region, however, does not have the same mucociliary mechanism. Insoluble particles deposited in this region may be engulfed by alveolar macrophages and transported to lymph nodes although generally it can take months or years to clear them. The total deposition fraction (*DF*) in the respiratory system according to International Commission on Radiological Protection model is:

$$DF = IF\left(0.0587 + \frac{0.911}{1+e^{(4.77+1.485\ln d_p)}} + \frac{0.943}{1+e^{(0.503+2.58\ln d_p)}}\right) \qquad (1.4)$$

where d_p is particle size in μm, and *IF* is the inhalable fraction defined as

$$IF = 1 - 0.5\left(1 - \frac{1}{1+0.00076d_p^{2.8}}\right). \qquad (1.5)$$

1.1.4. Aerosol particle chemical composition

Atmospheric aerosols are typically complex mixtures of inorganic and organic compounds. Variable amounts of sulphate, ammonium, nitrate, sodium, chloride, trace metals, crustal elements, water and carbonaceous materials are usually found as a fraction of atmospheric aerosols (Wallace and Hobbs, 1977; Whitby, 1978). The sulphate component originates from the atmospheric oxidation of the anthropogenic and natural sulphur-containing compounds such as sulphur dioxide, dimethyl sulphide etc. Nitrate is formed from atmospheric nitrogen dioxide. Sulphate and nitrate are initially present as sulphuric and nitric acid which are progressively neutralized by atmospheric ammonia, forming the corresponding ammonium salts. Ammonium nitrate gas-to-particle conversion is strongly dependent on the temperature. Moreover, because of the Kelvin effect, particulate nitrate is rarely found in the sub-micrometer particle size range (Seinfeld and Pandis, 2006). Studies in central Europe have shown the dominance of ammonium sulfate and carbonaceous components, both largely due to combustion sources, in the fine particle composition. Carbonaceous aerosol components account for a large fraction of atmospheric particulate matter. BC (optical definition) and element carbon (EC) (thermal definition) consist of carbon content of graphite-like material and other disordered stacks of graphene layers or large polycyclic aromatics. The EC mass fraction increases in winter. This can be explained by an increased combustion of fossil fuels during the cold season. The water-soluble fraction of organic carbon increases moving from urban environment to rural area. This can be attributed to different aerosol sources, chemical aging and oxidative transformation of the organic aerosol components, which generally increases the number of functional groups and thus the water solubility of organic molecules.

1.1.5. Volatility of aerosol particles

Volatility of a molecule determines the dynamics between gas and particulate phase. The easiest way to characterize volatilization temperatures, at which compounds evaporate, is to use the laboratory generated particles of a known chemical composition. For example, sodium chloride, which boiling point is much higher than 200^{o}C (~ 1400^{o}C), is known to be non-volatile in most thermo denuders operated under not oxidizing environments (Scheibel and Porstendoerfer, 1983). Citric acid, as a reference substance for rather high volatility secondary organic aerosols, completely evaporates at 120^{o}C. Thermal studies of ammonium sulfate have shown the decomposition process before it changes into the gaseous state. 150 nm pure sulfuric acid particles evaporate completely at 300^{o}C, even though residence time of the particles in the conditioning field is as low as 32 ms. Nitrates are found to be more volatile than sulfates (Raatikainen et al., 2010).

Polydisperse aerosol particles consisting of a sulfuric acid, ammonium nitrate and chloride were found to evaporate at temperatures between 60 and 200^{o}C, typically at 100^{o}C for a sulfuric acid. Ammonium sulfate and bisulfate were found to evaporate at the temperatures between 180 and 220^{o}C. However, compared to the polydisperse particles, quasi-monodisperse population exhibit a different volatile behavior due to their smaller mass. This is mainly because of different equilibrium dynamics between gaseous and a solid particulate state.

Almost all volatility observations of ambient particles smaller than 1 μm have indicated the non-volatile cores that do not evaporate at temperatures of 300^{o}C. Polluted environment studies revealed a strong correlation between the non-volatile aerosol fraction and the light-absorption coefficient suggesting a close correspondence between refractory and light-absorbing particle fractions (Birmili et al., 2010). Even newly formed particles have shown the non-volatile residuals at temperatures, which are considered to be high enough to volatilize most of the organics (Wehner et al., 2005).

1.1.6. Hygroscopicity of fine aerosol particles

Water is a very important component of atmospheric aerosol (Rosenfeld et al., 2008). Most of the aerosol particles grow by taking up water when the relative humidity of the atmosphere increases. Particle hygroscopicity plays a crucial role in acid deposition, visibility reduction, formation of clouds and air quality in general. By interacting with water vapor particles can change their size. It influences the scattered light intensity (Fierz-Schmidhauser et al., 2010). The number size distribution and the hygroscopic properties of aerosols also determine which fraction of aerosol particles can act as a CCN and thus contribute to the indirect radiative effect. It is well known that most of the atmospheric aerosol particles containing soluble materials show a hygroscopic behavior (Zhou et al., 2002). Two main particle groups that can be separated from their hygroscopic growth spectra are called hygroscopic and hydrophobic particle fractions. Aerosol particles with a high affinity to the water molecules are called hygroscopic particles. Water uptake by atmospheric aerosols has been associated with their inorganic components, such as sodium chloride, ammonium sulfate and bisulfate, ammonium and sodium nitrates. Lots of attempts were made to understand hygroscopic behaviors of these salts (Gysel et al., 2002). However, not all questions are answered. For example, what is the chemical composition of freshly nucleated aerosol particles? How does organic species influence the water uptake, mixing state and optical properties of the inorganic fraction? Particles containing an organic fraction may exhibit vastly different hygroscopic behavior compared to pure inorganic species (Murphy et al., 2006). Some organics can decrease the surface tension of aqueous droplets and enhance hygroscopic growth (Facchini et al., 1999). Others can form surface layers that inhibit the uptake of water vapor influencing the wettability of solid particles (Kotzick and Niessner, 1999). The particles that does not take up water is called "hydrophobic" fraction. Single particle analysis supports the hypothesis that the less hygroscopic mode consists of hydrophobic soot particles. Pagels et al. (2009)

investigated the hygroscopic and optical properties of soot particles internally mixed with sulfuric acid. Fresh soot particles exhibited no change in mobility size at the sub-saturated conditions, whereas soot particles coated with a sulfuric acid experienced a lager hygroscopic growth with increasing RH. Saxena et al. (1995) used H-TDMA and impactor data to conclude that organic material from freshly produced aerosols hindered hygroscopic growth, while organic species found in aged air masses seemed to increase the growth. Cruz and Pandis (2000) suggested that the organic aerosol particle fraction decreases their hygroscopicity. Xue et al. (2009b) investigated the morphology and hygroscopicity of soot aerosol, internally mixed with dicarboxylic acids (succinic acid and glutaric acid). They found that internal soot and glutaric acid mixing transformed particles from hydrophobic to hydrophilic state and modified their morphology, enhancing their hygroscopic properties.

1.1.7. Mixing state of aerosol particles

Individual, nano-metric size particles control all the characteristics and effects of the aerosols. Because of the multitude of possible sources and transformation processes, individual particles in an air portion have their own characteristic properties. However, the available physical and chemical information about aerosol particles concerns bulk properties of a large number of aerosols. It gives wide range of uncertainties. Therefore, knowledge about state of mixing (distribution of particle properties among a population of particles with a common sorting property) is needed.

Two extremes can be distinguished when speaking about aerosol particle mixing: a) externally mixed aerosols, where essential particle properties differ between particles of a given sorting property; and b) internally mixed particles, where all particles of a given size range have similar properties. Atmospheric transformation processes, known as “aging”, alter particle properties making them more internally mixed as their residence time in the atmosphere gets longer. In the source regions aerosol particles are

expected to be mixed externally. Different approaches, such as electron-microscopy, aerosol mass spectrometry or the single soot particle photometers are used to study the mixing state and chemical composition of the individual aerosol particles. However, the traditional methods to distinguish the mixing state of aerosol particles reach their limitations when aerosol particle size gets below 100 nm. Aerosol particle hygroscopicity and/or volatility properties can be used to determine the state of mixture with high size and time resolution. At any given sub-micrometer particle size, these measurements reveal the information about physical properties of an aerosol. Their characteristic behavior gives an insight about particle chemical composition. Studies have shown that internally mixed aerosol particles absorb more light compared to externally mixed ones (Jacobson, 2001). Carbonaceous compounds are known to absorb less light when they are 100% externally mixed (Bond and Bergstrom, 2006). Numerous atmospheric processes alter aerosol particle properties by a process called “aging”. Hydrophilic particulate organic matter, co-emitted together with BC can coagulate and/or condensate on carbonaceous particles increasing their hydrophilic potential. Optical models show 2 to 4 times amplified specific absorption cross section of internally mixed BC compared to the externally mixed cases. The global climate models assume that all BC is mixed externally (Cooke et al., 1999). It results in high uncertainties and a need to properly evaluate the mixing state of aerosol particles.

A concept of a mixture of two different aerosol species, presented by Junge (1952), is shown in Fig. 1-3. Let us assume that at the source point primary particles are not affected by any processes. This would lead to a non-volatile material to be equally distributed within a particle volume where particles are mixed internally. The volatility size distribution of internally mixed, one volatility type aerosol particles, will have a mono-modal shape distribution. Internally mixed particles from a different source will correspond to different residual mode diameters. When at least two particle populations are mixed together without the transformation processes, the resulting aerosol

system represents an external mixture of internally mixed particles. This is rather rare in the atmosphere, where processes such as gas-to-particle mass transport, coagulation, mixing of different air masses and deposition change the mixing state of aerosols to a combination of internally and externally mixed particles.

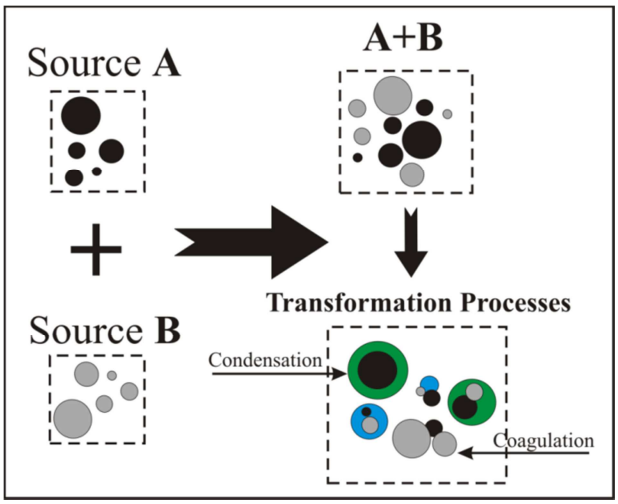

Fig. 1-3. The Mixing state of aerosol particles represented as two different aerosol particle species from source A and B. A+B illustrates an external mixing state. Aerosol transformation processes (condensation, coagulation) change the mixing state into internal.

The volatility and hygroscopicity measurements are used to investigate the aerosol particle mixing concept with respect to an aerosol population consisting of two components, either volatile or hygroscopic compounds. To simplify, it will be assumed that all non-volatile (at 300^{o}C) and hydrophobic material is mainly combustion carbonaceous matter (BC). In different scientific literature light absorbing carbonaceous have had various denominations including BC, "elemental carbon" (EC) or soot. Nomenclature strongly depends on what analysis was carried out to identify the carbonaceous aerosol particles and/or in which context light absorbing species are used. The Intergovernmental Panel of Climate Change defines soot as combustion-generated, light absorbing aerosol particles (Shine et al., 1996; IPCC, 2007). Meanwhile, combustion researchers' link the term "soot" to their scientific object – aerosols which are generated in a combustion process. Because

indistinct composition of soot, which may include variety of carbon-containing, dark-appearing compounds generated in a combustion process, the term “soot” is suggested to be replaced with BC (Cachier, 1998). Climate modelers’ use the term BC to denote carbonaceous aerosol particles with strong light absorption efficiency. Difference between BC and EC arise from the measurement method used to characterize specific aerosol properties (Orgen et al., 1983).

The volatility size distributions of the conditioned (thermally) atmospheric particles are shown in Fig. 1-4. In part A, particle population selected by a Differential Mobility Analyzer (DMA-1) consists of completely volatile species – after passing a thermal conditioning unit all particles are converted into a gas phase - both, initial particle number and volume concentrations after heating turn to zero. No particles are detected by a Condensation Particle Counter (CPC-2). Most of the newly formed particles will evaporate completely shortly after their formation. Fig. 1-4 part B shows two different internally mixed aerosol particle types which are mixed externally. On one hand, the completely volatile fraction of particles evaporates at 300^{o}C, on the other - the non-volatile fraction remains unaltered by thermal conditioning. Such particle composition produces uni-modal residual size distribution, which is not shifted in size. And while this type of distribution is rare under real atmospheric conditions, it is known that controlled emission studies of the diesel vehicles produce a mono-modal structure with only slight shift towards the smaller particle size range. Heavily “aged”, only internally mixed atmospheric aerosol particle volatility distribution is shown in Fig. 1-4 (part C). This situation represents the non-volatile cores which are exclusively coated with the volatile compounds. After thermal conditioning such aerosol population shows a multi-modal residual size distribution which is shifted towards the smaller sizes. Under the real atmospheric conditions, aged, internally mixed aerosol particles are always appended with externally mixed, non-volatile particles, resulting in a residual size distribution shown in part D.

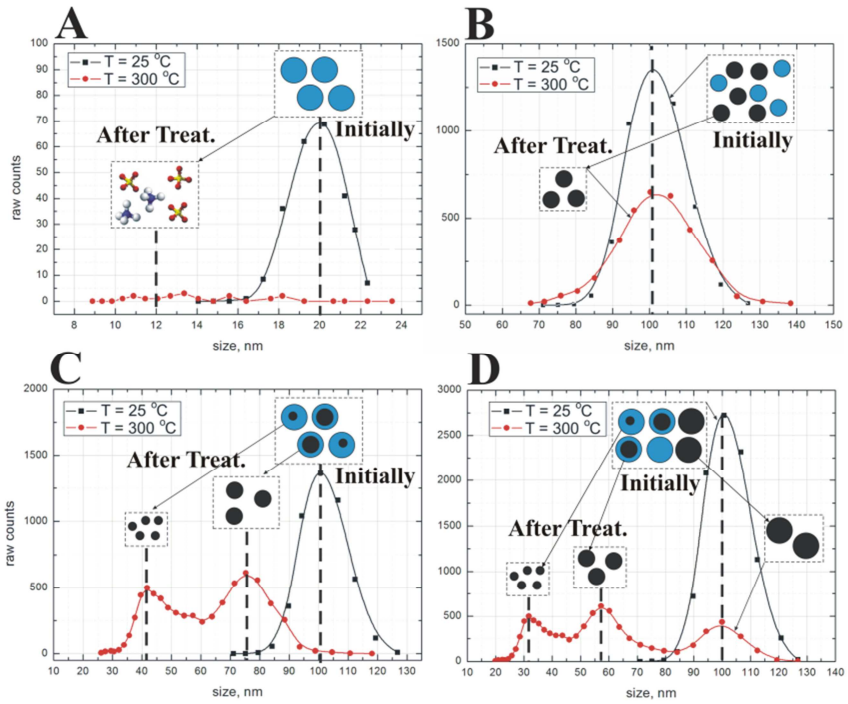

Fig. 1-4. Particle volatility size distributions when particles were exposed to ambient and elevated temperatures of 25 and 300°C, respectively.

Besides the volatility approach, mixing state of atmospheric aerosol particles can also be examined using particle hygroscopicity measurements. Accumulation of water onto aerosol particles leads to a hygroscopic growth. The ability of a particle to take up water depends mainly on the relative humidity, particle size and chemical composition. The most common particle hygroscopicity distribution is shown in Fig. 1-5.

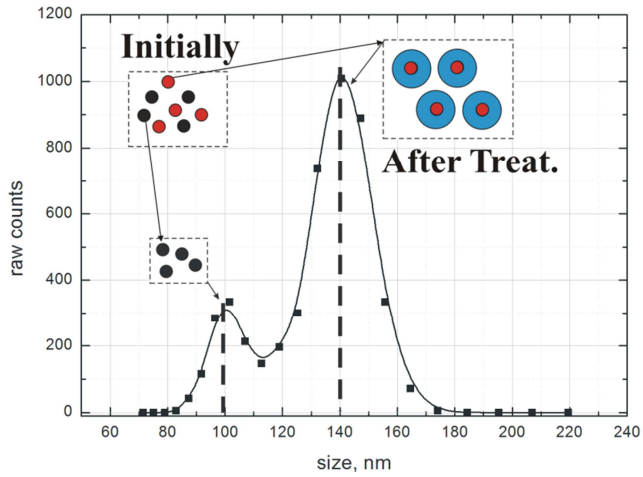

Fig. 1-5. Hygroscopicity distributions of the conditioned (RH = 87%) particles.

Suppose that the initial particle population is composed of two different chemical composition species which are defined by its own hygroscopic properties – some particles are hydrophobic, some - hydrophilic. After the treatment in a humidification chamber, the hydrophilic fraction will uptake water vapor and grow, while the hydrophobic particles will not change in their size. It results in a distinct separation between different origin particles.

1.2. Biomass burning aerosol particles

Biomass burning emission significantly contributes to the global climate change. Biomass burning aerosol is a regular feature of the Worlds temperate, tropical and boreal forests, the savanna grasslands and agricultural fields following the harvest. Currently, a pace of global fires is accelerated due to anthropogenic intervention (Simoneit, 2002). Particulate matter emitted during biomass burning episodes makes approximately 7% of the total global particulate matter emission. More than 86% of the total emitted elemental carbon originates from biomass burning. Due to high sorption capacity and optical properties, particles released from biomass burning play an important role in the Earth's radiation balance. Moreover, the published data suggests that the biomass fires create a large number of aerosol particles that are effective CCN. Biomass burning accompanied with a long range transport became a trans-boundary problem that can have significant impacts onto particulate matter levels in background European areas (Beverland et al., 2000). The pollutants from fires were also observed in Canada, USA, Russia and Eastern Europe (Damoah et al., 2004; Müller et al., 2005). Studies of a long range particulate matter transport in Northern Europe have shown that under favorable air mass transport conditions, biomass burning can have a notable impact on the particulate matter ($PM_{2.5}$) levels (Karppinen et al., 2004). The long range transport (LRT) of emissions from biomass burning in the Ukraine and European part of Russia increases the particulate matter concentrations in these countries during the spring and summer months

(Saarikoski et al., 2007). This leads to an ongoing need for analyses on the regional, continental, and global scale, to better understand how does biomass burning alter chemical and physical properties of the background environment atmospheric aerosol particles. Measurements of BC are carried out in various environments. Global effects of BC aerosols can be analyzed most explicitly using the data gathered from background regions, where clean air masses arrive from oceans or seas. Unique location of the Preila Environmental pollution research station makes it the representative background area for the East Baltic region. The surrounding regions are famous for the periodically occurring biomass burning. However, only limited information on how this process does change the background environment aerosol properties is accessible in this area. Additional studies on the atmospheric aerosol physico-chemical properties are necessary to obtain a more complete picture of the global distribution of BC. Analysis of aerosol particle properties in Preila contributes to a comprehensive understanding of the temporal variation in BC mass concentration, particle number size distribution and optical properties.

1.3. Ship traffic emissions

Ship emissions are one of the largest and least regulated sources of various atmospheric pollutants such as sulfur and nitrogen oxides (estimated to be between 9 and 15% of global emissions, respectively) and volatile organic compounds contributing up to 1.7 million tons of global particulate matter annually. BC emissions in the Arctic are predicted to increase from 0.88 kilo tones (kt) per year in 2004 to between 2.7 to 4.7 kt per year by 2050 (Eyring et al., 2010). These significant anthropogenic particulate loads affect the chemical composition of the atmosphere, local and regional air quality and are further increasing due to intensifying international co-operation and economic growth. On a global scale, more than 60000 cardiopulmonary and lung cancer related deaths, as well as changes in radiative balance over the marine environment are associated with particulate matter emitted from ships (Song et al. 2010). Most

ship-emission related research is focused on the ship engines (e.g. Sarvi et al., 2008), single ship plumes (e.g. Ault et al., 2010) or harbor and single shipping lane influence onto coastal areas (e.g. Kivekäs et al., 2014). In a review study by Kumar et al. (2013) no information about the total ship emission influence on the coastal environment aerosol properties was given. Ship emissions have been modeled on large scales and even globally (e.g. Jalkanen et al., 2009). Nevertheless, long term measurement data concerning ship-related emissions is missing.

One of the fastest growing cruise markets and a constant expansion of the busiest shipping routes in the world can be found in the Baltic Sea, Europe (Fig. 1-6**)**. According to a land-based Automatic Identification System network operated by the Baltic Marine Environment Protection Commission (HELCOM, also known as Helsinki Commission), the Baltic Sea Skaw line (Fig. 1-6) was crossed 62743 times during 2009, resulting in 20% growth since 2006.

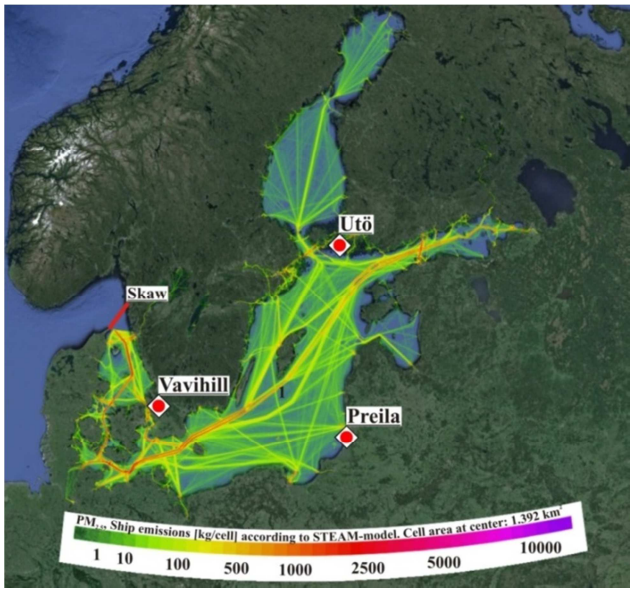

Fig. 1-6. Shipping lanes and Skaw line in the Baltic Sea using Automatic Identification System (AIS, HELCOM, 2013), as well as location of the stations.

The location of the Baltic Sea is surrounded by a continental land mass. Beside lately growing sea logistics, data on long-term physical properties of ship-exhaust aerosol species in the Baltic Sea is still rare, making it difficult to

provide a proper evaluation of the pollutants impact on the coastal regions. Viana et al., (2014) reported a comprehensive literature review focusing on the particulate matter and gaseous pollutants, main chemical tracers of shipping emissions, the particle number size distribution of ship-derived particulates and their contributions to population exposure and atmospheric deposition in Mediterranean basin, Atlantic coast of Europe and North Sea. However, the Baltic Sea coastal areas (especially western part) received either minor or no attention at all. This is mainly because only a few aerosol research stations exist in this region. Pugatshova et al., (2007) conducted a research on the characteristics of atmospheric aerosol particle number size distribution in the Baltic Sea region by means of the air mass trajectories. However, no ship-emission related effects were discussed. Isakson et al., (2001) reported that in the harbor of Göteborg in Sweden, ultra-fine particle number concentration increased by a factor of 3 when a ship plume was recorded. Kivekäs et al., (2014) estimated the ship traffic contribution to be from 5 to 9% of annual total particle number on the western coast of Denmark. Matthias et al., (2010) found that the increase of sulphate, nitrate and ammonium aerosol particle concentrations by 50% in northern Germany and Denmark can be assigned to ships' emission. Saxe and Larsen, (2008) used an operational meteorological air quality model to calculate the urban dispersion of air pollutants in Danish ports. They showed that particulate emission from ships corresponds to 15% of the total urban road traffic PM_{10} emission.

The present and increasing traffic in the Baltic Sea necessitates evaluation of the ship pollutant impact on coastal regions. The main problem with long term measurements of particles downwind of one or several shipping lanes is the separation of the ship emissions from background particle properties. Two approaches exist: 1) to identify the ship plumes in the data and estimate the background particle properties from the non-plume periods (Kivekäs et al., 2014). This approach can only be used close to the shipping lane, where the individual plumes can be separated (Kivekäs et al., 2014); 2) if particle properties in the same air mass are measured prior to and after the air

trajectory crossing with a ship lane, all changes can be attributed to phenomena taking place between the measurement sites.

1.4. Aerosol particles in densely populated environment

“China's air pollution blamed for 8-year-old's lung-cancer”, “Choking smog paralyzes cities in northeast China, closing schools, airports”, “Pollution Halves Visitors to Beijing”, “Beijing Region Tops China Pollution List in 3rd-Quarter Air Quality Survey” and other headlines emphasize not only growing scientific but also public concern on air quality during the economic bloom in People's Republic of China (The Guardian, 2013; Washington Post, 2013). In January, 2013, extraordinary pollution event has attracted the world wide attention when the daily $PM_{2.5}$ concentrations up to 6.7 times exceed new China National Ambient Air Quality Standard (MEP, 2012).

Intensive economic growth and industrialization demands a great supply for energy. This makes China to be first and second largest producer/consumer of a coal and oil in the World, respectively. 18.6% of the World’s steel production, 30.0% China’s coal and 13.6% of cement are produced in Hebei province. As a result seven of the top ten most polluted cities in China are found in this province (Wang et al., 2013). Vast amounts of BC aerosols are emitted from vehicles, fossil fuel and biomass burning. It permanently disturbed the natural equilibrium between aerosol production and aerosol removal. Not only has the overall quantity of aerosol emissions increased. Large amounts and diversity of trace gas overcame natural processes and lead to both, nucleation and secondary aerosol particle formation.

New particle formation (NPF) is usually observed during the daytime. It is emphasized that it occurs because of a low preexisting particle surface concentration and photochemical production of gaseous precursors (Kulmala and Kerminen, 2008). Elevated concentrations of SO_2 and H_2SO_4 were found to correlate well with nucleation event occurrences (Kirkby et al., 2011). Laboratory experiments showed that volatile organic compounds might also

play an important role in new particle formation. The possible pathways for new particle formation are paved through the binary and ternary nucleation (Merikanto et al., 2007; Kulmala and Laaksonen, 1990). H_2SO_4 is formed from SO_2 and OH (Seinfeld and Pandis, 2006). However, Wiedensohler et al., (1997) and Suni et al., (2008), among many others, have also reported nocturnal new particle formation events. Because scientific interest is mainly drawn towards the daytime NPF events, neglected scientific interest in nighttime nucleation veiled the knowledge about it. Compared with daytime nucleation events, the understanding about nocturnal ones is still sparse. Previously mentioned pathways do not apply to nocturnal nucleation because the major OH sources are photochemical production from ozone and water. Studies in Australia carried out by Suni et al., (2008) suggested that the nocturnal nucleation events might be associated with high concentrations of radon and/or presence of Eucalypt trees (source of VOCs). In polluted environments SO_2 conversion to H_2SO_4 might take place throughout NO_3 (Brown et al., 2006a, 2006b). However, neither the detailed nucleation mechanism, nor the complete sets of reaction partners are known. Moreover, only a sparse knowledge exists about how nocturnal NPF affects the mixing state of aerosol particles. Thus, a more intense investigation of this phenomenon would help to improve climate models and lead to a better understanding of their direct scattering of solar radiation as well as indirect effects on climate throughout increase in the CCN number.

1.5. Chapter conclusions

Observations of atmospheric ultrafine aerosol particles began in the late 1800s and is the subject of great scientific interest ever since. Despite the vast scientific knowledge about their relevance for both, global climate and human health, a great uncertainty still remain about how aerosols interact with the environment. It was shown that the particle impact onto various processes greatly depends on their physical and chemical properties among which

particle number size distribution and concentration are of great importance. It was also shown that the mixing state of the aerosol particles is a key feature which describes not only black carbon cloud condensation nuclei activity, but also characterize their light absorption and scattering properties thus being significantly important in reducing uncertainties in global and regional aerosol model studies. Because of the unique location of the Preila Environmental Pollution Research station, representing East Baltic region, two characteristic processes for this region were overviewed, i.e. biomass burning (wildfire) and ship related emissions in the Baltic Sea. Despite these processes relevance, no attempts were made to identify how regional biomass burning and shipping in the Baltic Sea influences the background aerosol particle physical properties. Moreover, the highly polluted environment processes, such as nocturnal new particle formation impact on the mixing state of aerosol particles, are not well understood.

2. INSTRUMENTS AND METHODS

2.1. Condensation particle counter

The basic physical parameters of an aerosol particle number concentration can be measured using a Condensation Particle Counter (CPC) (Fig. 2-1) (Mordas et al., 2005). Instrument parameters are as follows: working fluid – butanol; aerosol sample flow – 1 l/min.; condenser temp. + 10 °C; saturator temp. + 43 °C; cut-size – 4.35 nm; the minimum measured number concentration of aerosol particles - 0.003 cm^{-1}; maximum – 150000 cm^{-1}; accuracy – 5 to 10%. The principle on which the condensation technique is based involves three processes: super-saturation of working fluid; growth of particles by condensation of vapor; and detection of particles. The standard optic particle counters struggle to measure particles smaller than 50 nm. In a CPC particles are grown by condensation to a micron sizes, thus allowing easy detection by simple optics. The critical super-saturation for homogeneous nucleation is typically around 300%. The smallest size at which condensation will occur is referred to Kelvin diameter. This size dependence occurs because the vapor molecules are able to escape more easily from a curved surface. In a CPC, super-saturation is controlled to be around 100 – 200%. However, a critical super-saturation must be avoided. If this critical value is reached, droplets will form in particle free air.

In a diffusional thermal cooling CPC particle laden air passes through a heated chamber which is saturated with working fluid vapor. A sheath flow is split from an inlet flow, filtered and used to constrain the particles in the growth chamber. The sample flow is then injected into the center of the laminar sheath flow through a capillary to assure that particles will experience the highest possible super-saturation. At the end of the saturator, the air is cooled in the condenser. It becomes super-saturated and causes particles to grow. Grown particles are then focused through a laser beam where they are counted.

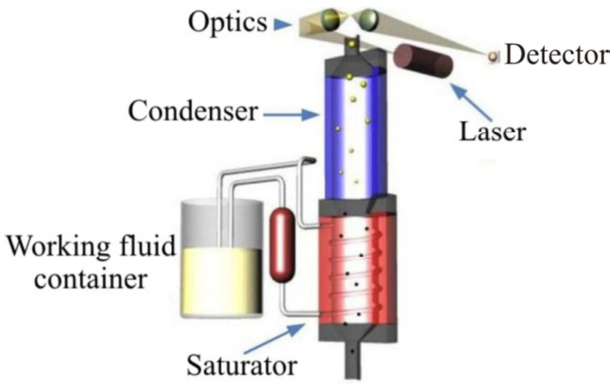

Fig. 2-1. Principal scheme of the CPC showing the main instrument components: working fluid container, saturator, condenser and particle detection section consisting of a laser and optics.

CPCs are mainly used to provide information about the total particle number concentration. Any information on the original size of particles is lost because of condensational growth. Differential Mobility Particle Sizer (DMPS) or Scanning Mobility Particle Sizer (SMPS) combined with a CPC can be used to measure the aerosol particle number size distribution. Additionally, several CPC's with the different lower cuts can be used to provide a course, but fast response size distribution of the smallest particles (Kulmala et al., 2007).

2.2. Differential mobility analyzer

The Differential Mobility Analyzer (DMA) is the fundamental component of the experimental set-up used in this work. DMA can be considered as a capacitor and is used to create a well-defined electric field, which is then used to determine the electrical mobility of charged aerosol particles. DMA for submicron aerosol size distribution measurements was firstly presented by Knutson in 1976. This technique has become a prime choice for submicron particle classification mainly because it enables to investigate the finest particle size range (down to 2 nm) with high precision, time and size resolutions while keeping aerosol particles suspended in air. Different DMA configurations do exist (Fissan et al., 1996). However, the most common geometry is the cylindrical DMA in which the classification takes place in the flow between concentric cylinders (Heim et al., 2005). Though

DMAs may differ in their design, the operational basics remain the same as presented in Fig. 2-2.

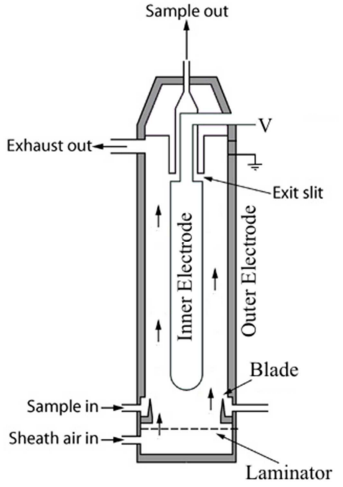

Fig. 2-2. Construction of a DMA.

Basic DMA consists of two inlets and two outlets (Fig. 2-2). Close loop or compressor/vacuum pump driven particle-free sheath flow is introduced through a laminator, which directs the flow towards a central (inner) electrode. Charged, poly-disperse aerosol particles are introduced in a smaller flow near the outer electrode through a smooth, blade sharp slit, which ensures that aerosol particles merges with a sheath flow without any turbulence. The rate of particle migration in the classification zone (space around inner electrode) depends on the electrical mobility of the particles. Mobility, in turn, depends on both, the size and electrical charge of the particles. If all the particles have the same charge, then particles of a given mobility will all be of the same size. By applying an electric field between the two electrodes, charged particles migrates from the poly-disperse aerosol entrance flow to the classified aerosol outlet flow for a subsequent use, which might be either particle counting or further conditioning. A small flow is then withdrawn through the slit in the central electrode at a downstream location, while most of the flow is exhausted. It is important to mention that electric mobility analysis does not directly measure particle size. It measures the particle transport property, an electric mobility. The particle size can be calculated from this mobility.

2.2.1. Aerosol particles charging

Particle charging by ions is a subject of great importance in the field of aerosol science. For charge-based aerosol characterization, the electrical particle charging must be well controlled and result in a known, preferably narrow distribution of charges (Wiedensohler, 1988). The most widely used charging technique is to pass the aerosol particles through a cloud of bipolar air ions. The ions are usually generated by the interaction of the molecules present in air with a radiation emanating from a radioactive source. The radiation ionizes the air/carrier gas molecules. The ions collide with the particles and form charged particles. Various radioactive sources can be used to reach charge equilibrium. Most frequent one is a Kr-85 bipolar neutralizer ($\tau_{1/2}$ = 10.76 year, 57 and 370 MBq), where emitted β radiation generates positive and negative ions through the ionization. The Kr-85 noble gas is located inside a hermetically sealed stainless steel container, which is integrated in a metal cylinder. In the space between the stainless steel container and the metal cylinder, the aerosol passes through the neutralizer. Moving through the metal cylinder the aerosol carrier gas is ionized by a high-energy radioactive radiation. As a result, positively charged gas ions and free electrons are generated. Charges are created by β radiation interaction with nitrogen gas molecules. Afterwards, neutral gas molecules with a strong electron affinity (e.g. O_2) collect the free electrons to build negatively charged ions. If these ions are brought together with an aerosol, a defined equilibrium charge distribution is set. The neutralizer does not neutralize charges, but rather brings the particles into a well-known charge distribution. The gas ions' velocities are distributed by Boltzmann distribution, therefore it is expected, that charged particles will also follow Boltzmann distribution:

$$f(n, d_p) = \frac{2e}{\sqrt{\pi d_p k_B T}} e^{-\left(\frac{n^2 e^2}{d_p k_B T}\right)}, \qquad (2.1)$$

where e - elementary electrical charge, d_p - particle diameter, k_B - Boltzmann constant, n - the number of elementary units of charge. The number of charges acquired by diffusion charging during a time t is:

$$n(t) = \frac{d_p kT}{2K_E e^2} \ln\left[1 + \frac{\pi K_E d_p \bar{c}_i e^2 N_i t}{2k_B T}\right], \tag{2.2}$$

where $n(t)$ - number of charges acquired by a particle of diameter d_p in time t, $\bar{c}_i$ -mean thermal speed of the ions (240 m/s at STP), k_B - Boltzmann constant, K_E - constant of proportionality (= 1 for cgs units; = $9.0 \cdot 10^9$ $Nm^2 C^{-2}$ for SI) and N_i -ion concentration. For typical diffusion chargers: $N_i \cdot t > 10^{12}$ s/m^3. For nanoparticles, the Boltzmann distribution leads to an under prediction, thus Fuchs charging should be used. The probability for a particle smaller than 1 μm, to get singly or doubly charged can be written from (Wiedensohler, 1988):

$$p(D_p, n) = 10^{\left[\sum_{i=0}^{5} a_i(n)\left(\log\frac{D_p}{nm}\right)^i\right]}, \tag{2.3}$$

where $a_i(n)$ are the fit parameters from Table 2-1.

Table 2-1. Fit parameter for specific charge of the fifth-degree polynomial approximation of Wiedensohler (1988).

N					
$a_i(N)$	**-2**	**-1**	**0**	**+1**	**+2**
a_0	-26.3328	-2.3197	-0.0003	-2.3484	-44.4756
a_1	35.9044	0.6175	-0.1014	0.6044	79.3772
a_2	-21.4608	0.6201	0.3073	0.4800	62.8900
a_3	7.0867	-0.1105	-0.3372	0.0013	26.4492
a_4	-1.3088	-0.1260	0.1023	-0.1553	-5.7480
a_5	0.1051	0.0297	-0.0105	0.0320	0.5059

The fraction of particles with three or more elementary charge units can be calculated using the following expression (Gunn, 1955):

$$p(D_p, n) = \frac{1}{\sqrt{2\pi\sigma}} exp\left[-\frac{(n-\sigma \ln 0.875)^2}{2\sigma}\right], \quad (2.4)$$

where $\sigma = \frac{2\pi\epsilon_0 D_p k_B T}{q_e^2}$, ϵ_0 -vacuum permittivity, q – electric charge, D_p – particle diameter, k_B – Boltzmann constant, T - temperature, and n – number of elementary charge units on particle. Table 2-2 gives the bipolar charge distributions calculated using the Fuchs theory.

Table 2-2. Electrical charging probabilities during a bipolar neutralization

D_p [nm]	Electrical charging probabilities f(n)										
	n=-5	**n=-4**	**n=-3**	**n=-2**	**n=-1**	**n=0**	**n=1**	**n=2**	**n=3**	**n=4**	**n=5**
2	0	0	0	0	0	0.97	0	0	0	0	0
5	0	0	0	0	0.02	0.96	0.01	0	0	0	0
10	0	0	0	0	0.05	0.91	0.04	0	0	0	0
20	0	0	0	0	0.10	0.79	0.08	0	0	0	0
50	0	0	0	0.01	0.22	0.58	0.16	0	0	0	0
100	0	0	0	0.05	0.27	0.42	0.21	0.03	0	0	0
200	0	0	0.03	0.12	0.26	0.29	0.20	0.07	0.01	0	0
500	0.02	0.05	0.09	0.14	0.18	0.18	0.14	0.08	0.04	0.01	0
1000	0.05	0.08	0.11	0.12	0.13	0.12	0.10	0.07	0.05	0.02	0.01

2.2.2. Differential mobility analyzer transfer function

To evaluate the performance of a DMA, the concept of the DMA transfer function is utilized (Knutson and Whitby 1975a, 1975b). The DMA transfer function Ω is defined as the probability of a particle with a given size successfully traversing the classifier. Specifically, it is the probability of the particle, starting at the aerosol entrance of the classification zone and reaching the aerosol exit. The DMA transfer function itself is characterized by the midpoint mobility and the shape of the transfer function. The midpoint mobility and Ω shape depend on various parameters, such as voltage applied to the DMA, flow rates in the DMA and its design (Stolzenburg, 1988). The ideal transfer function of a cylindrical DMA has a triangular shape as shown in

Fig. 2-3 (part a). The relative half width β depends only on the DMA flow rates. However, particle losses caused by the diffusion processes, especially in the ultrafine particle range (D_p < 20 nm), may broaden transfer function as shown in Fig. 2-3 (b and c). A schematic of an axial flow DMA is shown in Fig. 2-3, left. R_1 and R_2 are the inner and outer radii of the annular classification zone. L is the axial length between the midpoints of the aerosol inlet and outlet slits. Q_a and Q_s are the aerosol inlet and outlet flows. Q_c and Q_m are the entering particle-free and exiting particle-laden sheath flows. The voltage, V, applied to the center rod is used to select particle size.

Centroid mobility Z_p^* for non-diffusing transfer function Ω_{nd} can be written as:

$$Z_p^* = \frac{(Q_c+Q_m)}{4\pi\Delta\phi}. \tag{2.5}$$

The base half width is defined as:

$$\Delta Z_p = \frac{(Q_a+Q_s)}{(Q_c+Q_m)} Z_p^*. \tag{2.6}$$

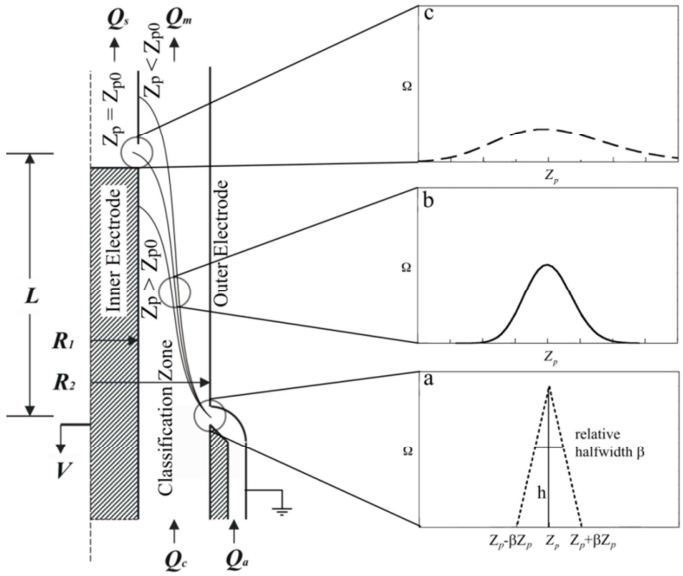

Fig. 2-3. Schematic of axial flow DMA showing non-diffusing particle streamline (a) and Gaussian cross-stream probability distributions of the diffusing particles (b).

For the axial flow DMA, the change in the electrical flux from the aerosol inlet to the outlet is:

$$\Delta\phi = \frac{LV}{\ln\frac{R_2}{R_1}}. \tag{2.7}$$

Then non-diffusing transfer function has the form:

$$\Omega_{nd}\left(Z_p, Z_p^*, \Delta Z_p\right) = \frac{1}{Q_a} max\left(0, \left[min\left(Q_a, Q_s, \left[\begin{array}{c}\frac{(Q_a+Q_s)}{2} - \\ -\left|2\pi Z_p \cdot \Delta\varphi + \frac{(Q_c+Q_m)}{2}\right|\end{array}\right]\right)\right]\right). \tag{2.8}$$

In a non-dimensional form:

$$\Omega_{nd}\left(\tilde{Z}_p, \beta, \delta\right) = \frac{1}{2\beta(1-\delta)}\left[\begin{array}{c}\left|\tilde{Z}_p - (1+\beta)\right| + \left|\tilde{Z}_p - (1-\beta)\right| - \\ -\left|\tilde{Z}_p - (1+\beta\delta)\right| - \left|\tilde{Z}_p - (1-\beta\delta)\right|\end{array}\right], \tag{2.9}$$

where the dimensionless mobility and flow parameters are as follows:
$\tilde{Z}_p = \frac{Z_p}{Z_p^*}$, $\beta = \frac{(Q_s+Q_a)}{(Q_m+Q_c)}$ and $\delta = \frac{(Q_s-Q_a)}{(Q_s+Q_a)}$.

In a case when diffusion cannot be neglected, the Gaussian cross-stream profile about the corresponding non-diffusing particle streamline can be used to approximate diffusing particle spread (Stolzenburg, 1988). Standard deviation of a Gaussian cross-stream profile in non-dimensional form is written as:

$$\sigma^2 = \omega \cdot \widetilde{D}, \tag{2.10}$$

where ω is non-dimensional geometry factor, $\widetilde{D} = \frac{4\pi LD}{(Q_m+Q_c)}$, and D is the particle diffusion coefficient. The diffusing transfer function Ω_d in non-dimensional

form is defined as:

$$\Omega_d\left(\tilde{Z}_p,\beta,\delta,\sigma\right)=\frac{\sigma}{\sqrt{2}\beta(1-\delta)}\begin{bmatrix}\varepsilon\left(\frac{\tilde{Z}_p-(1+\beta)}{\sqrt{2}\sigma}\right)+\varepsilon\left(\frac{\tilde{Z}_p-(1-\beta)}{\sqrt{2}\sigma}\right)-\\-\varepsilon\left(\frac{\tilde{Z}_p-(1+\delta\beta)}{\sqrt{2}\sigma}\right)-\varepsilon\left(\frac{\tilde{Z}_p-(1-\delta\beta)}{\sqrt{2}\sigma}\right)\end{bmatrix}, \quad (2.11)$$

where $\varepsilon(x)=x\cdot erf(x)+\frac{e^{-x^2}}{\sqrt{\pi}}$ and erf(x) is the error function.

2.3. Scanning mobility particle sizer

This work presents a variety of aerosol number size distributions measured with SMPS system, which consists of a sequential setup of a neutralizer, DMA and CPC. Raw data provided by such system contains information about particle electrical mobility. These measurements can then be converted to a size distribution by using the distribution of charges produced by a charger and the known relation between mobility and size (Wiedensohler 1988).

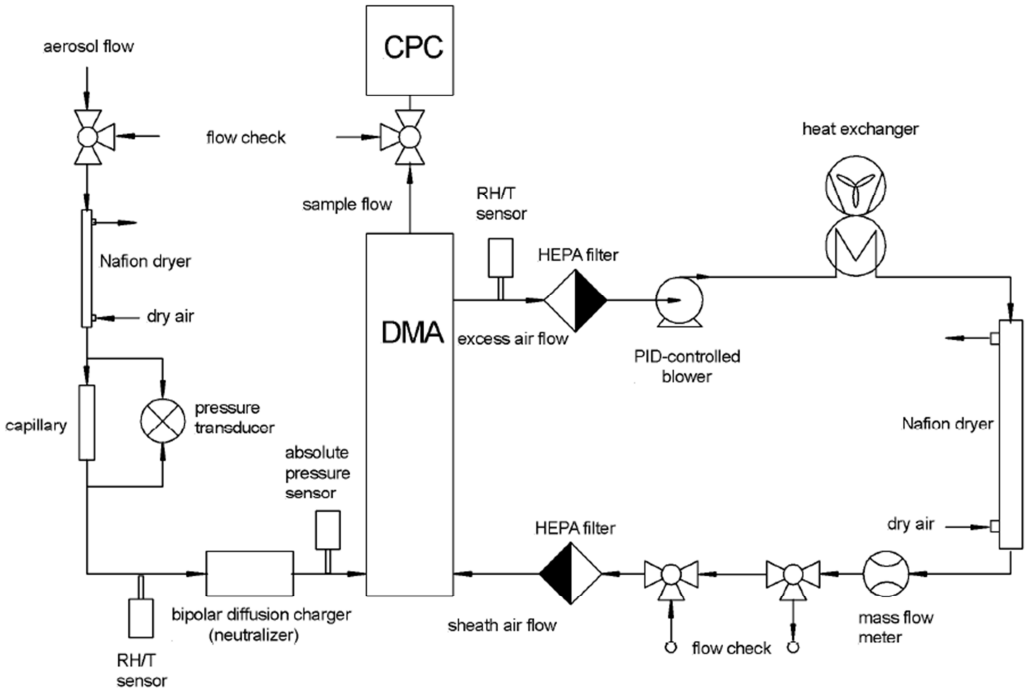

Fig. 2-4. Schematic sketch of the mobility particle size spectrometer. Picture is taken from Wiedensohler et al., 2012.

The working principle of SMPS system (Fig. 2-4) can be described as follows. After aerosol particles pass the pre-impactor, they are brought to bipolar charge equilibrium in a bipolar diffusion chamber, so called neutralizer. The highest particle number concentration, which can be measured by mobility particle size spectrometers, is defined by the equilibrium ion pair concentration, which is believed to be approximately 10^7 cm^{-3}. Therefore, SMPS can only be used for the total particle number concentrations reaching up to 10^6 cm^{-3}. After passing through neutralizer, well-conditioned aerosol particles are carried into a DMA - a cylindrical capacitor where they are injected through an annular slit close to the outer electrode in the DMA and then merged with the particle-free sheath air flow. All flows are strictly laminar. In the DMA, under the influence of an electric field, charged particles migrate into a clean sheath air flow. The migration rate depends on the electrical mobility, which itself depends on both, the size and electrical charge of the particle. By scanning through the voltages, certain mobility particles can be selected and withdrawn through a slit in a DMA. When the mono-disperse particles leave the DMA they are still suspended in air. These particles then can be used for various purposes, such as kinetic experiments on the rates of reactions between gases and particles. In the present work, particles were counted with a CPC to provide the size distribution of the aerosol entering the DMA. The electrical particle mobility distribution is determined by scanning the voltages through the entire electrical particle mobility range being investigated. In the SMPS system used in the present study the particle number concentration accuracy is measured to be 5 – 10% (Wiedensohler et al. 2012). Sizing accuracy is ± 2 nm. System technical information: sample flow – 1 l/min.; sheath flow – 10 l/min.; time resolution – 5 min.; neutralizer – Kr-85; inlet – PM_{10}; RH < 40%; sizing interval – 8 to 800 nm; sizing steps – 71. Measured aerosol particle mobility distributions were evaluated using multiple-charge inversion routine presented by Pfeifer et al., (2013). No other system exists to measure particle number size distribution in a range from 2 to 1000 nm. Therefore DMA based instrumentation was chosen in this work.

2.4. Volatility tandem differential mobility analyzer

The size-segregated atmospheric aerosol non-volatile fraction was defined by evaporating particle volatile components and successively quantifying resulting refractory material using the DMA. This method involves the following steps: selection of quasi-mono-disperse particles from a poly-disperse aerosol population; conditioning by heating to a specific temperature; and determining the residual number size distribution. A schematic of a used V-TDMA system is shown in Fig. 2-5. In the first part of the system, poly-disperse aerosol particles are dried in a diffusion dryer and passed thought a neutralizer to achieve bipolar charge equilibrium. Particles of a defined narrow mobility are selected from an aerosol population by a first DMA (DMA1). The sheath air is adjusted to a flow rate of 5 l/min, complying with an aerosol flow rate of 1 l/min, thus establishing aerosol-to-sheath air ratio of 1:5.

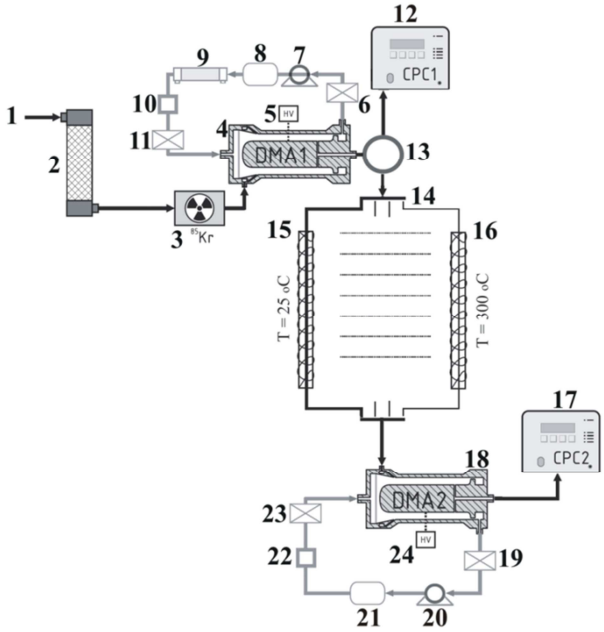

Fig. 2-5. Schematics of V-TDMA system: 1 – poly-disperse ambient aerosol sample, 2 – diffusion dryer, 3 – Kr-85 neutralizer chamber, 4 – DMA1, 5 – high voltage unit, 6 – total particle filter, 7 – blower, 8 – flow meter, 9 – nafion dryer, 10 – heat exchange, 11 – total particle filter, 12 – CPC1, 13 – aerosol mixing chamber, 14 – magnetic valves, 15 – reference, ambient temperature, heating column operated at 25^{o}C, 16 – conditioning heating column, operated at 300^{o}C, 17 – CPC2, 18 – DMA2, 19 – total particle filter, 20 – blower, 21 – flow meter, 22 – heat exchange, 23 – total particle filter.

The flow rates are manually adjusted to ensure flow equilibrium inside the DMA on a regular basis. The RH of the sheath air before the DMA1 and in its excess air (sheath air plus aerosol flow) is typically on the order of 10%. The resulting quasi-mono-disperse aerosol is then directed through a small mixing chamber to guarantee a homogeneous particle profile inside the sampling tube. The flow is subsequently split to simultaneously determine the number concentration of the initially selected particles and to direct the remaining part to a conditioning unit.

All V-TDMA system aerosol lines are made of stainless steel tubes with an inner and outer diameter of 4.0 and 6.35 mm, respectively. The transport tubes are designed to be of minimal length and number of bends. The flow through the sampling lines is maintained to be laminar. After size selection the quasi-mono-disperse particles are passed into a conditioning unit where they are thermally conditioned to a predefined temperature. The heating unit comprises four heating columns (Fig. 2-6). Each column is maintained at a fixed temperature between 25°C and a maximum of 300°C. The selection of a pertinent heating column is controlled by a valve assembly (Fig. 2-5, 14). Each column consists of an inner, 6.35 mm stainless steel tube for the aerosol flow. The tube is surrounded by a second, 25.4 mm steel tube filled with sand to act as a buffer between heating coil and aerosol line. A glass-silk heating wire is coiled around the outer tube and allows fast heating of the aerosol. Sand reacts slowly to small temperature changes and guarantees a stable and homogeneous temperature field. The tubes are furthermore surrounded by a thick layer of glass padding and an additional quartz fiber fleece for insulation. At the bottom of each column a thermocouple is inserted into the center of the aerosol to continuously measure the aerosol temperature. The software digitally controls the heater via software regulator to maintain the temperature inside the inner tube.

Thermal particle conditioning was performed at two different temperatures: 25°C and 300°C. Ambient temperature is selected as a reference for the unconditioned aerosol particles; 300°C is the maximum

temperature technically feasible for this setup to evaporate the volatile particle fractions. Temperatures above 300°C require carrier gases such as helium or nitrogen to avoid measurement artifacts due to charring of the organic matter which may lead to an overestimate of measured non-volatile material. Aerosol particles ensuing from the thermal conditioning process are passed to the third part of the system to determine their resulting number size distribution termed as non-volatility size distribution. The size distribution is determined by a second DMA and CPC.

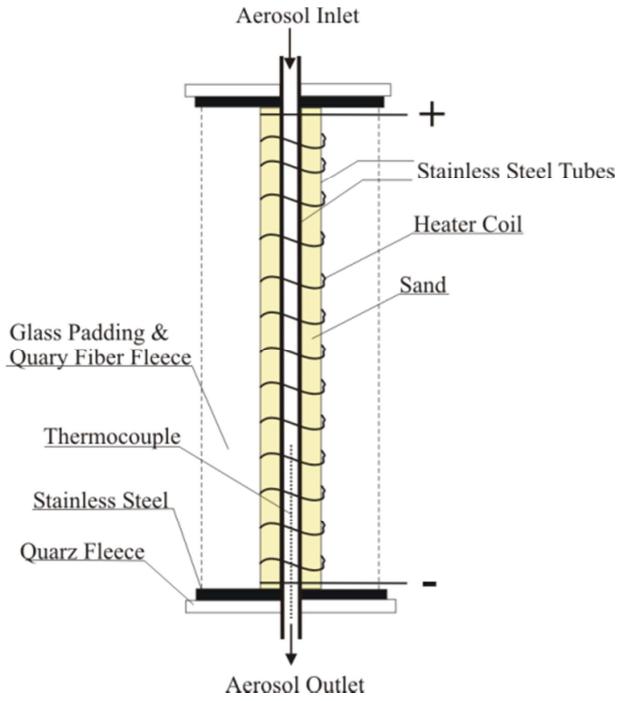

Fig. 2-6. Schematic of a single V-TDMA heating column.

The total time for a CPC to determine the concentration at one particular DMA2 channel is adjusted to be 10 sec during which the DMA voltage is kept constant. An additional 5 sec. between the different channels is set to allow CPC2 adapt to a new particle size. DMA2 is operated at aerosol-to-sheath air flow ratio of 0.1 (aerosol flow rate of 0.5 l/min, sheath air flow rate of 5 l/min). To obtain a compromise between high size and temporal resolution, the number of size bins and the DMA2 scan range vary during the different experiments and are optimized to measurement conditions.

2.5. Hygroscopicity tandem differential mobility analyzer

A Hygroscopicity Tandem Differential Mobility Analyzer (H-TDMA) is an instrument to measure hygroscopic diameter growth of individual particles when taken from a dry (RH < 20%) to a controlled humidified state. Measurements were performed with an H-TDMA designed at the Leipzig Institute for Tropospheric Research (TROPOS) (Fig. 2-7). The H-TDMA consists of similar parts as V-TDMA except different particle conditioning chamber is used. After the first DMA-1 selects a narrow, quasi-mono-disperse size range aerosol, it is passed to a humidification section with a distinctive relative humidity of 87%. In the humidification system a peristaltic pump is used to circulate water surrounding a micro-porous membrane, through which the aerosol flows. The tubing is made of GORE-TEX membrane. Because of a humidity gradient, water vapor is transported through the membrane and humidifies the dry air inside to a relative humidity of approximately 95%. Leaving the humidifier, the humid air is mixed with a dry air to reach the defined level of relative humidity. To obtain stable, well controlled conditioning, the aerosol and sheath air flows are treated in two separate humidifiers. Humid air is then circulated through a Nafion tube, where the aerosol and sheath flows are humidified due to humidity gradient. In a conditioning section particles grow in size by taking up water depending on their chemical composition and their initial dry diameter. This humidified aerosol is passed then into the second DMA-2. The sheath air in the second DMA-2 is humidified to the same relative humidity as the aerosol. The same aerosol/sheath flow ratio (0.5/5 l/min) is used in DMA-2. Since a high size resolution decreases the temporal resolution and vice versa, a diameter step of 5% is used in measuring atmospheric aerosol. Depending on optimized CPC-2 counting time and DMA-2 scanning size range and steps, a full measurement cycle takes less than one hour.

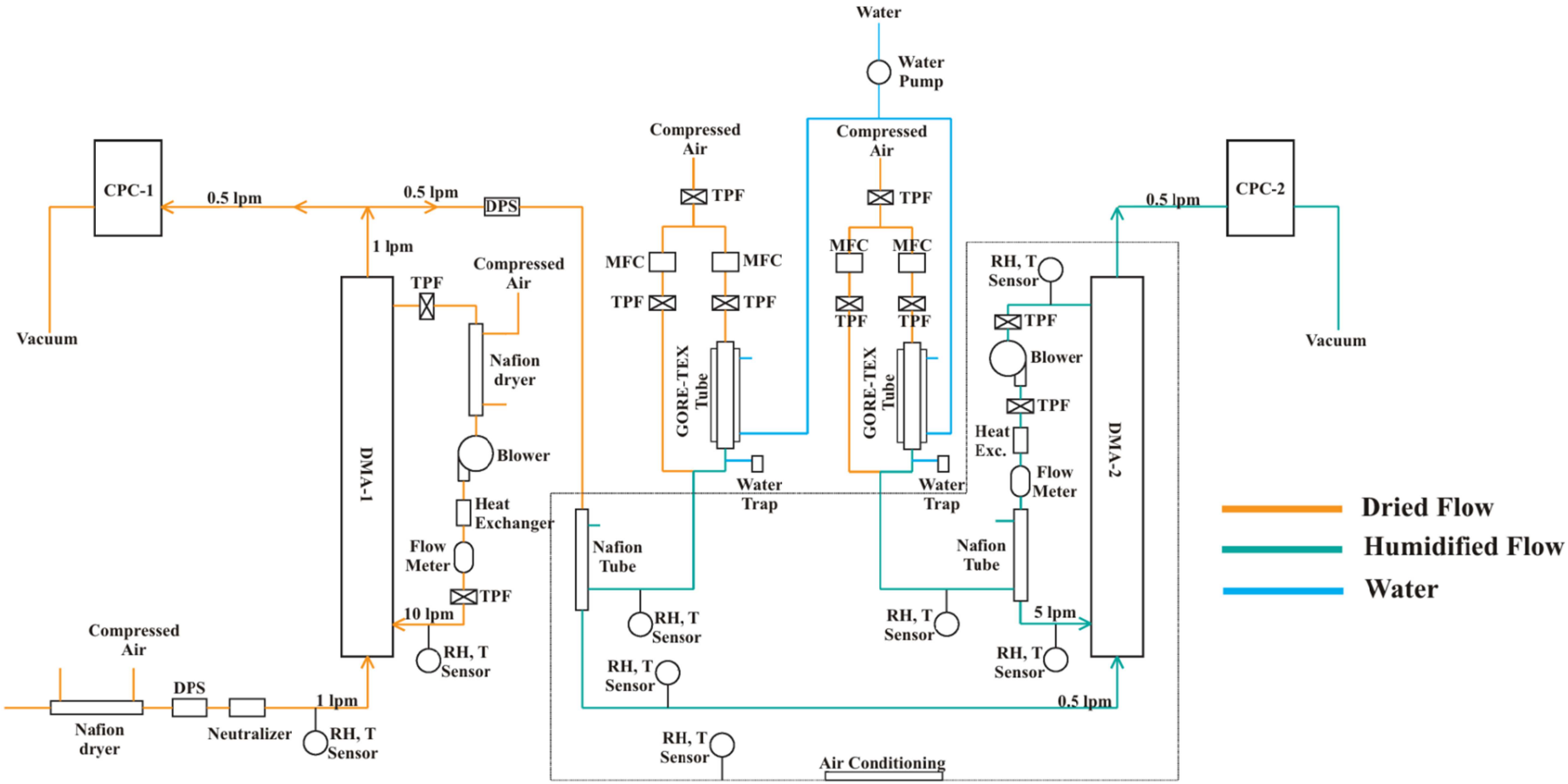

Fig. 2-7. Schematics of H-TDMA system. The following abbreviations are used: DPS – differential pressure sensor, TPF – total particle filter, CPC – condensation particle counter, DMA – differential mobility analyzer. Different line color represents different humidity flows and water lines.

2.6. Tandem differential mobility analyzer data inversion

In this work, V-TDMA and H-TDMA systems were used to determine non-volatile and hygroscopic fractions of the atmospheric aerosols. Measurement signal of both systems refers to the particle number concentration at the T-DMA system outlet as a function of the particle size set at the instrument. The measured aerosol size distribution downstream of the DMA-2 is not only related to the aerosol conditioning process, but also includes mobility transfer functions of both DMAs. Measured distribution function (MDF) is a skewed and smoothed integral transform of the particle's actual growth factor probability density function (GF-PDF). Therefore, an inversion algorithm has to be applied to the MDF of T-DMA measurements to retrieve the GF-PDF (Gysel et al., 2009). The underlying principle of T-DMA inversion approaches is to find an inverted GF-PDF such that a minimum χ^2-residual is obtained between the measured MDF and the retrieved MDF (R-MDF), which can be calculated from the inverted GF-PDF using the T-DMA's forward function. In an algorithm, inverted GF-PDF is described as a piecewise linear function at predefined growth factor values. TDMAinv minimizes the χ^2-residual between the R-MDF and the measured MDF by fitting the values of the piecewise linear GF-PDF at the predefined growth factor values. The kernel function is a key element for the inversion of T-DMA data. Two-dimensional T-DMA kernel function can be expressed as:

$$K_{TDMA}^{g,i}(g_{set}, \hat{g}, D_0) = \int_0^{\infty} T_{DMA1}^{g,i}\left(\frac{\hat{g}}{g''}, \frac{g''}{\hat{g}} D_0\right) \frac{1}{g''} T_{DMA2}^{g,i}\left(\frac{g_{set}}{g''}, g'' D_0\right) dg'', \quad (2.16)$$

$$T_{DMA}^{g,i}(g_{set}, D_0) = R\left(f_{z,1}\left(gD_{particle}\right), f_{z,i}\left(D_{particle}\right)\right), \quad (2.17)$$

where $R(z, z_{particle})$ is the electrical mobility transfer function. The idealized DMA electrical mobility transfer function for equal sheath and excess flow

rates is of symmetrical triangular shape, has a transfer probability of 1 at $z = z_{particle}$, and a constant full width at half maximum of $\frac{\Delta z}{z_{particle}} = \frac{Q_{sa}+Q_{ae}}{Q_{sh}+Q_{ex}}$, Q_{ae}, Q_{sa}, Q_{sh} and Q_{ex} are the poly-disperse sample, mono-disperse sample, the sheath and the excess flow rates, respectively. The kernel function is the normalized concentration of particles carrying i charges with dry diameter $D_i = u_i(D_0)$, which is observed at the T-DMA outlet, if DMA1 is set to diameter D_0, if DMA2 is set to diameter $D_{set} = g_{set}D_0$, if all particles of diameter D_i exhibit a true *GF* of $\hat{g}$. T-DMA kernel function is the kernel of the integral transform, which allows calculation of the MDF measured by a T-DMA for any given GF-PDF. The MDF is the particle concentration at the T-DMA sample outlet as a function of set *GF*, when DMA1 selects particles of single charge equivalent diameter D_0 and DMA2 selects at diameter $D_{set} = g_{set}D_0$ as:

$$m_{TDMA}^{g,total}(g_{set}, D_0) = \sum_{i=1,2\ldots} p_i\left(u_i(D_0)\right) \frac{dN_{poly}}{d\ln D}\left(u_i(D_0)\right) \int_0^{\infty} c\left(\hat{g}, u_i(D_0)\right) \cdot K_{TDMA}^{g,i}(g_{set}, \hat{g}, D_0) d\hat{g} \quad (2.18)$$

Where g_{set} is *GF* set at DMA2 ($g_{set} = D_{set}/D_0$), D_0 – single charge equivalent diameter, p_i – number fraction of particles in the poly-disperse aerosol with diameter D carrying i charges, $u_i(D)$ is function to calculate the mobility diameter of a particle carrying i charges and having equal electrical mobility as a singly charged particle with diameter D, $\frac{dN_{poly}}{d\ln D}$ is number size distribution of dried poly-disperse aerosol at T-DMA inlet, $c\left(\hat{g}, u_i(D_0)\right)$ is growth factor probability density function for particle with dry diameter D_0 to exhibit a $GF = g$. The total probability of exhibiting a certain *GF* is unity and $K_{TDMA}^{g,i}(g_{set}, \hat{g}, D_0)$ is T-DMA kernel as a function of g_{set} and D_0 for particles carrying i charges and giving a true $GF = \hat{g}$ factor to adjust the measurement uncertainty level due to variations of the particle concentration at the T-DMA inlet. An eq. (2.18) along with (2.16) and (2.17) is the T-DMA forward function, which fully describes the physical behavior of the T-DMA. Eq. (2.18)

describes how to calculate the MDF from a given GF-PDF. T-DMA response is an inverse solution of an eq. (2.18). If the number size distribution of the poly-disperse aerosol is of such shape that interference from multiply charged particles are small in the T-DMA, eq. (2.18) can be reduced to:

$$m_{TDMA}^{g,total}(g_{set}, D_0) = p_1(D_0)\frac{dN_{poly}}{d\ln D}(D_0)\int_0^{\infty} c(\hat{g}, D_0)K_{TDMA}^{g,1}(g_{set}, \hat{g}, D_0)d\hat{g}, \quad (2.19)$$

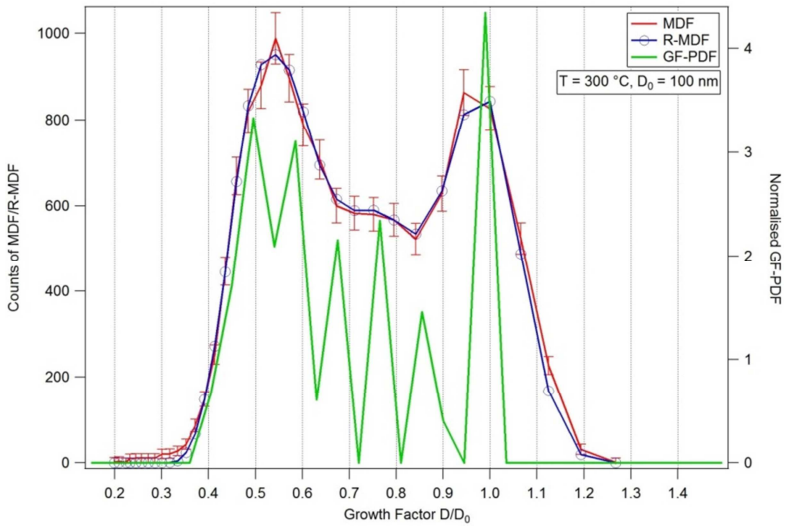

Fig. 2-8. Example of V-TDMA data inversion.

Piecewise linear approach is used to retrieve GF-PDF (Fig. 2-8). The integrated properties (refractory/volatile/hygroscopic fractions of particles) of a distinct shrink/growth mode are determined from the inverted GF-PDF.

As for all physical measurements, the counted particle number concentration in a data point of the MDF is affected by uncertainties. Poisson statistical limitation associated with low counts can be expressed as $\Delta n_{poiss} = \sqrt{n}$. Wiedensohler et al., (2012) carried out a SMPS workshop showing that integrated total number concentration of T-DMA system, Δn_{inlet}, exhibit 5 – 10% uncertainty. Uncertainty in the exact shape of the T-DMA kernel, Δn_{kernel}, is the product of the maximum number of counts in any data point of the MDF. Humidity fluctuations in H-TDMA conditioning unit bring uncertainties to a

measured *GF* and GF-PDF. For the atmospheric measurements, RH tolerance is reported to be around 2%. In our work we assume that the singly charged particles dominate such that the TDMA forward function simplifies to eq. (2.19).

2.7. Aerosol particle transport by air masses

The air mass trajectory analysis was used to identify the aerosol sources and their transport pathways. Backward trajectories were produced using the HYbrid Single-Particle Lagrangian Integrated Trajectory (HYSPLIT4) model (Draxler and Rolph, 2003) with the Final Analyses (FNL, 2008–2009) and the Global Data Assimilation System (GDAS) meteorological databases at the NOAA Air Resources Laboratory's web server (Rolph, 2003). In a biomass burning study 72-hour backward air mass trajectories, 500 and 2000 m above the ground level, were calculated. In ship related emission study the hourly trajectories at two different altitudes of 100 and 300 m above the ground level, representing the Baltic Sea atmospheric boundary layer (SMHI, 2013), were calculated. Possible higher altitude (3000 m) trajectories' influence has also been cross-checked using the atmospheric sounding profiles (Oolman, 2014). Analysis of rawinsonde data from three stations in the Baltic region, (Leba, Poland, 54.75°N, 17.53°E; Visby, Sweden, 57.65°N, 18.35°E and Greifswald, Germany, 54.10°N, 13.40°E) showed that the boundary layer, or a mixing height, was clearly less than 2000 m (and generally half that depth) in all but two instances during the periods when trajectories were calculated. In those two cases the winds at 700 mb were nearly identical to the winds at lower levels and the 700 mb trajectories did not deviate significantly from the lower level trajectories used for a comparison. In order to minimize the continental contamination, only the trajectories that did not pass over the major land masses between the two upwind sites and Preila were selected for further analysis. The upwind site and Preila were connected by advecting air masses into which mainly ship emissions were added to the background aerosol.

2.8. MODIS fire maps

Hotspot/fire locations were detected using MODIS (Moderate Resolution Imaging Spectroradiometer) data from the middle infrared and thermal infrared bands (Giglio, 2007). Each MODIS sensor achieves global coverage once per day and once per night every 24 h. Fig. 3-5, A and C show the locations of the active fires identified from MODIS. The MODIS monthly fire maps, available since 2001, showed that biomass burning events occur annually.

2.9. Measurement sites

Data from 4 measurement sites are presented in this work. To study the regional biomass burning influence onto aerosol particle properties, the particle light absorption and number size distribution measurements were performed at the Preila Environmental pollution research station (55°55′N, 21°00′E, 5 m above sea level) in the coastal/marine environment (Ulevicius et al., 2012). This station is located on the Curonian Spit, which separates the Curonian Lagoon and the Baltic Sea, and thus can be characterized as a regionally representative background area (Fig. 1-6). The climate in the Curonian Spit is intermediate between marine and continental and is characterized by frequent and intensive variableness of weather, by mild winter and moderately warm summer. The mean annual air temperature is 7°C, with the absolute minimum of -26°C in January and the absolute maximum of 31°C in June. The mean annual precipitation amount is 550 – 900 mm (April – October, 375 – 525 mm and November – March, 175 – 350 mm). Maximum precipitation falls in the period from October till February. One of the nearest industrial cities Klaipeda is at a distance of about 40 km to the north and the other major city Kaliningrad is 90 km to the south from Preila.

To study shipping influence onto background environmental particle properties, data from two additional stations were analyzed: Vavihill (Sweden)

and Utö (Finland) (Fig. 1-6). Vavihill, a background monitoring station, is located in Southern Sweden (56°01′N, 13°09′E, 172 m. a.s.l.). Surroundings of the site are dominated by deciduous forest. The distances to the densely populated areas of Helsingborg, Copenhagen and Malmö are 25 km west, 45 km south-west and 50 km south, respectively. Utö station (59°47′N, 21°23′E, 8 m a.s.l.) is located on a small island in the Baltic Sea some 60 km from the Finnish southwest coast and more than 10 km from the nearest islands around. Turku, the closest city, is about 90 km to the north-east of the almost treeless island. Local pollutant sources like passing large ships or motor vehicles could be easily detected since these sources produce high but short duration concentrations in certain size classes of the particle number size distribution. Detailed description of the station including some aerosol properties is available in Hyvärinen et al., (2008).

Aerosol particle physical properties were explicitly measured at a suburban site of Hebei province, Langfang county (39.753828° N, 116.960211° E), China, roughly 60 km south-eastward from Beijing (Fig. 2-9).

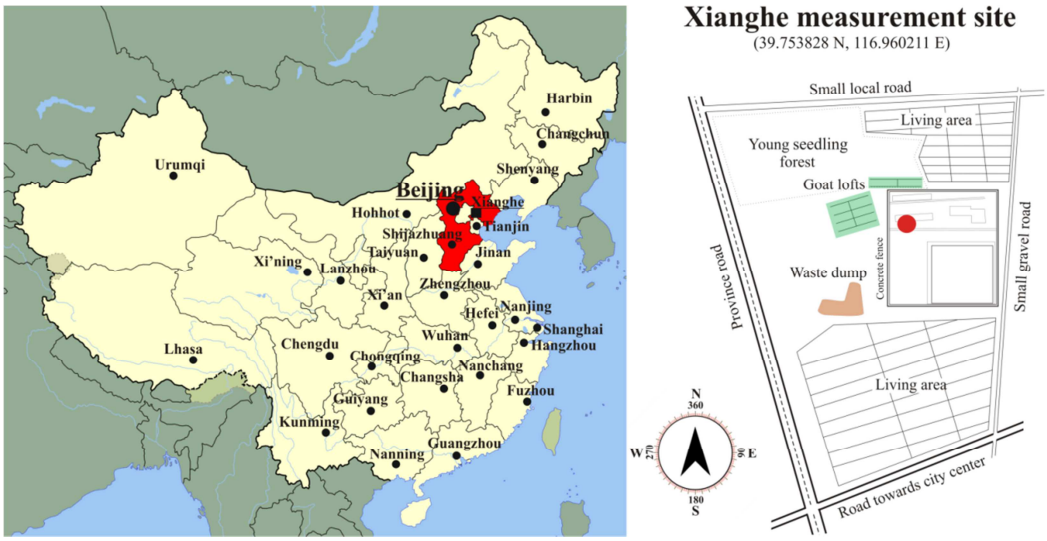

Fig. 2-9. Hebei province (red area, left figure). On the right – Xianghe measurement site. Red spot indicates the position of measurement container in the site.

Hebei province encloses two densely populous cities – Tianjin, a major seaport and the capital of China – Beijing. Large industrial production and its special location scores to seven of ten most polluted cities in China are located in this province (Wang et al., 2013). The measurements were performed as a part of the "Campaign of Air Quality Research in Beijing and Surrounding Region 2013" (CARE-Beijing 2013) measurement campaign during 8th of July to 9th of August, 2013. Measurement containers were located about 5 km to west of Xianghe town center (Fig. 2-9). The surroundings of the Xianghe site are mainly residential rural areas. During the measurement campaign median nighttime relative humidity (RH), temperature (T), wind direction (wd) ant speed (ws) were RH = 96.6%, T= 23 °C (min: 19 °C, max 27 °C) , wd = west-northwest and south-east, ws = 0.4 m/s, respectively. Mean daytime RH = 75%, T= 27 °C (min 20 °C, max: 36 °C), wd = south-west, north-west, ws = 1 m/s.

2.10. General remarks on instrumentation

2.10.1. Aerosol particle number size distribution

Four different mobility particle size spectrometers were used to measure aerosol particle number size distribution. The instruments were chosen because of their unique ability to measure particle number size spectrum with a high particle size resolution *in situ*. A Twin Differential Mobility Particle Sizer (T-DMPS), Differential Mobility Particle Sizer (DMPS), A TROPOS-type Scanning Mobility Particle Sizer (SMPS) and Neutral cluster and Air Ion Spectrometer (NAIS) were used in Vavihill, Utö, Preila and Xhianghe stations, respectively. Main instruments specifications are listed in Table 2-3. The aerosol particle number concentration at the Preila site was measured using condensation particle counter (CPC) UF-02proto developed by EUREKA COPAP project consortium (Mordas et al., 2005) and manufactured by State research institute Center for Physical Sciences and Technology, Lithuania (previous Institute of Physics, Lithuania). All instruments (except NAIS)

operate by aspirating dried air and using an ionizing radiation source to achieve an equilibrium bipolar charge-distribution in the sample (Wiedensohler., 1988), selecting particles based on their electrical mobility in cylindrical differential mobility analyzers and counting them with CPC to measure the resulting concentrations in each of the selected size ranges. The main differences between the instruments are their size ranges and the mode of operating voltage in the DMAs. While the DMPS steps through voltages during measurement sequence of size intervals, the SMPS scans through the voltage range and corresponding size intervals continuously. The T-DMPS, on the other hand, combines two different types of Differential Mobility Analyzers (medium long and ultrafine DMAs) to select a wider size range of aerosol particles (Birmili et al., 1999). The size range and time resolution of T-DMPS, DMPS or SMPS system depends on both system architecture and user choice or field of use and is in a range from 5 up to 15 min. Aerosol PNSD in Utö station was measured using a University of Helsinki type DMPS. The temperature difference between the saturator and the condenser of the CPC has been increased to lower the 50% cut off diameter limit. The T-DMPS system used at Vavihill consists of two Hauke-type (medium and short) DMAs to cover a size range from 3 to 850 nm (Kristensson et al., 2008).

In Xianghe, additionally to SMPS system, NAIS was used to investigate the finest aerosol particle number size distribution in a 2 to 15 nm size range. NAIS data was averaged to 5 min.

Table 2-3. Aerosol PNSD measurement instruments and their specifications at sampling sites.

Site	Inst.	CPC type	Size range (nm)	Size steps	Time resolution (min)	Flow rates (aerosol/sheath lpm)
Preila	SMPS	UF-02proto	8 – 800	71	5	1/10
Utö	DMPS	TSI 3010	7 – 500	30	5	1/10
Vavihill	TDMPS	TSI 3760 and 3025	3 – 850	37	10	1.5/19 and 0.91/5.9
Xianghe	SMPS	TSI 3025	8 - 800	51	5	1/5
Xianghe	NAIS	---	2 - 15	21	0.016(6)	54/60

2.10.2. Mixing state of aerosol particles

Two state of art conditioning TROPOS T-DMAs were used to determine aerosol particle mixing state in one of the most polluted regions in China – Hebei province, Xiange city. Aerosol particle hygroscopic growth was measured using TROPOS Hygroscopisity Tandem Differential Mobility Analyzer (H-TDMA) (Massling et al. 2003). Refractory aerosol fraction in Xianghe station was measured using TROPOS Volatility Tandem Differential Mobility Analyzer (V-TDMA) (Philippin et al., 2004).

2.10.3.Aerosol particle light absorption coefficient

At Utö and Preila sampling sites two Magee Scientific Company seven wavelength (370, 450, 520, 590, 660, 880 and 950 nm) Aethalometer™, Model AE31, were used to measure aerosol particle light-absorption properties. To compensate for filter loading effects an empirical algorithm was used (Virkkula et al., 2007; Weingartner et al., 2003).

Custom made, one wavelength (λ = 520 nm) Particle Soot Absorption Photometer (PSAP), constructed at the Department of Applied Environmental Science, Stockholm University, was used to measure aerosol particle light absorption coefficient at Vavihill station (Krecl et al., 2007). The absorption is calculated with the Bond (Bond et al., 1999) loading correction without any additional correction for scattering.

2.10.4.Data evaluation

Aerosol particle nucleation rate and condensational sink formalism was taken from Dal Maso et al., (2005). For detailed information, please refer to mentioned references. Shortly: nucleation rate, J_{nuc}, can be expressed as:

$$J_{nuc} = \frac{dN_{nuc}}{dt} + F_{coag} + F_{growth}, \quad (2.20)$$

where N_{nuc} is the number concentration of nucleation mode particles, F_{coag} – the loss of formed particles due to coagulation, F_{growth} – the flux of particles out of the specified size range; the particle condensational sink, *CS*, can be calculated using:

$$CS = 2\pi D \sum_i \beta_M D_{p,i} N_i. \quad (2.21)$$

Measured V-TDMA and H-TDMA growth/shrink factor distributions were inverted using TDMAinv method developed by Gysel et al. (2009). Hygroscopic growth factor (*GF*) refers to a ratio between particle mobility diameter, *D*(RH), at a given RH and the dry diameter, D_d:

$$GF(RH) = \frac{D(RH)}{D_{dry}}. \quad (2.22)$$

Shrink factor (*SF*, or *GF* < 1) is defined by a ratio between mobility diameter, $D(T_{300C})$, at a temperature of 300°C and ambient temperature diameter, D_{amb}:

$$SF(T) = \frac{D(300\ ^0C)}{D_{ambient}}. \quad (2.23)$$

Dry (RH = 25%) and ammonium sulphate scans were used to calibrate actual RH values and any size shift in between DMA1 and DMA2 in H-TDMA. All cases of size shift between DMA1 and DMA2 in V-TDMA system was referred as bad scan and eliminated in further data analysis. H-TDMA Growth Factor Probability Density Function (GF- PDF) was integrated in a range from 0.8 to 1.2 and 1.2 to 2.5 to identify hydrophobic and hydrophilic aerosol particle number fractions respectively. V-TDMA GF-PDF (GF-PDF < 1, or particle shrink) was integrated in a range from 0 to 0.8 and 0.8 to 1.4 to find refractory and volatile particle number fractions respectively.

2.11. Chapter conclusions

It was shown that aerosol spectrometry is applicable method to define the most important properties of atmospheric aerosol particles. A more general view about how aerosol particles are influencing the Earth's climate is only possible when analyzing the data from long term observations. While the short term measurements are enough to discuss the fundamental particles properties. Therefore, aerosol spectrometry methodology and instrumentation was developed over the decades to fulfill the need for a long term measurements. The chosen instrumentation and methods are both, the least expensive and the most effective to reach the goals set in this work. No other tools exist to provide on-line, cost-effective, relatively simple and long term measurements of aerosol physical properties.

3. RESULTS

3.1. Biomass burning impact onto atmospheric aerosol properties

In this part, the semi-continuous atmospheric aerosol particle number size distribution and particle optical properties measurements from Preila site during the 2008 to 2010 are presented. This study shows temporal aerosol particle number and BC mass concentration variation. Several pollution events are segregated to demonstrate the relevance of aerosol spectrometry as a tool for atmospheric research. The particle number size distribution, BC mass concentration, backward trajectories and satellite fire maps were used to identify and parameterize the biomass burning events which change aerosol particle physical properties in the background environment.

3.1.1. Particle number concentration

The temporal variation of hourly means of the integrated aerosol particle number concentrations in a range from 10 to 20, 20 to 60, 80 – 200 and 400 to 800 nm from 2009 to 2010 is shown in Fig. 3-1. As it can be seen, different size range particle number concentrations behave differently revealing several diverse processes. Nucleation mode particle, diameter of 10 to 20 nm, number concentration maximum is registered in the spring and autumn months (Fig. 3-1, D). Mean and maximum (in parenthesis) aerosol particle number concentration in nucleation mode during March, April, September and October were 400 ± 40 cm^{-3} (max: 5900 ± 590 cm^{-3}), 340 ± 30 cm^{-3} (max: 6400 ± 640 cm^{-3}), 950 ± 100 cm^{-3} (max: 11100 ± 1110 cm^{-3}) and 420 ± 40 cm^{-3} (max: 5000 ± 500 cm^{-3}), respectively. Here the mathematical sign "±" defines 10% measurement uncertainty (Wiedensohler et al., 2012). Diurnal nucleation mode particle number concentration variation, Fig. 3-1, part C, shows that a new particle formation at the Preila site occurs around noon. Aitken mode particle number concentration variation directly follows the nucleation mode particle

pattern. This is because of the growth of the newly formed particles. The Aitken mode particle number concentration maximum is shifted and reaches its peak at around 6 - 7 PM. Relatively high, compared to a nucleation mode, Aitken mode particle number concentration can be explained by a constant particle augmentation by a newly formed particles and reduced their removal by coagulation. The highest aerosol particle number concentration in a bigger particle mode (400 to 800 nm) was observed during the winter months. Particle number concentrations in December, January and February were 100 ± 10 cm^{-3} (max: 800 ± 80 cm^{-3}), 110 ± 10 cm^{-3} (max: 560 ± 60 cm^{-3}) and 130 ± 10 cm^{-3} (max: 720 ± 70 cm^{-3}), respectively. Elevated bigger size particle number concentration might be associated with a sea spray aerosols as it positively correlates with the higher wave frequency. The wave height might serve as an indirect evidence for a higher sea sprayed aerosol particles fraction. The particle number concentration variations essentially comprise an accumulation mode particle number concentration peaks in spring and winter, which is conspicuous in April (Fig. 3-1, A, marked with a grey shade, and a well pronounced peak in D). Diurnal accumulation mode particle number concentration pattern is different compared to other modes (Fig. 3-1, C). The highest particle number concentrations were observed during the nighttime period. This can be explained in terms of planetary boundary layer. Ma et al., (2011) has explained the change in aerosol optical properties in terms of diurnal cycle of the boundary layer height. Increase in boundary layer height enhances the atmospheric volume, where aerosol particles might be diluted. Decrease in boundary layer height locks particles in a lower volume increasing particle concentration. The increase in accumulation mode particle number concentration determines lower nucleation and Aitken mode particle number concentrations because of a higher coagulation sink.

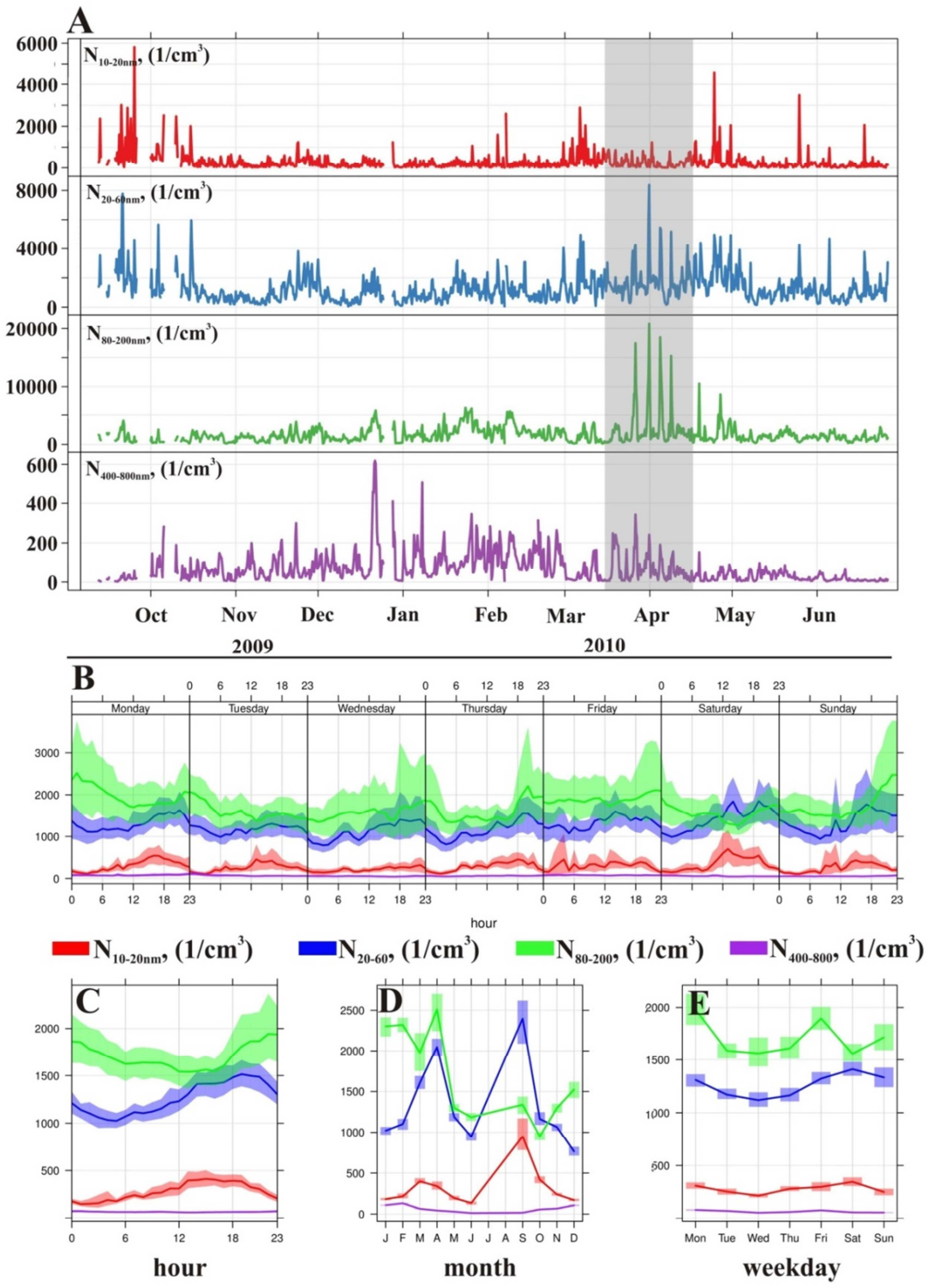

Fig. 3-1. The time variation of aerosol particle number concentration in four different size ranges.

When accumulation mode particles are assigned to wind direction, it can be seen that highest particle number concentration values (up to 3500 ± 350 cm^{-3}) are present when south – east winds prevail (Fig. 3-2).

In addition, it can be seen that higher particle number concentrations appear during the night hours. As discussed above, this can be explained by planetary boundary layer evolution during daytime. Weekday particle number concentration increase shows higher anthropogenic activities towards the weekend. This is reasonable, because Curonian Spit is a tourist beloved resort.

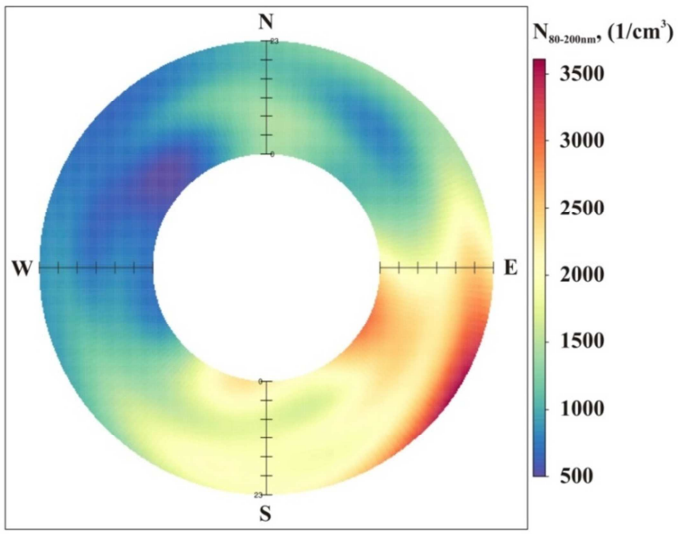

Fig. 3-2. Polar annulus plot of accumulation mode particle number concentration assigned to wind direction and day hour.

To investigate the possible reasons for an increased particle number concentration in a size range between 80 and 200 nm, auxiliary information about particle physical properties is needed. Next section presents the aerosol particle light absorption measurements which were accomplished together with particle number size distribution measurements.

3.1.2. Aerosol particle light absorption

The time variations of hourly means of black carbon mass concentration (mass concentration corresponding to wavelength of 880 nm) and some meteorological information (temperature, wind speed and direction) from 2008 to 2010 are shown in Fig. 3-3, part A. It can be seen that temperature and wind direction exhibits bimodality. Two different temperatures for warm and cold

seasons show up in density distribution graph as a separate peak (Fig. 3-3, part B). Temperature maximum is reached during July and August months with a mean temperature of 18°C (max: 28°C). After September the temperature starts to drop and reaches the minimum value of -5°C (min: -21°C) in January. The prevailing winds are south – east, north – west and north - east.

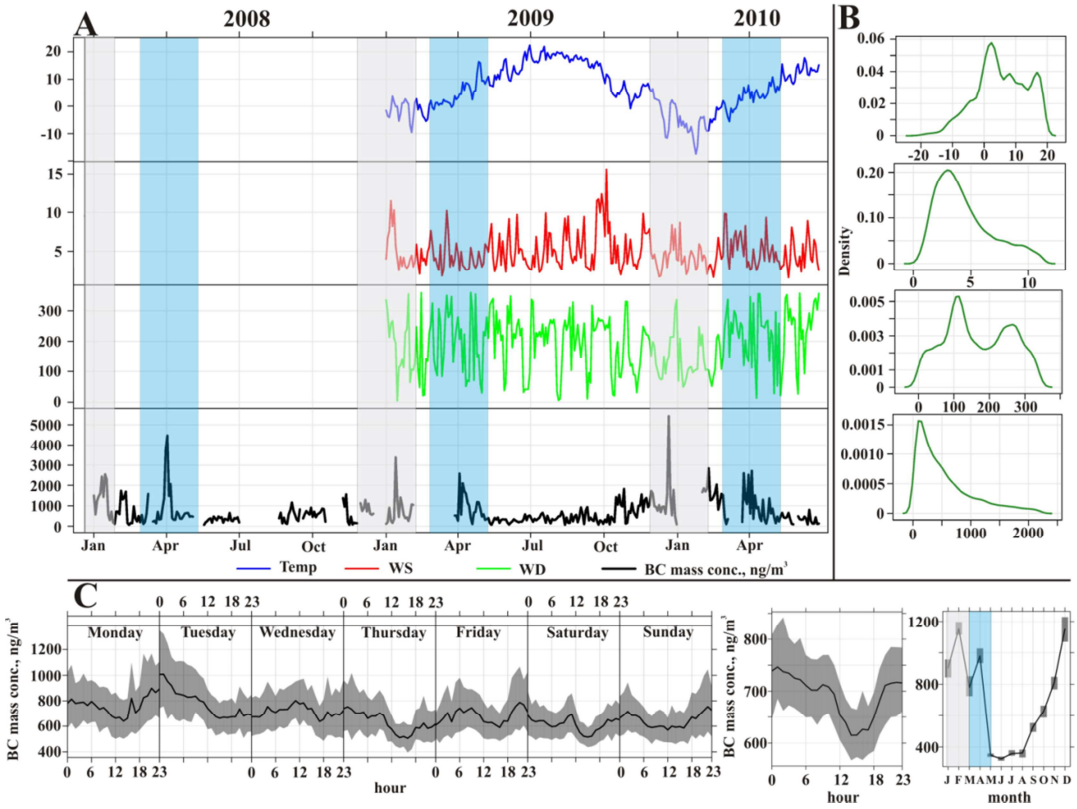

Fig. 3-3. Black carbon mass concentration variation in the Preila site. Temperature in Celsius (blue line), wind direction (WS, red line) and wind direction (WD, green line) are also shown here. Blue and grey shades mark the high BC mass concentration events.

There are three distinctive peaks in black carbon mass concentration in the late autumn, winter and spring months (Fig. 3-3, part C). The minimum BC mass concentration is reached during the summer months – June, July and August. The hourly mean BC mass concentration during those months were 320 ± 20 ng/m^3 (max: 6400 ± 320 ng/m^3), 360 ± 20 ng/m^3 (max: 2090 ± 110 ng/m^3) and 360 ± 20 ng/m^3 (max: 2820 ± 140 ng/m^3), respectively. After September, BC mass concentration gradually increases and reaches the maximum in November, December and January months with a mean mass

concentration of 810 ± 40 ng/m^3 (max: 5230 ± 260 ng/m^3), 1150 ± 60 ng/m^3 (max: 8250 ± 410 ng/m^3) and 1150 ± 60 ng/m^3 (max: 7780 ± 390 ng/m^3), respectively. This increase in BC mass concentration during the late autumn to early spring months correlates positively with a temperature decrease. In January temperature drops from 16 to -5^{o}C. Moreover, the wind speed from 6 m/s in September decreases to 4 m/s in February. This suggests a stronger anthropogenic pollution influence onto increased aerosol particle number and BC mass concentrations due to domestic heating. Decreased temperature results in a weak atmospheric mixing. Aerosol particles accumulate in a lower boundary layer leading to the increased number and mass concentrations.

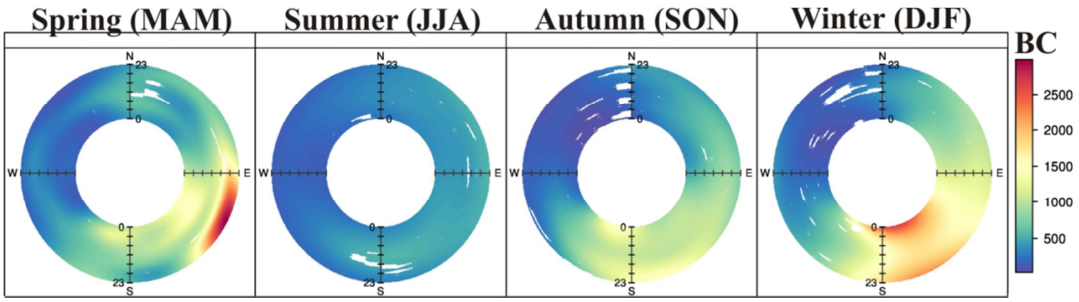

Fig. 3-4. BC mass concentration dependence on wind direction and daytime.

While aerosol particle number and BC mass concentration increase in cold season is trivial, change in particle physical properties during the spring months is not clear. Pronounced increase in BC mass concentration during the spring months (March, April), when the mean temperature is 6^{o}C, cannot be explained only by a domestic heating, boundary layer evolution or a low atmospheric mixing. Even though hourly mean concentrations are not high (780 ± 40 ng/m^3 and 980 ± 50 ng/m^3 for March and April, respectively), maximum concentrations are much higher compared to other months (10300 ± 510 and 11520 ± 580 ng/m^3 for March and April, respectively). The BC mass concentration polar annulus plot (Fig. 3-4) indicates that high BC mass concentration in spring is related with south – eastern winds. To elucidate the aerosol particle origin during high BC mass concentration episode, analysis of high pollution episode will be presented in the following section.

3.1.3. High particle number and BC mass concentration case study

This section will focus on the elevated aerosol particle number and BC mass concentration episode observed on 4-5th of April, 2010. Air mass backward trajectories, calculated using the NOAA-HYSPLIT model, have shown that air masses coming to Preila have passed over Kaliningrad (Fig. 3-5, C). To study the transport and geographical extent of the aerosol pollution the satellite measurements were also used. Data analysis of the BC and aerosol size distribution combined with TERRA/Moderate Resolution Imaging Spectroradiometer MODIS fire detections provided some insights into the regional aerosol transport. As shown in Fig. 3-5, part A, MODIS clearly illustrates the fire locations. During the event days, substantial concentrations of BC were observed when air masses arrived from the biomass burning regions. This confirmed that pollutants were transported from the Kaliningrad region to the Lithuanian lower troposphere. The peak value of particle number and BC mass concentrations on the event days were from 10 to more than 30 times higher than a background concentration, respectively.

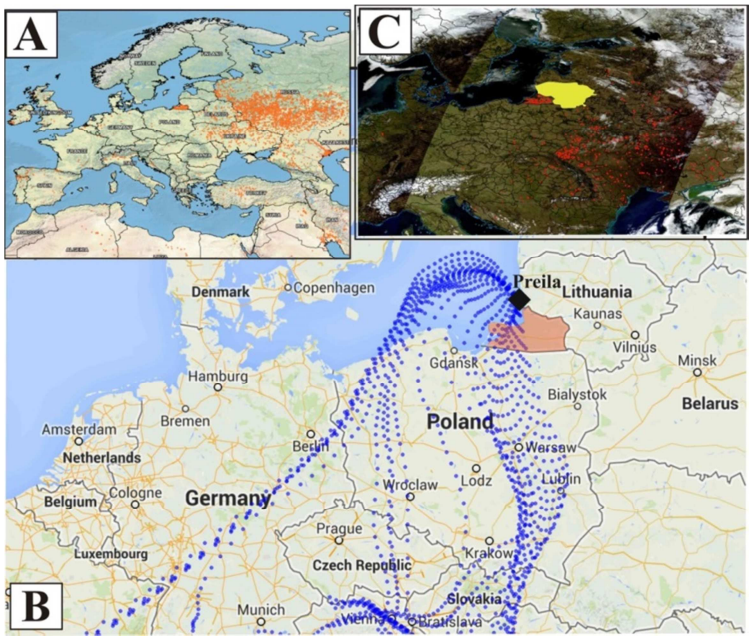

Fig. 3-5. The locations of the active fires identified from MODIS (A, C) and backward air mas trajectories during 2010 year April high pollution episode (B). Red shade in part B marks Kaliningrad as a potential source of high aerosol load.

The hourly means of light absorption coefficient Ångström exponent (α), aerosol particle mode geometric mean diameter (d2, d3 in nm), mode standard deviation (σ2, σ3), total mode concentration (N2, N3 in cm^{-3}), wind speed (WS in m/s), wind direction (WD in degrees), temperature (T in ^{o}C) and particle BC mass concentration (BC in ng/m^3) during the event days are shown in Fig. 3-6.

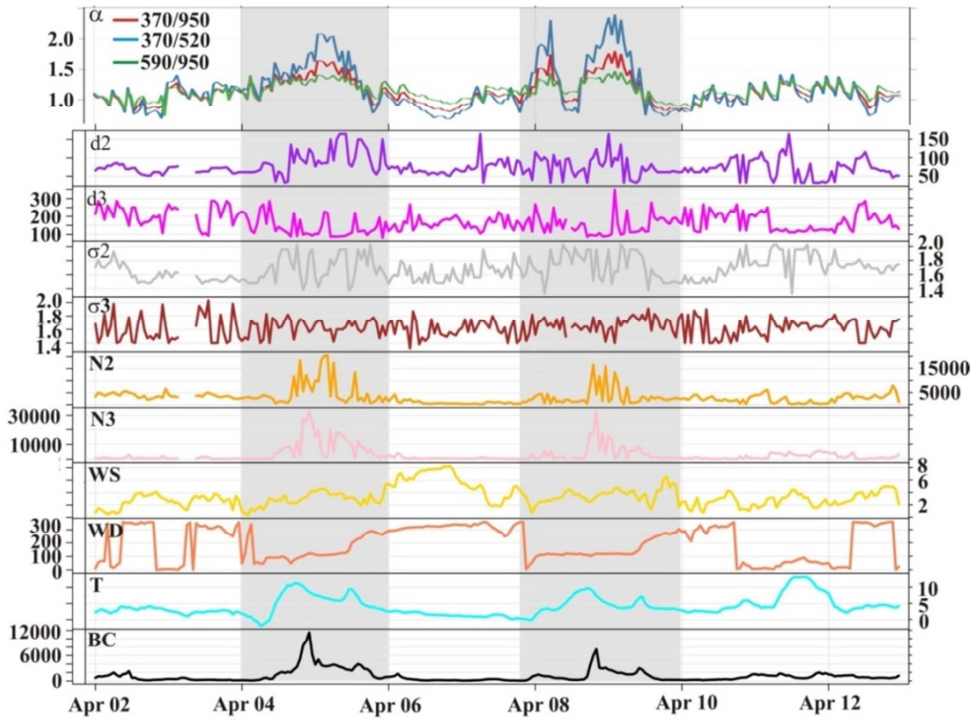

Fig. 3-6. High aerosol particle pollution episode on 4-5th of April, 2010 (marked with a grey shade).

Both, particle number and BC mass concentrations observed during this event were clear outliers in their respective series, both for hourly concentrations and 24-hour means (see the grey shaded area). During the event, wind speed (daily mean) was 3 m/s, wind direction - south-east, temperature – $5^{o}C$. BC mass and aerosol number concentrations rose to unusually high levels. The maximum 1-hour average aerosol particle number (integrated from SMPS) and BC concentrations reached 40800 ± 4080 cm^{-3}, BC — 11500 ± 580 ng/m^3, respectively. Background concentration values

were about 3790 ± 380 cm^{-3} and 340 ± 20 ng m^{-3}, respectively. It should be noted, that during such kind of events Lithuanian urban sites PM_{10} mass concentration was significantly higher. This increase coincided with the extensive biomass burning in southern Russia and Ukraine. The European PM_{10} mass concentration limit value was exceeded by a factor of 2.

For a detailed analysis of the event, diurnal pattern of the BC and the time dependent size distribution in Preila during 4-5th of April, 2010, is depicted in Fig. 3-7. It can be seen that high BC mass concentration is associated with high Aitken (Fig. 3-7) and accumulation (d3, N3) mode particle number concentrations.

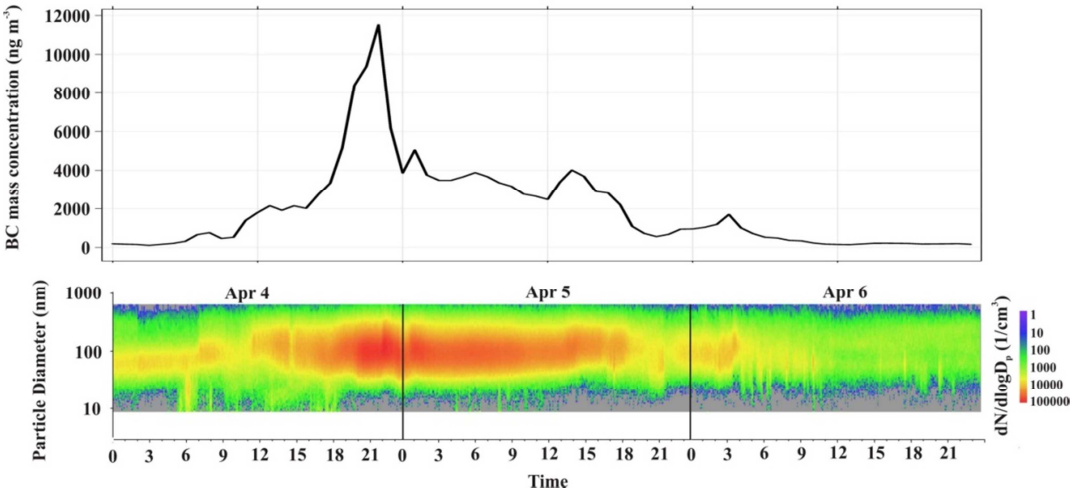

Fig. 3-7. Aerosol particle number size distribution and BC mass concentration during a high pollution episode on 4-5th of April, 2010.

Both, aerosol number size distribution and BC mass concentration showed a concentration maximum at night (April 4, 10 PM). As a result, regarding the aerosol physical properties, the SMPS measurements revealed that the key characteristic of such episodes is high accumulation mode particle number concentration. Particle number size distributions were fitted with several lognormal distributions. The result showed a very strong accumulation mode with particle number concentration of 20500 ± 2050 cm^{-3}, 150 nm geometric mean diameter and the standard deviation of 2.0. During the biomass burning event the accumulation mode geometric mean diameter was

approximately 160 nm (Fig. 3-7). The analysis of particle number size distribution showed that the Aitken mode geometric mean diameter shifted to a larger size during the night from around 60 to 165 nm. This behavior can be interpreted as a coagulation driven particle growth. Interestingly, the accumulation mode particle mean diameter did not change (Fig. 3-7, d3).

Information about the wavelength dependence of BC absorption can show possible aerosol particle sources. The wavelength dependence of the light absorption can be better interpreted by separating shorter (370 – 520 nm) and longer (660 – 950 nm) wavelength exponential fits. The Ångström exponents were calculated by fitting b_{abs} for the whole available wavelength intervals. The contrast between the events with a wood-smoke and those with less wood-smoke is most evident in the short wavelength interval. For reference, the value of α = 1.0 is known to be assigned to a purely diesel black carbon aerosol. Black carbon aerosol particles measured at the Preila site represents a long-range atmospheric transport rather than local sources. Backward trajectory analysis indicates that air masses passing through a continent in the east of the country can lead to a significant BC loading. The air masses originating from the west of the site are much cleaner. Fig. 3-6 shows the course of the BC mass concentration and Ångström exponent variation during the event days. It can be seen that Ångström exponents shows a very clear pattern during the event period. The α values were significantly higher when BC mass concentration increased. This change was larger and stronger for shorter wavelengths ($\alpha_{370–520}$ = 2.1) compared to the longer ones ($\alpha_{590–950}$ = 1.4) (Fig. 3-7). On the non-event days light absorption coefficients $\alpha_{370–950}$, $\alpha_{370–520}$ and $\alpha_{660–950}$ were within a narrow range of 1.2, with the weak diurnal cycles. During the 5th of April, the highest mean values of $\alpha_{370–520}$ and $\alpha_{590–950}$ were observed between 1 and 6 AM (2.1 and 1.4, respectively). During the 9th of April, the peak values ($\alpha_{370–520}$ = 2.4, $\alpha_{590–950}$ = 1.4) were observed in midnight and early morning. Sandradewi et al., (2008) showed that high Ångström exponent values are a representative indicator for biomass burning aerosol. Kirchstetter et al. (2004) reported α value of 2.2 for outdoor firewood burning, 1.8 for a savanna fire, and 0.8 – 1.1

for traffic dominated sites. Previous investigations showed that the type of wood being burned also influences α value. Fresh wood smoke from the seven types of forest wood was investigated using an aethalometer. Alpha values were between 0.9 and 2.2 (Day et al. 2006). Hoffer et al. (2006) showed $\alpha = 6$ for water-soluble humic-like substances (HULISs) isolated from the fine fraction of the biomass burning aerosol spectrophotometer measurement with $\lambda = 300 – 700$ nm.

3.1.4. Conclusions

Combination of ground-based and satellite observations were used to investigate the influence of biomass burning on the background aerosol particle physical properties. High aerosol particle number (integrated from SMPS) and BC mass concentrations were measured during the winter and early spring seasons. The lowest particle number concentrations were observed during May – December (4540 ± 450 cm^{-3}) and the highest ones during January – April (6380 ± 640 cm^{-3}) months. The lowest BC mass concentrations were observed during May – August (350 ± 20 ng/m^3) and the highest ones during the September – April (870 ± 40 ng/m^3) months. Trajectory analysis showed that long-range transport significantly influences aerosol particle physical properties in the East Baltic region. The periods of a high aerosol load and BC mass concentration are determined by the air mass transport from biomass burning regions. Biomass burning events in spring were associated with a high BC mass (up to 11500 ± 580 ng/m^3) and particle number (40800 ± 4080 cm^{-3}) concentrations. Accumulation mode geometric mean diameter and mode standard deviation were found to be 2.0 and 165 ± 2 nm, respectively. The presence of biomass burning products was confirmed by light absorption wavelength dependence. During the pollution episode the absorption Ångström exponent values were found to be $\alpha_{370–520} = 2.4$. This confirms the contribution

from a biomass burning. Moreover, the α values were higher for the shorter wavelengths ($\alpha_{370–520}$ = 2.1) compared to the longer ones ($\alpha_{590–950}$ = 1.4).

Observations from other countries demonstrate that particulate matter levels have been rising in northern Europe and Scandinavia during the spring periods. Biomass burning episodes are repetitive. This study gives a valuable insight how coastal physical aerosol particle properties might be influenced in the future.

3.2. Baltic Sea shipping influence onto background aerosol properties

10 months (September 2009 to June 2010) of atmospheric aerosol particle number size distribution and optical properties at three atmospheric observation stations along the Baltic Sea coast: Vavihill (upwind, Sweden), Utö (upwind, Finland), and Preila (downwind, Lithuania) have been examined. Differences in aerosol particle number size distributions and light absorption between the upwind and downwind stations during the situations of connected atmospheric flow were used to assess the contribution of ship emissions to aerosol physical properties in the Lithuanian background coastal environment.

After analyzing air mass trajectories and measurement data, 14 and 17 cases were chosen when air was transported directly from Utö to Preila or from Vavihill to Preila, respectively, as shown in Fig. 3-8. Only those air mass trajectories, which had passed as little land areas as possible between the sites were selected. Vavihill to Preila air mass transfer cases were distributed mainly in spring (1 case in March, 2 cases in April, 6 cases in May) and autumn (6 cases in September, 2 cases in October). Utö to Preila cases covered all four seasons: summer (2 cases in June), spring (2 cases in March, 1 case in April and 1 case in May), winter (2 cases in January, 1 case in February) and autumn (5 cases in October). The average PNSD and PVSD (Particle Volume Size Distribution) and aerosol particle optical properties are presented in Fig. 3-9 and Table 3-1. Optical data was often missing and rarely overlapped in time with suitable air mass trajectories.

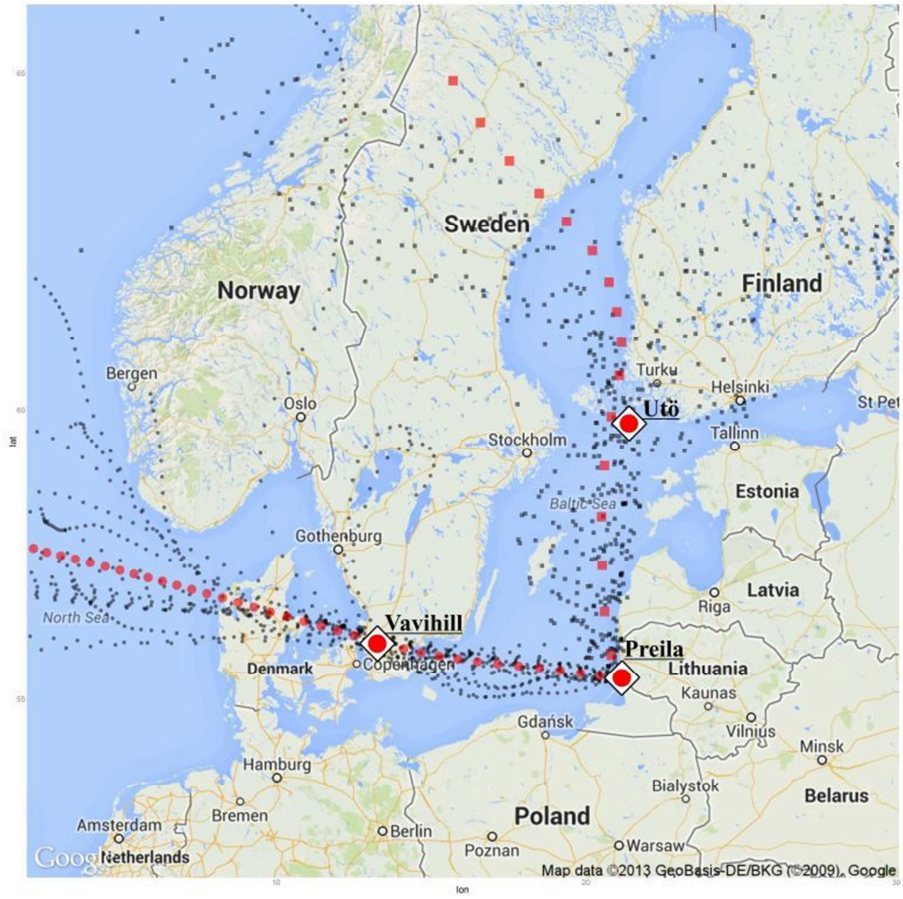

Fig. 3-8. Sampling sites location and backward air mass trajectories used for analysis: smaller dots represent hourly air mass flow, larger – the mean of trajectories.

All aerosol PNSDs were described as the sum of 2 or 3 log-normal modes using an automatic mode fitting algorithm. Nucleation (particle mean diameter 8 – 15 nm), Aitken (15 – 100 nm) and the accumulation (100 – 250 nm) modes were fitted to each PNSD. In all seasons and at both air mass transfer cases aerosol particle number concentration in a size range between 50 and 500 nm ($^{50\text{-}400}N$) was higher by a factor of 1.4 to 2.8 at the downwind-trajectory station. BC mass concentration ratio, $BC_{Preila}/BC_{Utö}$, at Preila station did not change in winter during the Utö to Preila air mass transfer ($BC_{Preila}/BC_{Utö} \approx 1.0$), but was as high as 2.9 in summer. It was found, that up to 60% of an aerosol particle number concentration, in the range from 50 to 400 nm, measured at Preila station, contributes to the particles generated over the Baltic Sea in Utö to Preila mass transfer. For Vavihill to Preila this value is close to 40%. The highest particle light (λ = 520 nm) absorption coefficient

and highest accumulation mode particle number concentrations, as well as particle mass concentration, were found in Utö and Preila sites during the winter season: $\sigma_{\text{Utö,520nm}} = 6.7 \pm 0.3$ (Mm^{-1}), $\sigma_{\text{Preila,520nm}} = 6.9 \pm 0.3$ (Mm^{-1}), ${}^{50\text{-}400}N_{\text{Utö}} = 1270 \pm 130$ (cm^{-3}) and ${}^{50\text{-}400}N_{\text{Preila}} = 2770 \pm 280$ (cm^{-3}), $M_{\text{Utö}} = 2.0 \pm 0.1$ ($\mu\text{g/m}^3$) and $M_{\text{Preila}} = 8.0 \pm 0.4$ ($\mu\text{g/m}^3$), respectively.

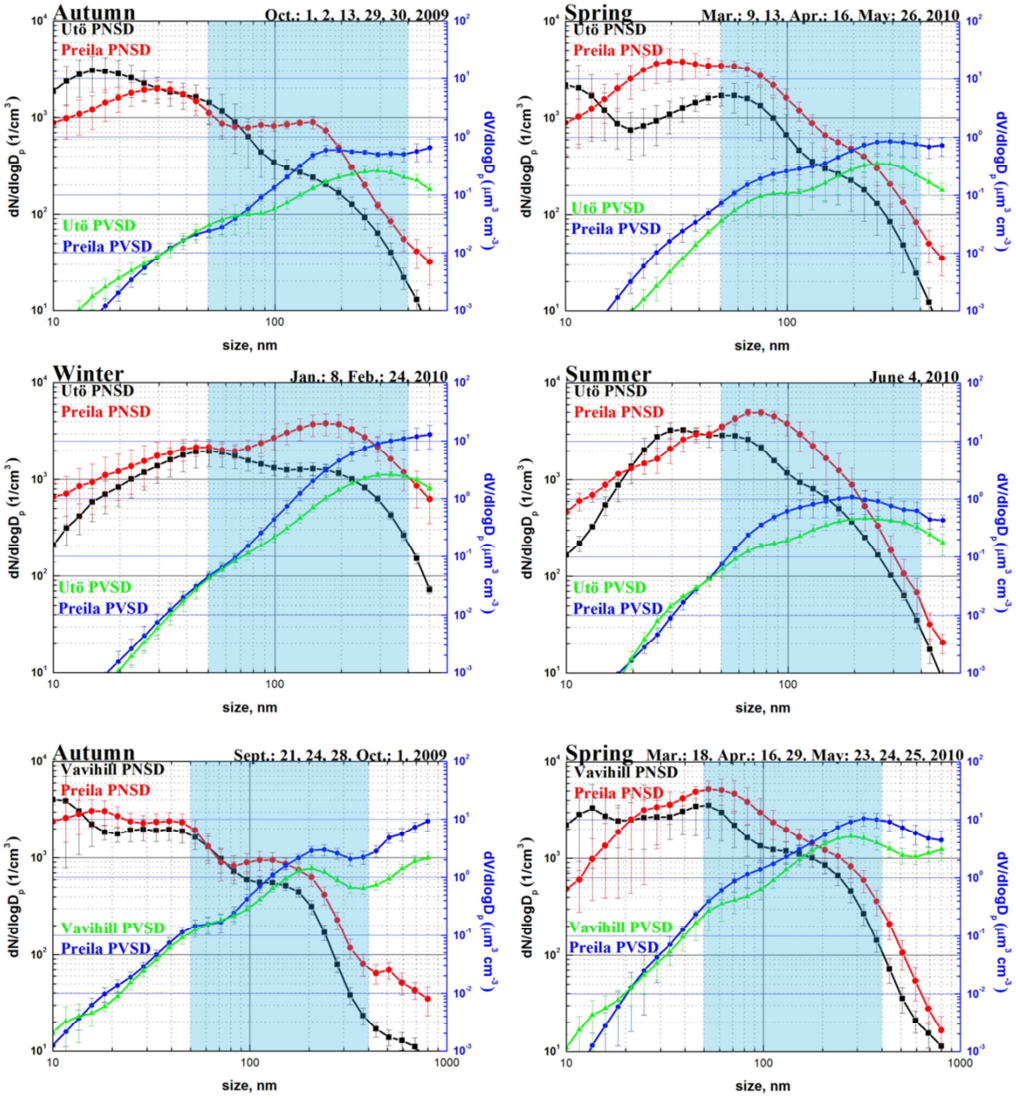

Fig. 3-9. Comparison of an average aerosol PNSD and PVSD at Utö, Vavihill and Preila stations. The 50 – 400 nm particle diameter range is highlighted with a blue color. Bars represent a time variability (standard deviation) over the hours sampled.

Second highest black carbon mass concentration and light absorption coefficient values, also outstanding accumulation mode was found in autumn: $\sigma_{\text{Utö,520nm}} = 0.9 \pm 0.1$ (Mm^{-1}), $\sigma_{\text{Preila,520nm}} = 1.9 \pm 0.1$ (Mm^{-1}), $BC_{Utö} = 60 \pm 10$

(ng/m^3) and BC_{Preila} = 140 ± 10 (ng/m^3). The lowest particle light absorption coefficient values were registered during spring months: $\sigma_{\text{Utö,520nm}}$ = 0.6 ± 0.03 (Mm^{-1}), $\sigma_{\text{Preila,520nm}}$ = 0.8 ± 0.04 (Mm^{-1}). The lowest particle number and mass concentrations were registered in autumn: $^{50\text{-}400}N_{\text{Utö}}$ = 420 ± 40 (cm^{-3}) and $^{50\text{-}400}N_{\text{Preila}}$ = 650 ± 70 (cm^{-3}), $M_{\text{Utö}}$ = 0.3 ± 0.02 (μg/m^3) and M_{Preila} = 0.7 ± 0.04 (μg/m^3), respectively. In Vavihill to Preila cases, particle properties were sensibly higher in spring than autumn months (Table 3-1).

Table 3-1. Average aerosol properties at the three sites: $^{50\text{-}400}N_{\text{tot}}$ - the total aerosol particle number concentration in a range from 50 to 400 nm derived from the PNSD, M_{tot} – integrated total mass concentration (assuming 1.5 g/cm^3 density) , $\sigma_{520\text{nm}}$ - aerosol particle light absorption coefficient (λ = 520 nm), $BC_{\text{MASS,800nm}}$ – black carbon mass concentration, α - absorption Ångström exponent.

Parameter	**Autumn**		**Winter**		**Spring**		**Summer**	
	Utö	**Preila**	**Utö**	**Preila**	**Utö**	**Preila**	**Utö**	**Preila**
$^{50\text{-}400}N_{tot}$, (cm^{-3})	420	650	1270	2770	650	1410	1130	2390
$^{50\text{-}400}(N_{Preila}/N_{Utö})$	1.5		2.2		2.2		2.1	
M_{tot}, (μg/m^3)	0.3	0.7	2.0	8.0	0.3	0.9	0.5	1.1
σ_{520nm}, (Mm^{-1})	0.9	1.9	6.7	6.9	0.6	0.8	0.5	1.2
$BC_{\text{MASS,800nm}}$, (ng/m^3)	60	140	490	500	50	60	40	120
$BC_{\text{Preila}}/BC_{\text{Utö}}$	2.2		1.0		1.2		2.9	
α	1.2	1.0	1.0	0.9	0.8	1.0	1.0	1.3
Average distance / average time of trajectory, (km/h)	546/18		556/17		575/22		484/15	

Parameter	**Autumn**		**Winter**		**Spring**		**Summer**	
	Vavihill	**Preila**	**Vavihill**	**Preila**	**Vavihill**	**Preila**	**Vavihill**	**Preila**
$^{50\text{-}400}N_{tot}$, (cm^{-3})	520	710			1220	2190		
$^{50\text{-}400}(N_{Preila}/N_{Vavihill})$	1.4				1.8			
M_{tot}, (μg/m^3)	1.6	4.9			4.5	8.9		
σ_{520nm}, (Mm^{-1})	no data		no data		0.9	2.4	no data	
Average distance / average time of trajectory, (km/h)	486/10				502/14			

Table 3-2. Aerosol PNSD log-normal fit parameters.

Mode parameters	**Autumn**		**Winter**		**Spring**		**Summer**	
Mode 1	**Utö**	**Preila**	**Utö**	**Preila**	**Utö**	**Preila**	**Utö**	**Preila**
N_1, (cm^{-3})	1200	---	190	410	1340	1900	---	---
$\sigma_{g,i}^2$	1.5	---	1.6	2.0	1.6	1.9	---	---
$d_{g,i}$, (nm)	14	---	17	13	8	28	---	---
Mode 2								
N_2, (cm^{-3})	970	1350	1160	1440	1010	1160	2080	890
$\sigma_{g,i}^2$	1.8	1.9	1.8	2.0	1.8	1.8	1.8	1.9
$d_{g,2}$, (nm)	37	26	49	49	50	62	40	26
Mode 3								
N_3, (cm^{-3})	60	340	530	1810	40	80	180	2380
$\sigma_{g,i}^2$	1.4	1.5	1.6	1.6	1.3	1.4	1.6	1.6
$d_{g,3}$, (nm)	178	131	181	186	213	251	139	75
Mode parameters	**Autumn**		**Winter**		**Spring**		**Summer**	
Mode 1	**Vavihill**	**Preila**	**Vavihill**	**Preila**	**Vavihill**	**Preila**	**Vavihill**	**Preila**
N_1, (cm^{-3})	2370	1320			1290	790		
$\sigma_{g,i}^2$	1.6	1.6			1.6	1.8		
$d_{g,1}$, (nm)	8	12			13	22		
Mode 2								
N_2, (cm^{-3})	1250	1330			1940	2900		
$\sigma_{g,i}^2$	1.8	1.8	no data		1.8	1.8	no data	
$d_{g,2}$, (nm)	34	37			47	58		
Mode 3								
N_3, (cm^{-3})	170	300			310	340		
$\sigma_{g,i}^2$	1.4	1.4			1.4	1.4		
$d_{g,3}$, (nm)	148	156			181	220		

Mobility particle size spectrometers' comparability study carried by Wiedensohler et al., (2012) has shown 5 to 10% measurement uncertainty in the total integrated particle number concentration. This suggests that the same order of uncertainty exists in the present study. However, the observed difference in integrated particle number concentration is still greater than the instrumental uncertainty might explain (i.e. the difference between $^{50\text{-}400}N_{Utö}$ = 420 ± 40 cm^{-3} and $^{50\text{-}400}N_{Preila}$ = 650 ± 70 cm^{-3}). For both, Utö to Preila and Vavihill to Preila air mass transport the highest concentration variation over all

aerosol PNSD was dominant in spring. Possible reason for this might be a relatively large wind speed - 8 m/s. In summer and autumn the wind speed was about 6 m/s, in winter - 3 m/s. Because of similar air mass flow conditions over a Baltic Sea, we did not expect significant differences in aerosol PNSD pattern for Vavihill to Preila and Utö to Preila air mass transfer events, in fact, aerosol particle number concentration in a range from 50 to 400 nm showed the same behavior. Particle number concentration and particle light absorption coefficient were sensibly higher in Preila than Vavihill for autumn and spring seasons. Moreover, it was observed that the longer air mass travels over the Baltic Sea, the greater change in both, aerosol optical and physical properties, were perceptible at downwind station (Table 3-1 and Fig. 3-9)

3.2.1. Continental aerosol particles

Air mass trajectory lateral position uncertainties with respect to upwind site locations are known to vary between 10 – 30% of the trajectory length (Stohl et al., 1998). The distance between Vavihill to Preila and Utö to Preila is about 490 and 530 km, respectively. It results in ± 50 km lateral uncertainty. The distance between Vavihill and Copenhagen is less than 60 km. Hence, the aerosol PNSD measured at Preila station might have a significant background anthropogenic contribution from Copenhagen even though the center of the trajectory does not pass through Copenhagen. Moreover, the air masses advecting over the Vavihill station pass over a 100 km stretch of land. This might result in a significant emission of primary aerosol particle from the land sources between Vavihill and Utö. Traffic, agricultural, domestic and biogenic emissions in southern Sweden are contributing to some extent. Hence, the Utö to Preila cases are least affected by the city and land emissions (the distance to Stockholm, Helsinki, and Turku is 190 km, 200 km, and 90 km respectively). If the land-based emissions were a significant contributor to the observed changes, much smaller changes should be observed on the Utö to Preila transport route. The observed change on Utö to Preila transport path was,

however, greater than at Vavihill to Preila transport path in both absolute and relative numbers.

3.2.2. Growth of pre-existing particles

Generalized qualitative evidence in particle number concentration biased over a Baltic Sea can be discussed using two-dimensional, aerosol PNSD mode geometric mean diameter and number concentration (from Table 3-2), classification of particle number size distribution (Fig. 3-10). Such diagram is useful in understanding the dynamics of aerosol particle transformations. If each mode is assumed to change as a whole, particle growth rates, required to explain the changes between the upwind stations and Preila, can be calculated. This was done for both transport routes.

In case of Utö to Preila transport the nucleation and Aitken modes at Utö could have contributed to the measured accumulation mode at Preila only if particle growth rates of at least 8.0 nm/h (for nucleation to accumulation mode) and 6.6 nm/h (for Aitken to accumulation mode) were assumed (using lowest averaged trajectory speed).

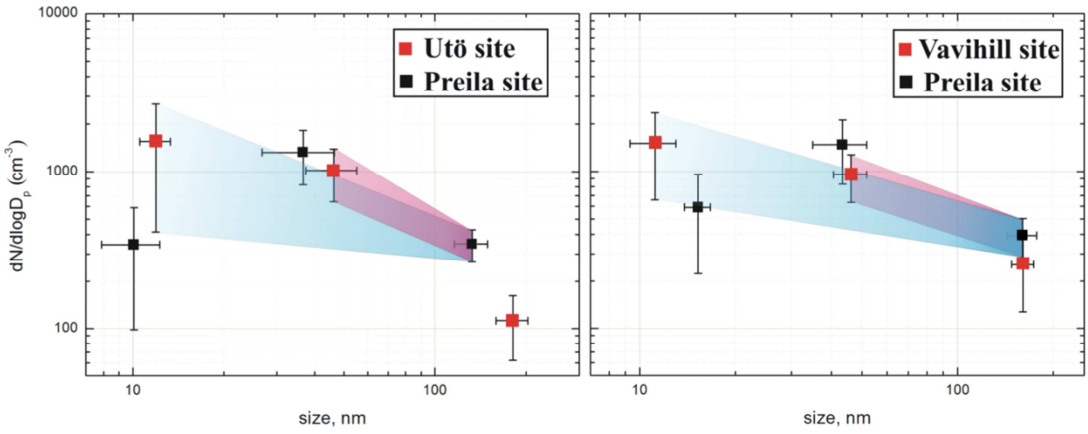

Fig. 3-10. Classification of the particle number size distribution. On the axes - geometric mean diameter and mode number concentration. Left – Utö to Preila, right – Vavihill to Preila cases. Bars show standard deviation of both, mode concentration and size.

For Vavihill to Preila air mass transport these numbers would have to be as high as 12.7 and 10.5 nm/h for nucleation to accumulation and Aitken to accumulation mode, respectively. Recent studies have shown that mean particle growth rate (GR) in a marine environment is 3 ± 0.5 nm/h (Ehn et al., 2010). This is clearly less than the GR required to explain the observed changes. For newly formed particles the required GRs are even higher. It rules out the emissions of organics or di-methyl-sulfide emitted from the sea surface as an explanation. The observed changes can only be explained if there was a source of accumulation mode particles between the sites.

3.2.3. Sea spray aerosol particles

A plausible cause for increased accumulation mode particle number concentration at a downwind marine environment station might be associated with a marine aerosols – products of bubble plumes and foams generated by the actions of a surface wave breaking (Lewis and Schwartz, 2004). Different laboratory methods are used to generate surrogate marine aerosols within enclosed tanks. These studies confirm the presence of accumulation mode particles in a marine environment with a geometric mean diameter of 200 nm (Stokes et al., 2013). As the aerosol chemical composition was not measured, the evidence for a sea spray aerosols cannot be supported. However, a sea spray influence onto particle number concentration can be sorted out by connecting a change in both, particle number and BC mass concentrations with a second part parameter, such as wave activity over the sea. Pettersson et al. (2012) have reported a series of environment fact sheets including monthly wave height variation over the Baltic Sea. It was shown that the minimum wave height is mostly common during the late spring to early fall months. Mean wave height in a Northern Baltic Proper was found to be 0.6 m. After the height minimum waves start to grow and reach their maximum (2.0 m) during the winter months. We suggest that wave height might serve as an indirect evidence for a higher sea sprayed aerosol particles fraction. Considering only a

number concentration in a range from 50 to 400 nm, 58, 61, 55 and 62% of particle number concentration were gained after air mass passed over the sea in autumn, winter, spring and summer seasons, respectively (for Utö to Preila case). The possible explanations for such phenomenon might be addressed to different origin and sources of aerosol particles. In winter and spring seasons, when the wave height over the Baltic Sea is peaking, sea sprayed aerosols might have increased an accumulation mode particle number concentration. This effect can be clearly seen in spring. Relatively low BC mass concentration, negligible increase in light absorption compared to a number concentration support the evidence of weak light absorbing particulate matter. The sea spray aerosol influence onto accumulation mode number concentration was checked using the parameterization provided by Sofiev et al., (2011). The following assumptions were made: a) wind speed at 10 m height is the same as trajectory speed; b) salinity is 9.2‰ (southern Baltic Sea); c) temperature of $+5^{o}$C in winter, $+15^{o}$C during other seasons; d) no deposition or coagulation processes are present; e) 300 m boundary layer is well mixed. Using the average trajectory speed (Table 3-1) the sea salt emissions, in a size range between 50 and 400 nm, were about 1-2 particles per cm^3. Using the highest study trajectory speed, the emissions were only slightly above 10 cm^{-3}. To get the observed increases in aerosol particle number concentration an average wind speed of 50 m/s would be needed. With this in mind, sea salt aerosol particles can explain only a tiny fraction of the observed increase in particle number concentration.

3.2.4. The effect of planetary boundary layer onto aerosol properties.

The observed increase in both, $^{50\text{-}400}N$ and BC concentration, was significant on both transport routes over the Baltic Sea. A change in observed particle number concentration can, in general, be a result of changed boundary layer (PBL) height (e.g. Ma et al., 2011). Increased PBL height during a daytime mixes the particles near the surface with air above. If the above air has

lower particle concentration, this results in dilution and a decrease in *N* at a surface level. The opposite has also been observed when the above air is more polluted (Clarke et al., 1998). During the nighttime turbulence weakens leaving the particles equally distributed in the air layer. New surface emissions are trapped in the low boundary layer leading to a higher increase in *N* at a surface per emission unit compared to the daytime situation. Gryning et al. (2002) have studied variables which influence the boundary layer height over the Baltic Sea. They showed that boundary layer height varies over different time scales. However, no clear diurnal variation, as seen in over land cases, was observed. This can be explained by high water heat capacity. Diurnal variation of a sea surface temperature is very small. PBL phenomenon is expected to have an effect only at Vavihill site, which is located inland. The boundary layer height was not examined in the present study. However, no systematic effects were found when comparing the cases in which the air mass passing upwind site at a daytime arrived to Preila at night, or vice versa. Moreover, 3000 m altitude trajectories have shown a very similar behavior to those at 100 and 300 m.

The light absorption coefficient and accumulation mode particle number concentration at Utö and Preila stations were highest during the winter months. It can be explained by a low boundary layer and strong inversion conditions. Regional scale anthropogenic sources, such as domestic heating, is well known to have an effect on the entire northern Europe. Weak vertical mixing leads to a higher aerosol particle transport efficiency over a longer distance compared to other seasons. This could explain high aerosol particle number and black carbon mass concentration values, but not their change during the air mass transport between the stations.

3.2.5. Shipping in the Baltic Sea

Baltic Sea Skaw line (Fig. 1-6) was crossed 62743 times during 2009. The presence of intensive ship activity is obvious. The main ship lanes in the Baltic Sea can be seen in Fig. 1-6. Most of the main shipping lanes are located

at least 100 km from Preila (except the one leading to Klaipeda harbor). The plumes have enough time to disperse, and individual peaks (such as in Kivekäs et al., 2014) can no longer be separated. In a recent study carried out by Diesch et al., (2013), bimodal aerosol PNSD was found to be common feature in a ship exhaust plumes. These modes were an ultra-fine particle mode at around 10 nm consisting mostly of sulfuric acid (González et al., 2011) and Aitken mode at 40 nm. An increase in 150 nm particle number concentration was also found. This carbon-containing mode is made up of mainly soot and absorbed organic materials. Our focus was mainly on the 50 – 400 nm particle diameter range where the carbon-containing mode is the most prominent. The observed Ångström exponents at Utö and Preila were consistent with the values measured in engine combustion studies (α = 1.0), but lower than the values associated with the wood burning soot (α > 1.8) (Sandradewi et al., 2008) all supporting the conclusion that ship-emitted, particulate matter contributes to the coastal aerosol properties in Lithuania.

3.2.6. Conclusions

Only limited data is available for particulate ship emissions from Baltic Sea shipping routes and their impact onto background aerosol properties. A previous study has shown that a single shipping lane can contribute up to 11 to 21% of the particle number concentration during a typical day at a coastal field site as the wind passes perpendicular through the shipping lane towards the field station (Kivekäs et al., 2014). Here the contribution from shipping lanes when the winds are passing over a much longer stretch of ship emissions, namely several hundreds of kilometers were investigated. During several of the chosen pristine study days, the ship emissions turned out to be the dominant contributor to the particle number concentration. Moreover, 40 to 60% of the aerosol particle (50 - 400 nm) number concentration measured at Preila station, contributed to the particles generated over the Baltic Sea in Vavihill and Utö to Preila mass transfer, respectively. High BC mass concentration values in winter

can be associated with intensive domestic heating in the northern Europe. It conceals the possible ship influence onto aerosol properties. It was found that the longer air mass spent over the sea, the bigger change in aerosol properties were observed in downwind station. Absorption Ångström exponent value (α = 1.0), increase in aerosol particle number and BC mass concentrations let us conclude that the aerosol particle physical properties, registered at the Preila, are determined by an intensive Baltic Sea marine traffic.

3.3. Nocturnal nucleation imposed mixing state of aerosol particles

The project "Campaign of Air Quality Research in Beijing and Surrounding Region" (CARE-Beijing) is a broad collaboration project where the physic and chemistry departments of the Leibniz Institute for Tropospheric Research e.V. (TROPOS), Leipzig, Germany, take place.

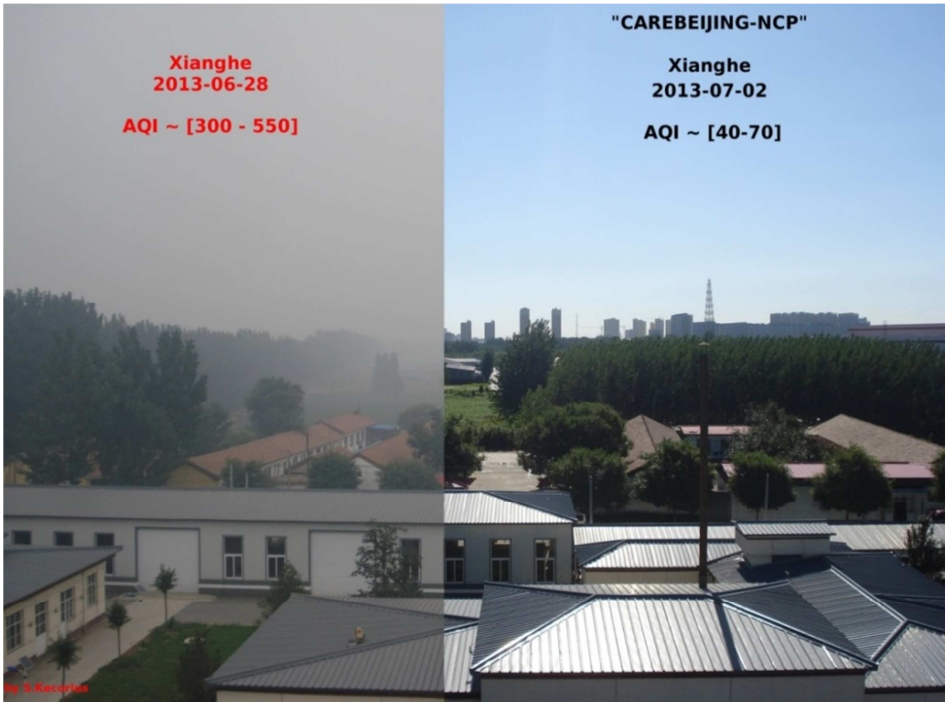

Typical high pollution episode in the North China Plain, Xianghe. Regional agricultural fires increase AQI to more than 500 drastically reducing visibility to less than 1 km.

The main goal of the project is to quantify the direct and indirect climate forcing in the North China Plain. In 2013 measurement campaign, which took place in Xianghe, China, my interest was to develop an aerosol spectrometry method by combining the aerosol particle volatility and hygroscopicity techniques to define how nocturnal new particle formation influences the mixing state of aerosol particles.

The measurement data set comprises 32 days of continuous measurements of aerosol particle physical properties. Because of the planetary boundary layer evolution during the day, this study dataset is sub-divided into daytime and nighttime periods. Sub-division necessity rises from the different physico-chemical processes as well as the sources of pollution shaping aerosol particle properties during the day. The mixing state of aerosol particles as a regional pollution phenomenon is analyzed during the time period when a boundary layer is well mixed. This is between 8 AM to 4 PM (Fig. 3-11).

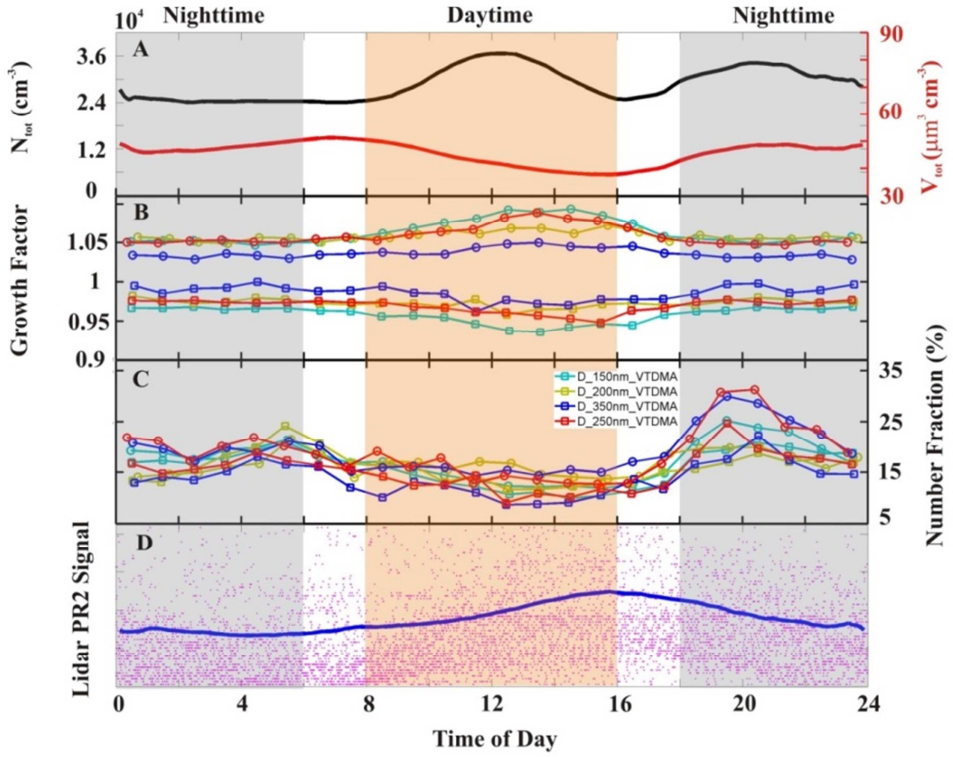

Fig 3-11. Diurnal variation of A – particle number and volume concentrations, B – volatility growth factor, C – number fraction of non-volatile particles (circles represents number fraction of nearly hydrophobic particles), and D – lidar signal. Orange and grey shades mark considered daytime and nighttime, respectively.

The altitude of the first main gradient in the lidar signal, corresponding to the inversion layer height, shows that PBL starts to develop at 8 AM and reaches the height peak at 4 PM. During this time period perceptible decrease in the non-volatile and nearly hydrophobic number fractions were registered (Fig. 3-11, C). It means that aerosol particles are less affected by a local pollution. In this time period regional air pollution effects is the most distinctive. Local pollution can be separated by a rapid increase in non-volatile and nearly hydrophobic number fractions at night (between 6 PM and 6 AM).

3.3.1. Mixing state of aerosol particles

The volatility growth factor probability density function (GF-PDF) is the probability size distribution of remained sub-micrometer particles after thermal treatment (at 300^{o}C). It represents non-volatile particle fractions which can be divided into two groups, corresponding to particles with a low and high volatility. Low volatility fraction represents externally mixed non-volatile material and can be considered as an externally mixed black carbon. Particles with a high volatility are known to be composed of a BC core and a non-light-absorbing volatile shell (Wehner, 2009). The same approach is also valid for hygroscopic growth factor probability density function interpretation. After particle humidification, GF-PDF represents two distinctive particle groups - nearly hydrophobic and hygroscopic particle fractions. High number fractions of nearly hydrophobic (NH) and low volatility (LV) particles observed at night indicate that the freshly emitted hydrophobic particles (e.g., fresh soot or primary organic aerosol) accumulate in the surface layer and mixes externally with the more hygroscopic and volatile particles. During the daytime, number fraction (NF) of NH particles is smaller, indicating the dominance of internally mixed aerosol particles due to aging process.

The averaged diurnal variations of number fraction (*NF*) and growth factor (*GF*) of 50 150 250 and 350 nm particle diameters during the whole campaign are presented in Fig. 3-11. The averaged *NF* derived from H - and V

- TDMA shows a similar diurnal variation. During the daytime, *NF* of NH and LV varies from 8% to 15%, depending on the different dry particle diameter. *NF* increases significantly during the nighttime to 35%. The *GF* of nearly hydrophobic particles (shown in Fig. 3-11, B, solid lines with circle) is around 1.05 during nighttime, and increases to 1.1 during a daytime. The shrink factor of low volatility particles (shown in Fig. 3-11, B, with square in solid lines) is around 1.0 during the night, and decreases to about 0.9 during the day. The differences between *GF* are much smaller during the nighttime than that during the daytime. It shows that particles exhibit different affinity to water and different volatility properties due to the aging process. Fig. 3-12 shows the average GF-PDFs from V- and H-TDMA measurements for different dry particle sizes. Hygroscopicity GF-PDFs measured in the range 85% < RH < 89% were corrected for RH = 87% according to eq. (3) and (6) in Gysel et al. (2009). The effect of instrumental RH fluctuation was corrected too. A dominant hygroscopic mode and a smaller but distinct NH mode can be found for each averaged GF-PDF. The hygroscopic mode is peaking at a *GF* from about 1.4 to 1.65 (RH = 87%). The hygroscopic mode peak shifts to a larger *GF* with increasing dry diameter. It indicates that hygroscopic particles with a larger dry diameter generally have a higher growth factor. This is because of both, reduced Kelvin effect and different aerosol chemical composition due to aging process (Liu et al., 2011).

Particle volatility GF-PDFs (blue lines in Fig. 3-12) show dominant volatile and smaller but noticeable low volatility fractions. The volatile mode is peaking at a *GF* from 0.38 to 0.3 at a temperature of 300℃. The volatile mode peak shifts to a smaller *GF* with dry diameter increasing, indicating that volatile particles with a larger dry diameter shrink more. Similar to NH mode, the LV mode for each dry diameter (except 50 nm) does not show significant shift. Exceptional 50 nm particle shrinkage might be explained by a nucleation induced particle volatility. Newly formed and slightly grown particle were observed to be highly volatile and hygroscopic. Summary of the hygroscopicity and volatility properties is shown in Table 3-3.

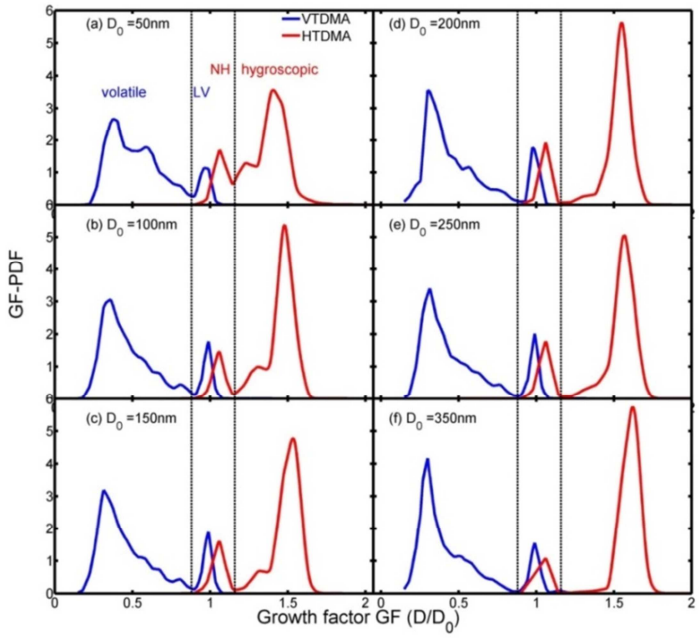

Fig. 3-12. Averaged hygroscopicity (red line) and volatility (blue line) GF-PDFs for the whole measurement period. "Volatile" marks the region of considered volatile particle fraction, "LV" – low volatility, "NH" – nearly hydrophobic, and "hygroscopic" – hydrophilic particle fractions.

Table 3-3. Summary of the H- and V-TDMA measurements (mean value ± standard deviation)

Dry diameter (nm)		50	100	150	200	250	350
Number of scans	H-TDMA	720	1300	1293	385	756	1095
	V-TDMA	823	688	862	180	685	422
Mean $GF \pm$ std		1.39 ± 0.07	0.37 ± 0.03	1.42 ± 0.07	1.46 ± 0.06	1.46 ± 0.09	1.49 ± 0.11
NF of $GF < 1.2$ group		0.23	0.16	0.17	0.16	0.18	0.18
High hygroscopic group, HYGROSCOPIC							
Number fraction		0.54 ± 0.25	0.72 ± 0.19	0.76 ± 0.17	0.81 ± 0.11	0.76 ± 0.17	0.81 ± 0.17
Mean $GF \pm$ std		1.44 ± 0.05	1.48 ± 0.03	1.51 ± 0.04	1.55 ± 0.03	1.56 ± 0.05	1.59 ± 0.05
Low hygroscopic group, NH							
Number fraction		0.19 ± 0.13	0.15 ± 0.09	0.16 ± 0.11	0.16 ± 0.09	0.18 ± 0.14	0.18 ± 0.16
Mean $GF \pm$ std		1.07 ± 0.03	1.06 ± 0.02	1.06 ± 0.03	1.06 ± 0.01	1.06 ± 0.02	1.04 ± 0.02
Low volatile group, LV							
Number fraction		0.16 ± 0.08	0.16 ± 0.09	0.16 ± 0.10	0.16 ± 0.08	0.15 ± 0.12	0.14 ± 0.11
Mean $GF \pm$ std		0.93 ± 0.03	0.95 ± 0.03	0.96 ± 0.02	0.97 ± 0.02	0.97 ± 0.02	0.99 ± 0.03
High volatile group, HV							
Number fraction		0.36 ± 0.21	0.5 ± 0.16	0.53 ± 0.16	0.54 ± 0.13	0.57 ± 0.18	0.60 ± 0.16
Mean $GF \pm$ std		0.37 ± 0.026	0.35 ± 0.032	0.35 ± 0.04	0.34 ± 0.03	0.33 ± 0.04	0.32 ± 0.04
Ensemble mean of all groups from H-TDMA							
Mean $GF \pm$ std		1.40 ± 0.07	0.37 ± 0.03	1.42 ± 0.07	1.50 ± 0.06	1.50 ± 0.09	1.50 ± 0.11

3.3.2. Nocturnal new particle formation

During the measurement period, nocturnal new particle formation events were observed on 59% of nights in the discrete manner without pronounced subsequently following particle growth. Nocturnal new particle formation (NPF) events usually started after 6 PM and continued to appear until next morning. Aerosol particle number size distribution during one of the events is shown in Fig. 3-13.

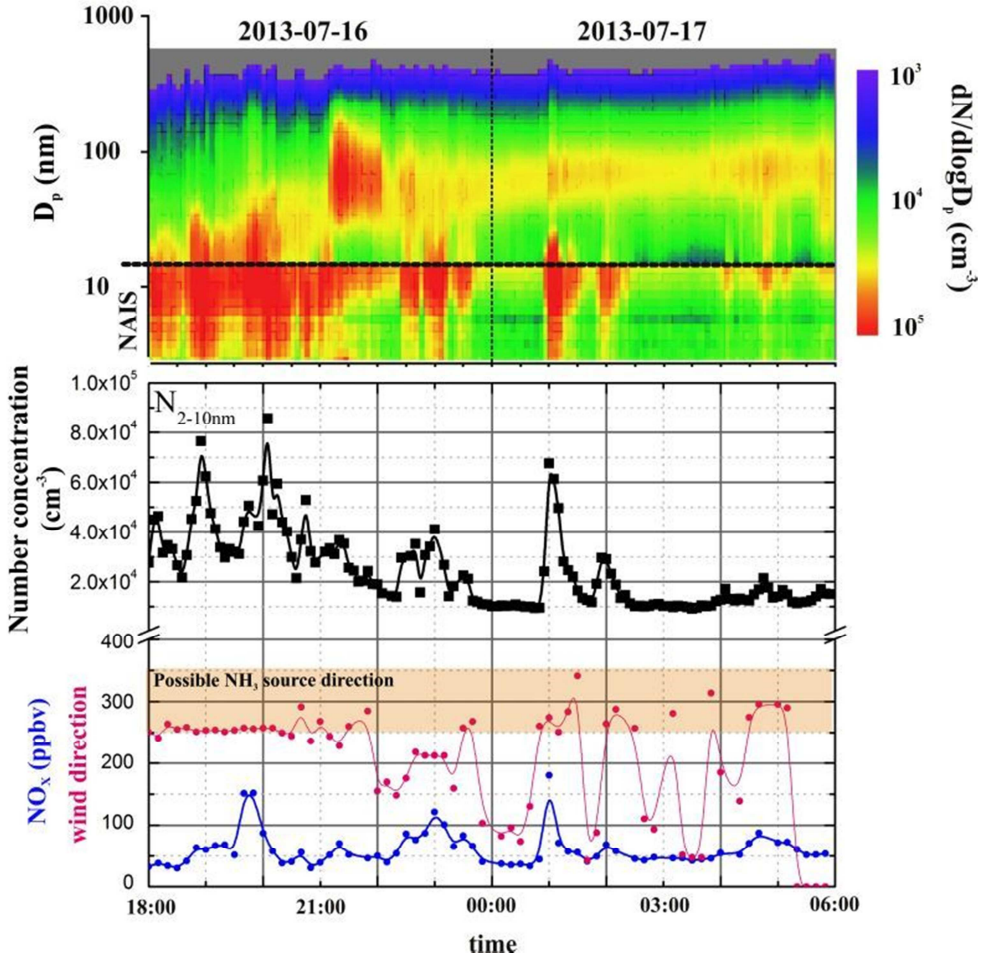

Fig. 3-13. Aerosol particle number size distribution, particle number concentration in a range from 2 to 10 nm, NO_X concentration and wind direction during 16 - 17th of July, 2013, nighttime new particle formation episode. Horizontal line marks the size range for NAIS and SMPS measurements.

Presented contour plot is a combination of the data measured with NAIS (particles between 2 and 15 nm) and SMPS (particles between 15 and 800 nm) systems. NPF classification is usually based on the visual inspection of the

distinct formation and growth shapes in the observed PNSD contour plot (Manninen et al., 2009). In NPF studies “non-banana-type” cases are regarded as “undefined” events (Heintzenberg et al., 2007). Our observed new particle formation does not follow a well-known “banana-shape” growth. Therefore NPF events were discerned according to rapid nucleation mode (2 to 10 nm) particle number concentration increase, lasting as short as 20 minutes (Wu et al., 2007). Example of observed NPF is presented in Fig. 3-13.

High concentrations of cluster ions in the size range from 0.34 – 1.8 nm also existed at all times making it difficult to determine the nocturnal new particle formation events, thus, was excluded from further data analysis. During the nighttime NPF ultra-fine particle (with diameters < 10 nm) number concentration increased up to $N_{2\text{-}10nm} = 7 \cdot 10^4 \pm 3600$ cm^{-3} and was at the same order of magnitude as the daytime events. The lower limit of the nocturnal new particle formation rate (particles in a size range from 2 to 10 nm, loss of formed particles due to growth and coagulation excluded) was 1.25 times higher than a daytime (45 ± 5 cm^{-3}s^{-1} versus 36 ± 4 cm^{-3}s^{-1}). Average condensational sink for the particles in the size range from 2 to 750 nm during nocturnal NPF was found to be $CS = 0.055$ s^{-1}. It is noticeably higher than ones observed in Beijing, China (between 0.02 and 0.045) by Wu et al., (2007).

Aerosol particle volatility and hygroscopicity profiles for V- and H-TDMAs are shown in Fig. 3-14. 150 nm particles were separately conditioned in 300^{o}C and around 87% RH environments to determine the mixing state of aerosol particles. Boxes in a contour plot indicate the regions between 6 PM to 6 AM, where aerosol volatility and hygroscopicity properties were significantly different compared to a daytime. Particle affinity to water, $GF \approx 1.5$, followed by a volatile fraction, $GF \approx 0.3$, notably increases during the nighttime. Interestingly, simultaneous increase in externally mixed particle fraction, $GF \approx 1.0$, suggests different processes occurring at the same time.

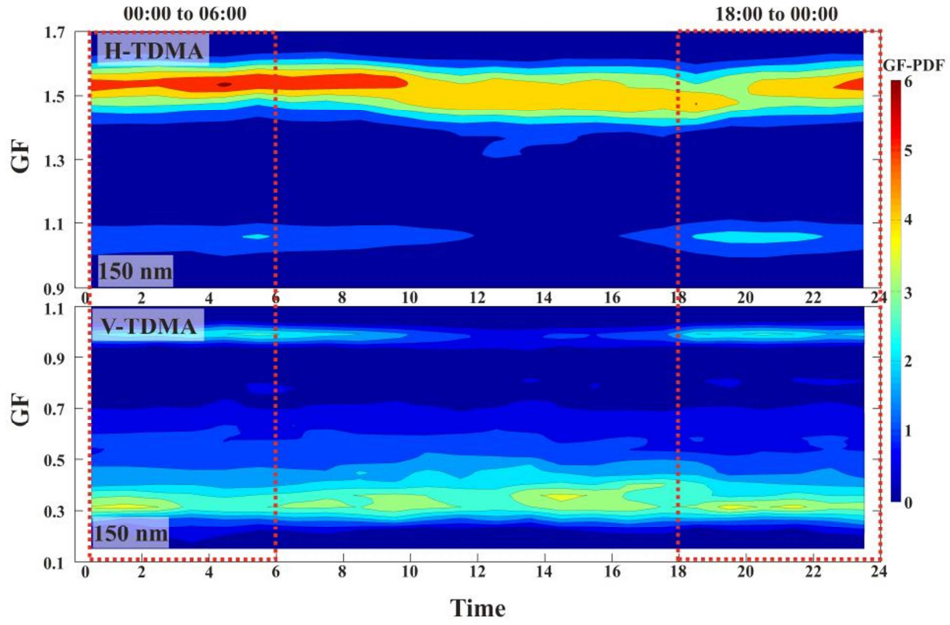

Fig. 3-14. 150 nm particle Growth Factor – Probability Density Function (GF-PDF) for both, H- and V-TDMA systems during all measurement period. Red rectangles mark the time period when nocturnal new particle formation was registered.

The extent of 150 nm aerosol particle volatility measured at night is somehow comparable to that observed during the daytime (Fig. 3-14, V-TDMA). Growth factor – probability density function of highly volatile aerosol particles, seen between 3 to 6 AM suggests that particle volatility increases during the period, when nocturnal nucleation is present and at daytime. It is when different vapors condense onto particles. Newly formed particle volatility and hygroscopic properties analysis have shown that particles between 20 and 35 nm (operating limit for V-TDMA and H-TDMA, respectively) were highly volatile and slightly hygroscopic (Fig. 3-15). During the new particle formation V-TDMA showed a significant increase in measurement distribution function (MDF) of 20 nm sized particles compared to non-event cases. After NPF episode particles were conditioned in 300^{o}C environment – only a minuscule refractory fraction (GF-PDF in Fig. 3-15), with a great uncertainty due to poor counting statistics, remained. Note that thermal conditioned particles were measured in the range from 9 to 23 nm. In H-TDMA system 35 nm particles experienced uni-modal growth to GF = 1.15 when exposed to 87% RH. Poor ultra-fine particle affinity to water can be explained by a Kelvin (curvature)

effect, a major limitation in the growth of atmospheric nanoparticles. Significantly elevated equilibrium vapor pressure above the small clusters limits its growth. However, the observed change was enough to distinguish between the different aerosol particle mixing states, revealing the episodes when particles were newly formed.

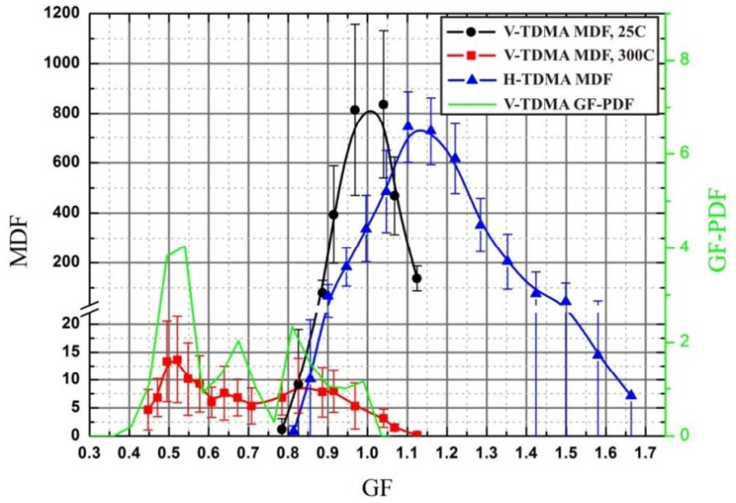

Fig. 3-15. Average of measurement distribution function (MDF, left scale) and growth factor probability density function (GF-PDF, right scale) for the nocturnal new particle formation episodes. Bars show a time variability (standard deviation) over the hours sampled.

Because V- and H-TDMA MDFs are narrow enough – inverted ambient temperature and hygroscopic growth GF-PDFs can be represented using only MDFs itself (Gysel et al., 2009).

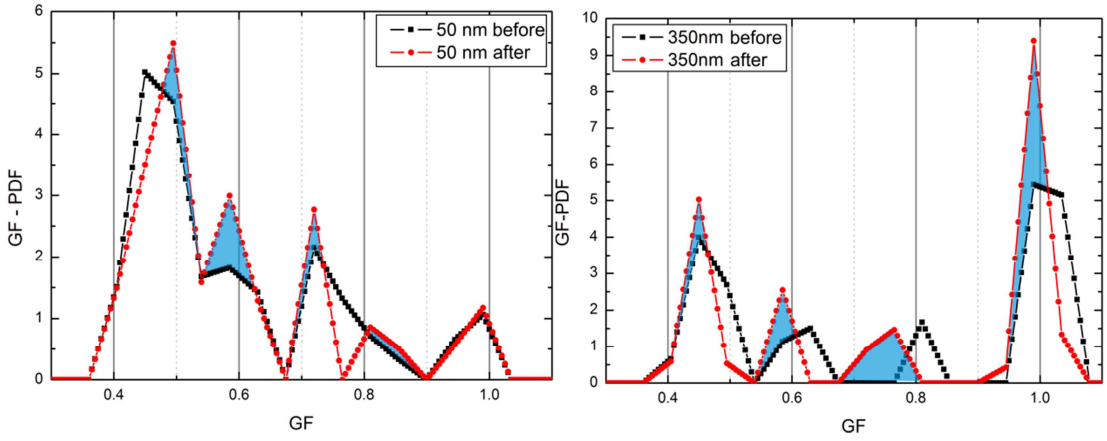

Fig. 3-16. V-TDMA volatile particle number fraction GF-PDF. Black line - GF-PDF before, read – GF-PDF after the nocturnal new particle formation. The blue shades mark increase in GF-PDF.

After analyzing the mixing state of 50 and 350 nm sized aerosol particles, the increase in particle volatile fraction after the new particle formation was noticed (Fig. 3-16). 50 nm sized particle volatile fraction GF-PDF was 1.3 times higher after NPF than before. Larger particle (350 nm) volatile number fraction increases by a factor of 3.0. Only a minuscular increase in hygroscopic particle (350 nm) number fraction was observed (not shown here). This can be explained by a volatile and hydrophobic species condensation onto pre-existing particles (Riccobono et al., 2012).

The wind direction during nocturnal NPF events was mainly between 250^{o} and 350^{o}; that is the wind arrived to the measurement site from the west or northwest direction. Wind speeds during the events were below 1 m/s. The correlation between RH, wind direction and NF of 50 nm volatile particles is shown in exceedance contour plot (Fig. 3-17). Section III, representing the west-north winds, shows that the *NF* of 0.8 for 50 nm particles were exceeded most frequently when RH was nearly ~ 100%. Other, less intense exceedance regions might also be seen in sections I and II. Exceedance contour is more quantitative rather than quantitative approach to investigate the dependences of variables revealing possible causes for NPF.

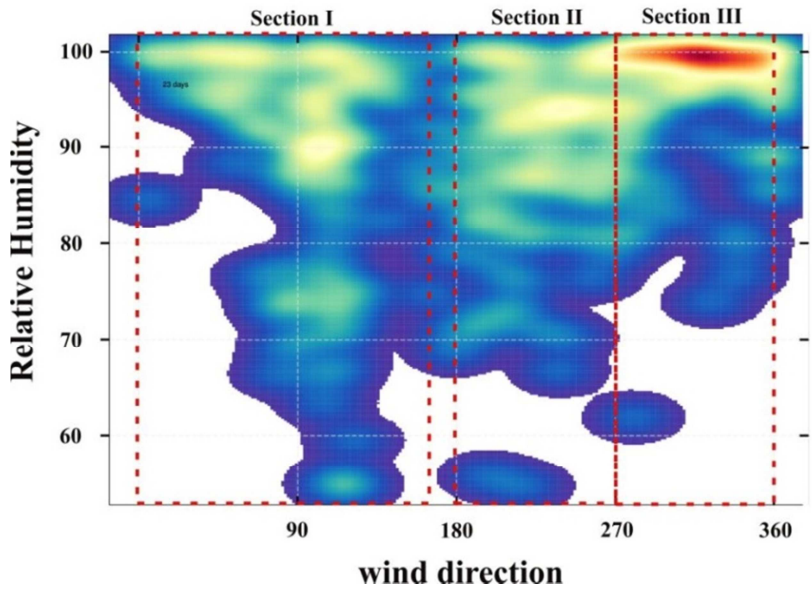

Fig. 3-17. Exceedance contour plot for all measurement period (nighttime), showing the conditions when NF of 50 nm volatile particle exceeded 0.8. Color intensity shows the strength of exceedance.

Plausible aerosol particle and precursor gas sources are indicated in Fig. 2-9. Those are the set of roads surrounding measurement site: provincial road with the relatively low traffic load, ~ 500 m to west, gravel road with intensive vehicle load, 200 m to east and heavily loaded main street towards the Xianghe center, 500 m to south-east. A periodically smoldering dump for domestic and small scale industrial (plastics, metal paint packages) waste, 200 m to south, was a strong aerosol particle source when winds were coming from south. The trace gases, such as SO_2, primarily come from anthropogenic emission sources in populated regions, largely - from coal combustion in the power plants. Nevertheless, coal enriched in potentially toxic trace elements such as mercury, arsenic, fluorine is still a popular fuel for the industrial and domestic use in rural China (Finkelman et al., 2002). Because measurements were conducted during the summer months, nocturnal SO_2 peaks cannot be associated with heating-period as explained by Ran et al., (2014). The maximum SO_2 hourly concentration average increased from 30 to 50 ppbvs during September to November, respectively. Non-heating period nighttime SO_2 concentrations were reported to be, on average, below 5 ppbv (Ran et al., (2014), Fig. 3d). However, the use of coal pellets for cooking, water heating and metal processing were evident around the site, which might justify elevated nighttime SO_2 concentrations when winds were coming from the living areas. During the observational period, NO_x and O_3 nighttime concentrations averaged at about 30 and 72 ppbv, respectively. 180 ppbv NO_x concentration peak was associated with a local emissions and the daytime evolution of planetary boundary layer (Ran et al., 2014).

In sulfur and nitrogen oxides abundance, that is in polluted plumes, nighttime SO_2 conversion to H_2SO_4 was observed by Brown et al., (2004). It was shown that OH radical production during the nighttime from the hydrocarbon ozonolysis and ozone reactions may be a very important process for a nighttime new particle formation (Donahue et al., 1998). On the other hand, nitrate radicals, NO_3 and N_2O_5, arising from the NO_2 and O_3, constitute an important chemical system in the nocturnal atmosphere (Allan et al., 2000).

Dinitrogen pentoxide (N_2O_5) can serve as a significant pathway for a conversion of NO_x into nitric acid via its heterogeneous hydrolysis on aerosol. Its nocturnal oxidation capacity is believed to be as large as that of the hydroxyl radical during the daytime (Geyer et al., 2001a). It can be clearly seen from Fig. 3-13 that increase in NO_x concentration is closely followed by a nucleation mode particle number concentration. Ultra-fine particles composed of ammonium sulfate or sulfuric acid increase in size significantly upon a humidification. During regional nucleation events in urban Atlanta, the hygroscopic growth factor of 10 nm ammonium sulfate aerosol particles were *GF* = 1.4 (Sakurai, H., et al. 2005). In the present study, much larger particles (35 nm) were found to be less hygroscopic, *GF* = 1.15 (Fig. 3-15). Moreover, because the measurement site was equally surrounded by living areas, no reason was found to justify the local SO_2 emissions being dependent on wind direction, at least during non-heating period. In fact, no correlation between SO_2, O_3 and ultra-fine particle number concentrations were observed during the nighttime NPF, suggesting additional components taking place in a new particle formation.

Studies of 2 to 9 nm particle affinity to water show that freshly nucleated particles are composed of less hygroscopic compounds, presumably organics, at the very early stage of particle formation and growth (Zhang et al., 2009). This agrees well with the observations in Xianghe if the abundance of amines in air is assumed. Emissions from cattle rumen and manure are known to be rich in both volatile amines and NH_3 (Kuhn et al., 2011). The cattle shed, 100 m to west (Fig. 2-9), might have served as a source for high volatile amines (methylamine, dimethylamine, trimethylamine, among others) and NH_3 concentrations. Studies on the formation and composition of the ultra-fine particles showed that NH_3 and amines is important constituent in new particle formation (Erupe et al., 2011). Amines are considered to be more important for nucleation than NH_3, even at low concentrations (thousandth of NH_3) (Loukonen et al., 2010). Under atmospheric conditions amines are able to form nitrate or sulfate salts. Quantum chemical computations show that for

nucleation processes involving nitric acid, amines may be more effective than ammonia in forming new particles (Murphy et al. 2007). Experiments by Bzdek et al., (2010) gave evidence that nucleation mode atmospheric salt particles are most likely amminium salts rather than ammonium salts, and amines rather than ammonia may be main components of nucleation. Although neither NH_3 nor amines were measured during the measurement campaign, the bursts in newly formed particle concentration were consistent with the winds coming from the direction of living areas and cattle lofts suggesting their participation in nucleation process. In ambient measurements RH is considered to be an indirect nucleation inhibitor. This is mainly because the surface area of existing particles increases due to their affinity to water molecules. In the present study it was observed that nucleation takes place with relatively high condensation sinks and RH. Looking at exceedance contour (Fig. 3-17) it is obvious that 50 nm particle volatility greatly depends on RH and wind direction. It agrees well with the theoretical models (Vehkamäki et al., 2002).

3.3.3. Conclusion

Nighttime concentration burst of the ultra-fine particles was shown, suggesting new particle formation process occurring despite the high concentrations of pre-existing particles. Several factors favoring new particle formation were found. High relative humidity, low wind speeds and, most important, wind direction correlate positively with the high ultra-fine particle number concentration. Because of the evolution of nocturnal boundary layer, high concentrations of NO_3, NH_3 and amines, were accumulated in the nearby living areas and life-stock lofts. These gases later were transported to the measurement site by weak winds enhancing nucleation process. The new particle formation and rapid their growth could have also taken place in the life-stock loft region. These particles later could have been transported to the measurement site by the northwest winds. Because we did not measure amines, the nighttime new particle formation mechanisms cannot be clearly identified.

However, the correlation between factors favoring NPF leads to the conclusion that the possible pathways for nighttime formation of ultra-fine particles include heterogeneous hydrolysis of NO_3. High concentration of ammonia and condensable organics (e.g. amines) might have also taken place in new particle formation and growth. Moreover, it can be concluded that nocturnal new particle formation process intensifies particle aging. It changes particle volatility and hygroscopicity thus having an effect onto particle mixing state.

THE MAIN CONCLUSIONS

1. Registered changes in the aerosol particle number and black carbon mass concentrations at Preila Environmental Research station are determined by a periodically occurring regional biomass burning. Air masses advecting over a high aerosol particle load regions are enriched in pollutants which are transported to a background environment altering aerosol particle number size distribution and optical properties. Condensation of the precursor gases onto pre-existing particles and particle coagulation leads to an increased accumulation mode geometric mean diameter of 124 nm and standard mode deviation of 2.0. Particle number and black carbon mass concentrations, light absorption coefficient Ångström exponent increase up to 40800 ± 4080 cm^{-3}, 11500 ± 580 ng/m^3 and 2.4, respectively.
2. After air masses advecting over Utö and Vavihill areas were transported over the Baltic Sea, 50 - 400 nm size aerosol particle number and BC mass concentrations measured in Preila were 1.4 to 2.2 and 1.2 to 2.9 times higher compared to upwind stations, respectively. The absorption Ångström exponent value (α = 1.0) was found to be specific for diesel exhaust (shipping-related emission) values.
3. Nocturnal new aerosol particle formation rate under a condensation sink of 0.055 s^{-1} was 1.25 times higher compared to a daytime value. Newly formed particle number concentration positively correlates with a relative humidity, wind speed and direction. Formation is favored by a highly volatile organic species (amines), high relative humidity and high concentrations of precursor gases, such as NH_3 and NO_X.
4. After a nocturnal new particle formation the volatile and hygroscopic particle fractions increased due to the condensation and coagulation processes up to 3.0 (350 nm) and 1.28 (50 nm) times, respectively.

APPENDIX A. Supplementary instrumentation

A.1. Aethalometer

Black carbon aerosol particle mass concentration was measured using an Aethalometer (Horvath, 1993). The simplest calculation of absorption coefficient for any filter based method is given by:

$$\sigma_{abs} = ln\left[\frac{I_o}{I}\right]\frac{A}{V\Delta t}, \quad \text{(A.1)}$$

where A is the area of the sample spot on a filter, V is the air volume drawn through and I_0, I are the average filter transmittances during the prior time period and the current time period, respectively (Bond et al., 1999). As the absorption coefficient decreases monotonically with wavelength, it can be approximated by a power-law expression, $\sigma_{abs} \sim \lambda^{-\alpha}$, where α is known as the absorption Ångström exponent. It is shown that the absorption Ångström exponent values for organic carbon varies from 1.5 to 3, while diesel exhaust aerosol particles α is close to 1 (Kirchstetter et al., 2004; Sandradewi et al., 2008). Absorption Ångström exponent was calculated using:

$$\alpha_{abs}(\lambda_1, \lambda_2) = -\frac{\ln\left(\frac{\sigma_{abs}(\lambda_1)}{\sigma_{abs}(\lambda_2)}\right)}{\ln\left(\frac{\lambda_1}{\lambda_2}\right)}, \quad \text{(A.2)}$$

where σ_{abs} is the absorption coefficient calculated using aethalometer (Weingartner et al., 2003; Virkkula et al., 2007).

A.2. Neutral cluster and air ion spectrometer

To sense the finest, nanometer-range particles and to measure their concentration, neutral cluster and air ion spectrometer (NAIS) was used. This instrument assesses the total concentration of particles (including the uncharged fraction) based on a known probability distribution of electric charge on a particle after the aerosol has been charged in well-defined conditions. Aerosol particles are neutralized by passing them through unipolar charger corona needle. NAIS consists of two parallel multichannel electrical mobility analyzer columns to differ the polarity of the measured ions (S. Mirme and A. Mirme, 2013). The aerosol is simultaneously mobility classified within 21 electrometer array per column. The mobility range is from 3.2 to 0.0013 $cm^2\ V^{-1}\ s^{-1}$ and covers the size range in particle mode from below 2 to 40 nm. Basic instrument diagram is shown in Fig. A-1.

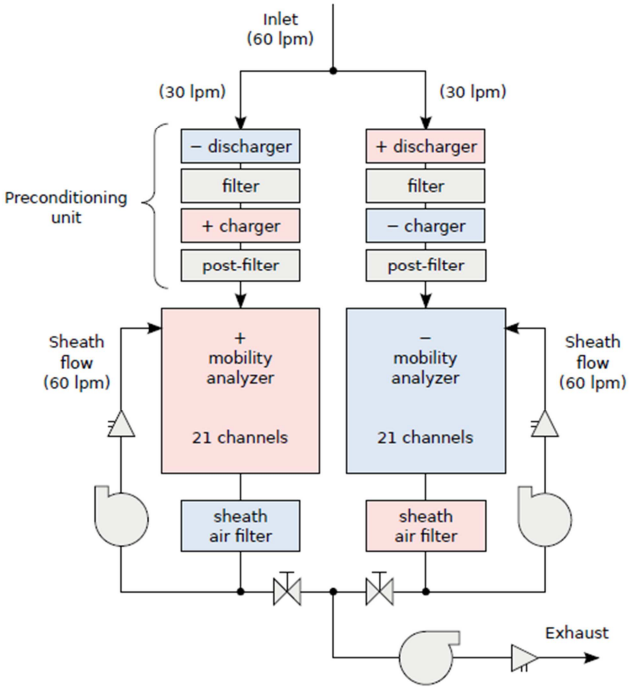

Fig. A-1. NAIS measurement flow process (S. Mirme and A. Mirme, 2013).

Before the aerosol sample enters the conditioning unit, it passes through a discharger, an electric filter, a charger and post-filter. When the instrument is

operating in an ion mode, all mentioned components are switched off. In particle mode, the main charger is switched on. The post-filter is used to remove the excess of charger ions.

Particle charge distribution as a function of charging conditions and particle size is crucial in accessing the right aerosol particle number size distribution. The NAIS uses unipolar corona charger – a corona needle on the axis of a cylindrical volume. The ions from the tip of the needle travel across the aerosol sample flow and attach to the particles mainly by thermal diffusion. The charging ion concentration is maintained at a constant level by stabilizing the current that reaches the electrode surrounding the charging space. Because ions generated by corona discharge are in the same mobility range as ions measured by the first channels of the analyzer, the lower size limit of NAIS in particle mode is ~ 2 nm (Manninen et al., 2011).

According to the theory, the movement of a charged particle with the electrical mobility *z* in analyzer is determined by the airflow rate Φ and the electric field (*CU* product, Tammet, 1970):

$$z = \frac{\Phi \varepsilon_0}{CU}. \tag{A.3}$$

Measured particle charge distribution is related to particle size via Millikan formula (Fuchs, 1964):

$$z_{Millikan} = e\frac{1+\frac{\lambda}{r}\left[a+be^{-c\frac{r}{\lambda}}\right]}{6\pi\eta r} \tag{A.4}$$

where *a*, *b* and *c* are empirical constants, *e* - the elementary charge, λ - the particle mean free path, η - the viscosity of air and *r* – particle radius.

APPENDIX B. Measurement quality

B.1. Aerosol sampling

To prevent the measurement artifacts, aerosol sampling line was designed according to the recommendations presented by a Global Atmospheric Watch (GAW) protocol. Commercially available PM_{10} impactor (flow rate of 16.6 l/min) was used upstream prior to all instruments. This ensures that all particles larger than the upper size limit of the mobility particle size spectrometer will be removed and no multiple charged particles with size larger than the measurement range will interfere with the measured electrical particle mobility distribution. Iso-kinetic aerosol splitter was used to feed the measurement instruments with the sample without under- or over- sampling the real particles concentrations. Aerosol sampling lines were made of stainless steel and conductive rubber tubing. Sampling flows were kept laminar with the Reynolds number below 2300. Aerosol sample relative humidity was kept below 40% using a custom-made drying chamber presented in the following paragraph.

B.2. Drying chamber

Relative humidity of the carrier gas is known to influence physico-chemical properties of aerosols (Wex et al., 2006). If the conditions of aerosol sample are not controlled, the investigations of aerosol effects on climate become somewhat difficult. Moreover, the ability to compare aerosol parameters from the different measurement sites with different humidity conditions would be nearly impossible. Because significant aerosol growth typically starts at relative humidity levels greater than about 50%, a common approach is to measure the aerosol below this threshold level (Baltensperger et al., 2003).

Presently, semi-permeable tubes (Nafion,Wilmington, DE or Gore-Tex,

W. L. Gore and Associates, Newark, DE) are used for aerosol drying. Commercially available single Nafion dryers are only suitable for aerosol flow rates up to 2 l/min. Higher flow rates would increase the turbulent deposition of particles in the dryer. Gore-Tex dryers with larger inner diameters can be built avoiding this restriction of commercially available Nafion dryers. However, neither Nafion nor Gore-Tex dryers do have a buffering capacity to smoothen fast fluctuations of the relative humidity of the ambient aerosol. Diffusion dryers using chemical adsorbents are specifically designed for the minimization of aerosol losses at high flow rates. The chemical adsorbent needs to be exchanged and regenerated on a regular basis.

Aerosol particle measurements were conducted using an automatically regenerating chemical adsorption dryer (Fig. B-1).

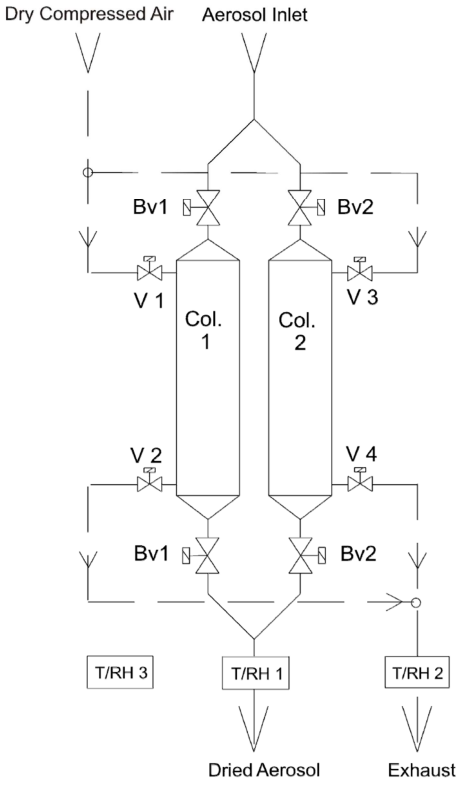

Fig. B-1. Schematic of aerosol dryer. Bv1/2 and V1/2 are the valves, T/RH – temperature and relative humidity sensor (Tuch et al., 2009).

The aerosol dryer is housed in a separate shelter which is deployed on the roof of a measurement laboratory. To prevent unwanted charging activity only

stainless steel tubing are used for aerosol sampling lines. All aerosol ducts are optimized for minimal losses at an aerosol flow rate of 1 m^3/h. Aerosol enters the shelter through a commercially available PM_{10} inlet. Subsequently, it is fed to one of two parallel stainless steel columns with an inner diameter of 70 mm and a total length of 800 mm. Each of these columns is filled with approximately 11 kg of Silica gel and houses seven aerosol ducts made of stainless steel mesh (wire diameter 0.25 mm, open area 0.4 mm^2) with an inner diameter of 10 mm. The calculated residence time of the aerosol in the columns is 1.6 s at a flow rate of 1 m^3/h. In operation, one of these columns is used for aerosol drying, while the other column is regenerated at ambient pressure by dry air, with a very low dew point temperature, supplied by a large compressor. For this purpose, each column can be shut at the top and bottom by motor actuated ball valves Bv1 or Bv2. During regeneration, the dry air is flushed through the column separated from the atmosphere using the magnetic valves V1/2 or V3/4, respectively. Operation of the aerosol dryer is controlled by a custom made LabView program (LabView 8.5, National Instruments, Austin, TX) (Tuch et al., 2009).

B.3. Correction for diffusion loss

Aerosol particle penetrating ratio can be described as:

$$P = 1 - 5.50\mu^{\frac{2}{3}} + 3.77\mu, \text{ for } \mu < 0.007, \quad \text{(B.1)}$$

and

$$P = 0.819e^{-11.5\mu} + 0.0975e^{-70.1\mu} + 0.0325e^{-179\mu}, \text{ for } \mu \geq 0.007. \quad \text{(B.2)}$$

Where:

$\mu = \frac{DL}{Q}$, $D = 1.38e^{\frac{16TC_C}{0.0003\pi\eta D_p}}$ is diffusion coefficient,

$C_C = 1 + \frac{2}{0.752PD_p}(6.32 + 2.01e^{-0.0823PD_p})$ - Cunningham slip correction factor and $\eta = 0.0001708\left(\frac{T}{273.15}\right)^{1.5}\frac{393.396}{T+120.246}$ – air viscosity. L - tube length in cm, Q - air volume flow rate in cm^3/sec, D_p - particle diameter in μm, T – temperature in K and P – pressure in KPa.

B.4. Correction for sedimentation loss

Penetrating ratio of particles due to sedimentation loss can be expressed as:

$$P = 1 - \frac{2}{\pi}\left(2k\sqrt{1-k^{2/3}} - k^{1/3}\sqrt{1-k^{2/3}} + arcsin(k^{1/3})\right). \quad \text{(B.3)}$$

Where $k = \left(\frac{3LV_{ts}}{4dU}\right)cos(\theta)$, $V_{ts} = \frac{\rho_p D_p^2 g C_C}{18\eta}$ - sedimentation velocity, ρ_p - particle density, D_p - particle diameter, C_C - Cunningham slip correction factor, η - air viscosity, T – temperature, P – pressure, L – tube length, d – inner diameter of the tube, U – air velocity in the tube, θ - angle of the tube against horizontal.

B.5. Correction for bend-deposition loss

Penetrating ratio due to bend-deposition loss can be written as:

$$P = 1 - S_{tk}\theta, \quad \text{(B.4)}$$

where $S_{tk} = \frac{\rho_p D_p^2 U C_C}{18\eta d}$ - Stokes number, ρ_p - particle density, D_p - particle diameter, C_C - Cunningham slip correction factor, η - air viscosity, d – inner diameter of the tube, U – air velocity in the tube, θ - angle of the tube bend.

B.6. SMPS measurement quality

In this long-term study mobility particle size spectrometer measurement quality was insured concerning the following items:

- Aerosol and sheath air flow rate was regularly measured once per week with an independent flow standard electrical bubble flow meter.
- The response function of the high voltage (HV) supply was calibrated twice per week. The calibration function of the high voltage was implemented into the scanning software.
- The sizing accuracy of mobility particle size spectrometers was verified each week using 203 nm latex spheres.
- Pluming time was determined by the latex sphere check. It was corrected when up- and down-scans did not agree.
- The Zero-check of the system was performed each week.

B.7. High voltage supply calibration

Sizing of the small particles is highly sensitive to the high voltage supply fluctuations. Particular care is hence required in the low voltage range. A HV-probe with ultra-low impedance was used to measure HV block response for the HV values presented in Table B-1.

Table B-1. Voltages mandatory for HV check

Set-point value (mV)	Measured value (V)
0	0 ± 3%
4	5 ± 25%
8	10 ± 25%
80	100 ± 10%
800	1000 ± 1%

B.8. Sizing accuracy

A mandatory part of a performance check of a mobility particle size spectrometer concerns the sizing accuracy (Wiedensohler et. al., 2012). It was accomplished using the mono-disperse spherical PSL (polystyrene 203 nm latex) particles. Particle diameters are certified by the manufacturer to be within ± 2.5% of the nominal diameter. The uncertainty of the sheath air flow rate is about ± 1%. Thus maximum deviation of ± 3.5% from the nominal diameter of the PSL particles is tolerable.

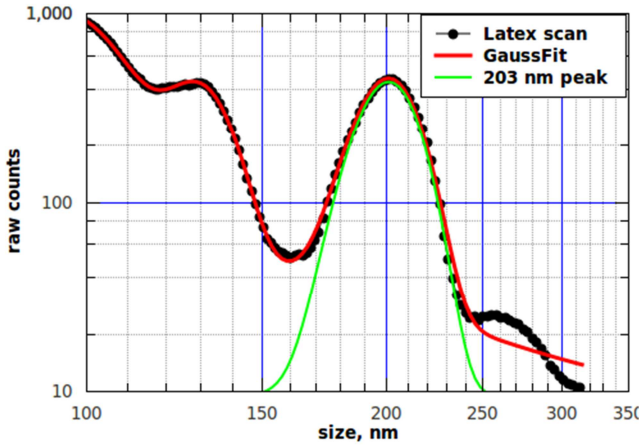

Fig. B-2. PSL spherule (203 nm) measurements of the mobility particle size spectrometer to determine the sizing accuracy under laboratory conditions.

The nebulized PSL particles were charged using a custom-made bipolar diffusion charger (85 Kr; 370 MBq) and then fed into mobility particle size spectrometers. Particle number size distribution of 203 nm PSL spheres are plotted in Fig. B-2. The centroid diameters of mobility particle size spectrometers were within the uncertainty range of 3.5% at a peak of 201 nm.

REFERENCES

Albrecht, B. A. 1989. Aerosol, cloud microphysics, and fractional cloudiness. *Science*, 245, 1227-1230.

Allan, B. J., McFiggans, G., Plane, J. M. C., Coe, H., and McFadyen, G. G. 2000. The nitrate radical in the remote marine boundary layer. *J. Geophys. Res*., 105, 24, 191–204.

Aschmann, S. M., Arey, J., and Atkinson, R. 2002. OH radical formation from the gas -phase reactions of O-3 with a series of terpenes. *Atmos. Environ*., 36, 4347-4355.

Ault, A. P., Gaston, C. J., Wang, Y., Dominguez, G., Thiemens, M. H., and Prather, K. A. 2010. Characterization of the Single Particle Mixing State of Individual Ship Plume Events Measured at the Port of Los Angeles. *Environ. Sci. Technol*., 44, 1954–1961.

Baltensperger, U., Barrie, L., Fröhlich, C., et al. 2003. WMO/GAW aerosol measurement procedures, guidelines and recommendations. *World Meteorological Organization Global Atmosphere Watch No*. 153 (September 2003) WMO TD No. 1178.

Beverland, I.J., Tunes, T., Sozanska, M., Elton, R.A., Agius, R.M., Heal, M.R. 2000. Effect of long-range transport on local PM_{10} concentrations in the UK. *Int. J. Environ. Health Res*. 10, 229–238.

Birmili, W., Heinke, K., Pitz, M., Matschullat, J., Wiedensohler, A., Cyrys, J., Wichmann, H. E., and Peters, A. 2010. Particle number size distributions in urban air before and after volatilization. *Atmos. Chem. Phys*., 10, 4643–4660.

Birmili, W., Stratmann, F., and Wiedensohler, A. 1999. Design of a DMA-based size spectrometer for a large particle size range and stable operation. *J. Aerosol Sci*., 30, 549–553.

Birmili, W., Wiedensohler, A., Heintzenberg, J., and Lehmann, K. 2001. Atmospheric particle number size distribution in central Europe: Statistical relations to air masses and meteorology. *J. Geophys. Res*., 106,

32005–32018.

Bond T.C., Anderson T.L. and Campbell D. 1999. Calibration and Intercomparison of Filter-Based Measurements of Visible Light Absorption by Aerosols. *Aerosol Sci. Technol*., 30, 582-600.

Bond, T. C., Habib, G. and Bergstrom, R. W. 2006. Limitations in the enhancement of visible light absorption due to mixing state. *J. Geophys. Res*., 111.

Brown, S. S., et al. 2004. Nighttime removal of NOx in the summer marine boundary layer. *Geophys. Res. Lett*., 31, L07108.

Brown, S. S., et al. 2006a. Variability in nocturnal nitrogen oxide processing and its role in regional air quality. *Science*, 311, 67–70.

Brown, S. S., et al. 2006b. Nocturnal odd-oxygen budget and its implications for ozone loss in the lower troposphere. *Geophys. Res. Lett*., 33, L08801.

Bzdek, B. R., et al. 2010. Amine exchange into ammonium bisulfate and ammonium nitrate nuclei. *Atmos. Chem. Phys*., 10, 3495–3503.

Cachier, H. 1998. Carbon combustion aerosols. In Atmospheric Particles. *John Wiley and Sons Ltd., New York*, 295-348.

Cheng, Y. F., et al. 2009. Influence of soot mixing state on aerosol light absorption and single scattering albedo during air mass aging at a polluted regional site in northeastern China. *J. Geophys. Res*., 114, D00G10.

Clarke, A. D., Varner J. L., Eisele F., Mauldin R. L., Tanner D., and Litchy M. 1998. Particle production in the remote marine atmosphere: Cloud outflow and subsidence during ACE 1. *J. Geophys. Res*., 103, D13.

Collaud-Coen, M., Weingartner, E., Schaub, D., Hueglin, C., Corrigan, C., Henning, S., Schwikowski, M., Baltensperger, U. 2004. Saharan dust events at the Jungfraujoch: detection by wavelength dependence of the single scattering albedo and first climatology analysis. *Atmos. Chem. Phys*. 4, 2465–2480.

Cooke, W. F., Liousse, C., Cachier, H., and Feichter, J. 1999. Construction of a 11 fossil fuel emission data set for carbonaceous aerosol and

implementation and radiative impact in the ECHAM4 model. *J. Geophys. Res*., 104, 22, 137–22.

Cruz, C. N., and Pandis, S. N. 2000. Deliquescence and hygroscopic growth of mixed inorganic organic atmospheric aerosol. *Environ. Sci. Technol*., 34, 4313–4319.

Dal Maso, M., Kulmala, M., Riipinen, I., Wagner, R., Hussein, T., Aalto, P. P., and Lehtinen, K. E. J. 2005. Formation and growth of fresh atmospheric aerosols: eight years of aerosol size distribution data from SMEAR II, Hyytiälä, Finland. *Boreal Environ. Res*., 10, 323–336.

Damoah, R., Spichtinger, N., Forster, C., James, P.,Mattis, I.,Wandinger,U., Beirle, S., Stohl, A., 2004. Around the world in 17 days — hemispheric-scale transport of forest fire smoke from Russia in May 2003. *Atmos. Chem. Phys*., 4, 1311–1321.

Day, D.E., Hand, J.L., Carrico, C.M., Engling, G., Malm, W.C. 2006. Humidification factors from laboratory studies of fresh smoke from biomass fuels. *J. Geophys. Res*. 111, D22202.

Diesch, J. M., Drewnick, F., Klimach, T. and Borrmann, S. 2013. Investigation of gaseous and particulate emissions from various marine vessel types measured on the banks of the Elbe in Northern Germany. *Atmos. Chem. Phys*., 13, 3603-3618.

Donahue, N. M., Kroll, J. H., Anderson, J. G., and Demerjian, K. 1998. Direct observation of OH production from the ozonolysis of olefins. *Geophys. Res. Lett*., 25, 59–62.

Draxler, R. R. and Rolph, G. D. 2003. HYSPLIT (HYbrid Single-Particle Lagrangian Integrated Trajectory), Model access viaNOAAARL READYWebsite http://www.arl.noaa.gov/ready/hysplit4.html). NOAA Air Resources Laboratory, Silver Spring, MD.

Eyring, V., Isaksen, I.S.A., Berntsen, T., Collins, W.J., Corbett, J.J., Endresen, Ø., Grainger, R.G., Moldanova, J., Schlager, H., Stevenson, D.S. 2010. Transport impacts on atmosphere and climate: Shipping. *Atmos. Env*., 44, 4735-4771.

Erupe, M. E., Viggiano, A. A., and Lee, S.-H. 2011. The effect of trimethylamine on atmospheric nucleation involving H2SO4. *Atmos. Chem. Phys*., 11, 4767–4775.

Facchini, M., Mircea, M., Fuzzi, S., and Charlson, R. 1999. Cloud albedo enhancement by surface-active organic solutes in growing droplets. *Nature*, 401, 257–259.

Fierz-Schmidhauser, R., Zieger, P., Wehrle, G., Jefferson, A., Ogren, J. A., Baltensperger, U., and Weingartner, E. 2010. Measurement of relative humidity dependent light scattering of aerosols. *Atmos. Meas. Tech*., 3, 39–50, 2010.

Finkelman, R. B. Orem, W., Castranova, V., et al. 2002. Health impacts of coal and coal use: possible solutions. *International Journal of Coal Geology*, 50, 425-443.

Fissan, H., Hummes, D., Stratmann, F., Buescher, P., and Neumann, S. 1996. Experimental Comparison of Four Differential Mobility Analyzers for Nanometer Aerosol Measurements. *Aerosol Sci. Technol*., 24, 1-13.

Friedlander, S. K. 2000. Smoke, Dust, and Haze. *Oxford U. Press, New York*.

Fuchs, N. A. 1964. The Mechanics of Aerosols. *Pergamon Press, Oxford*.

Geyer, A., et al. 2001a. Long-term observation of nitrate radicals in the continental boundary layer near Berlin. *Atmos. Env*.,35, 3619–3631.

Giglio, L. 2007. Characterization of the tropical diurnal fire cycle using VIRS and MODIS observations. *Remote Sens. Env*., 108, 407–421.

Gysel, M., McFiggans, G. B., and Coe, H. 2009. Inversion of tandem differential mobility analyser (TDMA) measurements. *J. Aerosol Sci*., 40, 134–151.

Gysel, M., Weingartner, E. and Baltensperger, U. 2002. Hygroscopicity of Aerosol Particles at Low Temperatures. 2. Theoretical and Experimental Hygroscopic Properties of Laboratory Generated Aerosols. *Env. Sci. Technol*., 36, 63–68.

González, Y., Rodríguez, S., García, J.C.G., Trujillo, J.L., García, R. 2011. Ultrafine particles pollution in urban coastal air due to ship emissions.

Atmos. Env., 45, 4907-4914.

Griffin, R. J., Nguyen, K., Dabdub, D., and Seinfeld, J. H. 2003. A coupled hydrophobic-hydrophilic model for predicting secondary organic aerosol formation. *J. Atmos. Chem*., 44, 171–190.

Gryning, S-E., Batchvarova, E. 2002. Marine Boundary Layer And Turbulent Fluxes Over The Baltic Sea: Measurements And Modelling. *Boundary-Layer Meteorology,* 103, 29.

Guardian. 2014. Online: http://www.theguardian.com/environment/chinas-choice/2013/nov/07/china-air-pollution-eight-year-old-cancer

Gunn, R. 1955. The statistical electrification of aerosols by ionic diffusion. J. *Colloid Sci*., 10, 107–119.

Haywood, J. M., and Shine, K. P. 1995. The effect of anthropogenic sulfate and soot on the clear-sky planetary radiation budget. *Geophys. Res. Lett*., 22, 603– 606.

Heim, M., Mullins, B., Wild, M., Meyer, J., Kasper, G. 2005. Filtration efficiency of aerosol particles below 20 nanometers. *Aerosol Science and Technology*, 39, 782-78.

Heintzenberg, J. 1994. The life cycle of the amospheric aerosol, in Topics in atmospheric and interstellar physics and chemistry. *Les Editions de Physique, Les Ulis*, 251-270.

Heintzenberg, J., Charlson, R. J., Clarke, A. D., Liousse, C., Ramaswamy, V., Shine, K. P., Wendisch, M., and Helas, G. 1997. Measurements and modeling of aerosol single scattering albedo: Progress, problems and prospects. *Beitr. Phys. Atmos*., 70, 249–263.

Heintzenberg, J., Wehner, B., Birmili, W. 2007. 'How to find bananas in the atmospheric aerosol': new approach for analyzing atmospheric nucleation and growth events. *Tellus 59B,* 273 – 282.

Hinds, W. C. 1982. Aerosol Technology: Properties, Behavior, and Measurement of Airborne Particles. *John Wiley and Sons, New York.*

Hyvärinen, A.-P., Komppula, M., Engler, C., Kivekäs, N., Kerminen, V.M., Dal Maso, M., Viisanen, Y. and Lihavainen, H. 2008. Atmospheric new

particle formation at Utö, Baltic Sea 2003-2005. *Tellus B*, 60, 345-352.

Hoffer, A., Gelencser, A., Guyon, P., Kiss, G., Schmid, O., Frank, G.P., Artaxo, P., Andreae, M.O., 2006. Optical properties of humic-like substances (HULIS) in biomass burning aerosols. *Atmos. Chem. Phys*. 6, 3563–3570.

Horvath, H. 1993. Atmospheric light absorption—A review. *Atmos. Env., Part A*, 27, 293–317.

IPCC (2007), Climate Change 2007 - The Physical Science Basis, edited by: Solomon, S. *Cambridge University Press, New York, USA.*

Isakson, J., Persson, T. A., Lindgren, E. S. 2001. Identification and assessment of ship emissions and their effects in the harbour of Göteborg, Sweden. *Atmos. Env*., 35, 3659-3666.

Jacobson, M. Z. 2001. Strong radiative heating due to the mixing state of black carbon in atmospheric aerosols. *Nature*, 409, 695–697.

Jalkanen, J.-P., Brink, A., Kalli, J., Pettersson, H., Kukkonen, J. and Stipa, T. 2009. A modelling system for the exhaust emissions of marine traffic and its application to the Baltic Sea area. *Atmos. Chem. Phys*., 9, 9209-9223

Junge, C. E. 1963. Air chemistry and Radioactivity. *New York and London, Academic Press*.

Junge, C.E., 1952. Die konstitution des atmosphärischen aerosols. *Annalen der Meteorologie* 5, 1–55.

Karppinen, A., Härkönen, J., Kukkonen, J., Aarnio, P., Koskentalo, T. 2004. Statistical model for assessing the portion of fine particulate matter transported regionally and long-range to urban air. *Scand. J. Work Environ. Health* 30, 47–53.

Kirchstetter, T. W., Novakov, T., Hobbs, P. V., 2004. Evidence that the spectral dependence of light absorption by aerosols is affected by organic carbon. *J. Geophys. Res*., 109, D21208.

Kirkby, J. et al. 2011. Role of sulphuric acid, ammonia and galactic cosmic rays in atmospheric aerosol nucleation. *Nature*, 476: 429–433.

Kivekäs, N., Rusnak, V., Carreno Correa, S., Massling, A., Skov, H., Lange,

R. and Kristensson, A. 2014. Contribution of ship traffic to aerosol particle concentrations downwind of a major shipping route. *Atmos. Chem. Phys. Discuss*, 14, 8419-8454.

Knutson E .O. and Whitby K. T. 1975b. Accurate measurement of aerosol electric mobility moments. *Journal of Aerosol Science*, 6, 453-460.

Knutson E. O. and Whitby K. T. 1975a. Aerosol classification by electric mobility: Apparatus, theory, and applications. *Journal of Aerosol Science*, 6:443-451.

Knutson, E. O. 1976. Extended Electric Mobility Method for Measuring Aerosol Particle Size and Concentration. *Fine Particles*, 739–762.

Kottler, F. 1950a. The distribution of particle sizes: Part I. *J. Franklin Inst.*, 250, 339-356.

Kottler, F. 1950b. The distribution of particle sizes: Part 2. *J. Franklin Inst.* 250, 419-441.

Kotzick, R., and Niessner, R. 1999. The effects of aging processes on critical supersaturation ratios of ultrafine carbon aerosols. *Atmos. Env.*, 33, 2669-2677.

Krecl, P., Ström, J., Johansson, C. 2007. Carbon content of atmospheric aerosols in a residential area during the wood combustion season in Sweden. *Atmos. Env.*, 41, 6974-6985.

Kristensson, A., Dal Maso, M., Swietlicki, E., Hussein, T., Zhou, J., Kerminen, V.-M., and Kulmala, M. 2008. Characterization of new particle formation events at a background site in Southern Sweden: relation to air mass history. *Tellus B*, 60, 330–344.

Kuhn, U., Sintermann, J., Spirig, C., Jocher, M., Ammann, C., and Neftel, A. 2011. Basic biogenic aerosol precursors: Agricultural source attribution of volatile amines revised. *Geophys. Res. Lett.*, 38, L16811.

Kulmala, M., and Laaksonen, A. 1990. Binary nucleation of water–sulfuric acid system: Comparison of classical theories with different H2SO4 saturation vapor pressures. *J. Chem. Phys.*, 93, 696–701.

Kulmala, M., Kerminen, V. M. 2008. On the formation and growth of

atmosperic nanoparticles. *Atmos. Res*., 90, 132-150.

Kulmala, M., Mordas, G., Petäjä, T., et al. 2007. The Condensation Particle Counter Battery (CPCB): A New Tool to Investigate the Activation Properties of Nanoparticles. *J. Aerosol Sci*., 38, 289–304.

Kumar, P., Pirjola, L., Ketzel, M., Harrison, R. M. 2013. Nanoparticle emissions from 11 non-vehicle exhaust sources – A review. *Atmos*. *Env*., 67, 252-277.

Levin, Z., and Cotton, W. R. 2009, Aerosol pollution impact on precipitation. *Springer*, 386.

Lewis, E. R., Schwartz, S. E. 2004. Sea Salt Aerosol Production: Mechanisms, Methods, Measurements, and Models—A critical review. *Geophysical Monograph Series*, v. 152, *American Geophysical Union, Washington, D. C*., pp. 413.

Liu, P. F., Zhao, C. S., Gobel, T., et al. 2011. Hygroscopic Properties of Aerosol Particles at High Relative Humidity and their Diurnal Variations in the North China Plain. *Atm. Chem. Phys., Discuss*., 11, 2991-3040.

Lohmann, U., and Feichter, J. 2005. Global indirect aerosol effects: a review. *Atmos. Chem. Phys*., 5, 715-737.

Loukonen, V., et al. 2010. Enhancing effect of dimethylamine in sulfuric acid nucleation in the presence of water: A computational study. *Atmos.Chem. Phys*., 10, 4961–4974.

Ma, N., Zhao, C. S., Nowak, A., et al. 2011. Aerosol optical properties in the North China Plain during HaChi campaign: an in-situ optical closure study. *Atmos. Chem. Phys*., 11, 5959-5973.

Manninen, H. E., Franchin, A., Schobesberger, S., et al.2011. Characterisation of corona-generated ions used in a Neutral cluster and Air Ion Spectrometer (NAIS). *Atmos. Meas. Tech*., 4, 2767–2776.

Maßling, A., Wiedensohler, A., Busch, B., Neusuß, C., Quinn, P., Bates, T., and Covert, D. 2003. Hygroscopic properties of different aerosol types over the Atlantic and Indian Oceans. *Atmos. Chem. Phys*., 3, 1377–1397.

Matthias, V., Bewersdorff, I., Aulinger, A., Quante, M. 2010. The contribution

of ship emissions to air pollution in the North Sea regions. *Env. Poll.*, 158, 2241-2250.

MEP. 2012. China National Ambient Air Quality Standards. [Online], available at: http://www.mep.gov.cn

Merikanto, J., Zapadinsky, E., Lauri, A., and Vehkamäki, H. 2007. Origin of the failure of classical nucleation theory: Incorrect description of the smallest clusters. *Phys. Rev. Lett.*, 98.

Mirme, S. and Mirme, A. 2013. The mathematical principles and design of the NAIS – a spectrometer for the measurement of cluster ion and nanometer aerosol size distributions. *Atmos. Meas. Tech*., 6, 1061–1071.

Morawska, L., Thomas, S., Jamriska, M., Johnson, G. 1999c. The modality of particle size distributions of environmental aerosols. *Atm. Env*., 33, 4401–4411.

Mordas, G., Kulmala, M., Petäjä, T., Aalto, P.P., Matulevicius, V., Grigoraitis, V., Ulevicius, V., Grauslys, V., Ukkonen, A., Hämeri, K. 2005. Design and performance characteristics of a condensation particle counter UF-02proto. *Boreal Env*. Res., 10, 543–552.

Müller, D., Mattis, I., Wandinger, U., Ansmann, A., Althausen, D., Stohl, A., 2005. Raman lidar observations of aged Siberian and Canadian forest fire smoke in the free troposphere over Germany in 2003: microphysical particle characterization. *J. Geophys. Res*. 110.

Murphy, D. M., Cziczo, D. J., Froyd, K. D., Hudson, P. K., Matthew, B. M., Middlebrook, A. M., Peltier, R. E., Sullivan, A., Thomson, D. S., and Weber, R. J. 2006. Single-particle mass spectrometry of tropospheric aerosol particles. *Journal of Geophysical Research-Atmospheres*, 111.

Murphy, S. M., Sorooshian, A., Kroll, J. H., Ng, N. L., Chhabra, P., Tong, C., Surratt, J. D., Knipping, E., Flagan, R. C., and Seinfeld, J. H. 2007. Secondary aerosol formation from atmospheric reactions of aliphatic amines. *Atmos. Chem. Phys*., 7, 2313–2337.

Oolman, L. University of Wyoming, College of Engineering, Department of Atmospheric Science. Worldwide Radiosonde Soundings of the

Atmosphere. Online: http://weather.uwyo.edu/upperair/sounding.html.

Orgen, J. A., Charlson, R. J. and Groblicki, P. J. 1983. Determination of elemental carbon in rainwater. *Anal. Chem*. 55, 1569-1572.

Pagels, J., Khalizov, A. F., McMurry, P. H., and Zhang, R. Y. 2009. Processing of Soot by Controlled Sulphuric Acid and Water Condensation-Mass and Mobility Relationship. *Aerosol Sci. Technol*., 43, 629–640.

Pettersson H., Lindow H., Brüning T. 2012. Wave climate in the Baltic Sea in 2012 . HELCOM Baltic Sea Environment Fact Sheets. Online. 2014, http://www.helcom.fi/baltic-sea-trends/environment-fact-sheets/

Pfeifer, S., Birmili, W., Schladitz, A., Müller, T., Nowak, A., and Wiedensohler, A. 2014. A fast and easy-to-implement inversion algorithm for mobility particle size spectrometers considering particle number size distribution information outside of the detection range. *Atmos. Meas*. Tech., 7, 95–105.

Philippin, S., Wiedensohler, A., Stratmann, F., 2004. Measurements of non-volatile fractions of pollution aerosols with an eight-tube Volatility Tandem Differential Mobility Analyzer (VTDMA-8). *Journal of Aerosol Science* 35, 185–203.

Pugatshova, A., Reinart, A., Tamm, E. 2007. Features of the multimodal aerosol size distribution depending on the air mass origin in the Baltic region. *Atmos. Env*., 41, 4408-442.

Raatikainen, T., Vaattovaara, P., Tiitta, P., Miettinen, P., Rautiainen, J., Ehn, M., Kulmala, M., Laaksonen, A., andWorsnop, D. R. 2010. Physicochemical properties and origin of organic groups detected in boreal forest using an aerosol mass spectrometer. *Atmos. Chem. Phys*., 10, 2063–2077.

Ran, L., et al. 2014. Surface Trace Gases at a Rural Site between the Megacities of Beijing and Tianjin. *Atmospheric And Ocean Science Letters*, 7, 3, 230-235.

Riccobono, F., Rondo, L., Sipilä, M., et al. 2012. Contribution of sulfuric acid and oxidized organic compounds to particle formation and growth.

Atmos. Chem. Phys., 12, 9427-9439.

Rissler, J., Swietlicki, E., Bengtsson, A., Boman, C., Pagels, J., Sandström, T., Blomberg, A., Löndahl, J. 2012. Experimental determination of deposition of diesel exhaust particles in the human respiratory tract. *J. A. Sci*., 48, 18-33.

Rolph, G. D. 2003. Real-time Environmental Applications and Display sYstem (READY) (http://www.arl.noaa.gov/ready/hysplit4.html). NOAA Air Resources Laboratory, Silver Spring, MD.

Rosenfeld, D., Lohmann, U., Raga, G. B., O'Dowd, C. D., Kulmala, M., Fuzzi, S., Reissell, A., and Andreae, M. O. 2008. Flood or Drought: How Do Aerosols Affect Precipitation? *Science*, 312, 1309–1313.

Saarikoski, S., Sillanpää, M., Sofiev, M., Timonen, H., Saarnio, K., Teinilä, K., Karppinen, A., Kukkonen, J., Hillamo, R. 2007. Chemical composition of aerosols during a major biomass burning episode over northern Europe in spring 2006: experimental and modelling assessments. *Atmos. Environ*. 41, 3577–3589.

Sakurai, H., Fink, M. A., McMurry, P. H., et al. 2005. Hygroscopicity and volatility of 4–10 nm particles during summertime atmospheric nucleation events in urban Atlanta. *J. Geophys. Res*., 110, D22S04.

Sandradewi, J., Prevot, A. S. H., Weingartner, E., Schmidhauser, R., Gysel, M., Baltensperger, U. 2008. A study of wood burning and traffic aerosols in an Alpine valley using a multi-wavelength Aethalometer. *Atmos. Environ*., 42, 101–112.

Sarvi, A., Fogelholm, C. J., and Zevenhoven, R. 2008. Emissions from large-scale medium-speed diesel engines: 2. Influence of fuel type and operating mode. *Fuel Process Technol*. 89, 520–527.

Saxe, H., Larsen, T. 2008. Air pollution from ships in three Danish ports. *Atmos. Env*., 38, 4057-4067.

Saxena, P., Hildemann, L. M., McMurry, P. H. and Seinfeld, J. H. J. 1995. Organics alter hygroscopic behaviour of atmospheric particles. *J. Geophys. Res*., 100, 18755–18770.

Scanlan, C.L., Wilkins, R.L., Stoller, J.K. 2003. Eds. Egan's Fundamentals of Respiratory Care, Eighth Edition, Mosby.

Scheibel, H. G. and Porstendoerfer, J. 1983. Generation of monodisperse Ag and NaCl aerosol with particle diameters between 2 nm and 300 nm. *J. Aerosol Sci*., 14, 113–126.

Schwartz, J., Dockery, D. W., Neas, L. M. 1996. Is daily mortality associated specifically with fine particles? *J. Air Waste Manage Assoc*., 46, 2–14.

Schwartz, S. E. 1996. The Whitehouse Effect - shortwave radiative forcing of climate by anthropogenic aerosols: An overview. *J. Aerosol Sci*., 27, 359-382.

Seinfeld, J. H. and Pandis, S. N. 2006. Atmospheric Chemistry and Physics: From Air Pollution to Climate Change. John Wiley & Sons, Hoboken, New Jersey, second edition.

Shine, K. P., Fouquart, Y., Ramaswamy, V., Solomon, S. and Srinivasan, J. 1996. Radiative forcing of climate change. *Cabridge University Press*, 108-118.

Simoneit, B. R. T. 2002. Biomass burning - a review of organic tracers for smoke from incomplete combustion. *Applied Geochemistry*, 17, 129 - 162.

SMHI. 2013. Online: www.smhi.se/oceanografi/istjanst/havsis_en.php.

Sofiev, M., Soares J., Prank M., de Leeuw G., and Kukkonen J. 2011. A regional-to-global model of emission and transport of sea salt particles in the atmosphere. *J. Geophys. Res*., 116.

Song, S.K., Shon, Z.H., Kim, Y.K., Kang, Y.H., Oh, I.B., Jung, C.H. 2010. Influence of ship emissions on ozone concentrations around coastal areas during summer season. *Atmos. Env*., 44, 713-723.

Spracklen, D. V., Carslaw, K. S., Kulmala, M., et al. 2008. Contribution of particle formation to global cloud condensation nuclei concentrations. *Geophys. Res. Lett*., 35.

Stohl, A. 1998. Computation, accuracy and applications of trajectories – A review and bibliography. *Atmos. Env*. 32, 947–966.

Stokes, M.D., Deane, G. B., Prather, K., Bertram, T. H., Ruppel, M. J., Ryder, O. S., Brady, J. M., and Zhao, D. 2013. A Marine Aerosol Reference Tank system as a breaking wave analogue for the production of foam and sea-spray aerosols. *Atmos. Meas*. Tech., 6, 1085-1094.

Stolzenburg, M. R. 1988. An Ultrafine aerosol size distribution measuring system. Ph.D. thesis, University of Minnesota.

Suni, T., Kulmala, M., Hirsikko, A., Bergman, T., Laakso, L. and coauthors. 2008. Formation and characteristics of ions and charged aerosol particles in a native Australian Eucalypt forest. *Atmos. Chem. Phys. Discuss*. 7, 10343–10369.

Tammet, H. 1970. The aspiration method for the Determination of Atmospheric-Ion Spectra. The Israel Program for Scientific Translations Jerusalem, National Science Foundation, Washington.

Tuch, T. M., Haudek, A., Muller, T., Nowak, A., Wex, H., and Wiedensohler, A. 2009. Design and performance of an automatic regenerating adsorption aerosol dryer for continuous operation at monitoring sites. *Atmos. Meas. Tech*., 2, 417–422.

Twomey, S. 1974. Pollution and the planetary albedo. *Atmos. Environ*., 8, 1251-1256.

Ulevicius V., Bycenkiene S., Remeikis V., et al. 2010. Characterization of pollution events in the East Baltic region affected by regional biomass fire emissions. *Atmos. Res*., 98, 190–200.

Vehkamäki, H., Kulmala, M., Napari, I., et al. 2002. An improved parameterization for sulfuric acid – water nucleation rates for tropospheric and stratospheric conditions. *J. Geophys. Res*., 107, 4622.

Viana M., Hammingh P., Colette A., Querol X., Degraeuwe B., Vlieger I., Aardenne J. 2014. Impact of maritime transport emissions on coastal air quality in Europe. *Atmos. Env*., 90, 96-105.

Virkkula, A., Makela, T., Hillamo, R., Yli-Tuomi, T., Hirsikko, A., Hameri, K., Koponen, I.K. 2007. A simple procedure for correcting loading effects of Aethalometer data. *J. Air Waste Manage. Assoc*., 57, 1214–1222.

Wallace, J. M., and Hobbs, P. V. 1977. Atmospheric science: An introductory survey. Academic Press, New York, 467.

Wang, L., Jing, Z., Pu, Z., Xiujuan, Z., Zhe, W., Fenfen, Z., Jie, S., and Chenchen, M. 2013. A Review of Air Pollution and Control in Hebei Province, China. *Open Journal of Air Pollution* 2, 47.

Washington Post. 2014. Online: http://www.melbournedailystar.com/choking-smog-paralyzes-cities-in-northeast-china-closing-schools-airports-washington-post/

Wehner B., Petäjä, T., Boy, M., Engler, C., Birmili, W., Tuch, T.,Wiedensohler, A., and Kulmala, M. 2005. The contribution of sulfuric acid and non-volatile compounds on the growth of freshly formed atmospheric aerosols. *Geophys. Res. Lett*. 32.

Wehner, B., et al. 2009. Mixing state of nonvolatile aerosol particle fractions and comparison with light absorption in the polluted Beijing region. *J. Geophys. Res*., 114, D00G17.

Weingartner, E., Saathoff, H., Schnaiter, M., Streit, N., Bitnar, B., and Baltensperger, U. 2003. Absorption of light by soot particles: determination of the absorption coefficient by means of aethalometers. *Journal of Aerosol Science*, 34, 1445-1463.

Wex, H., Kiselev, A., Ziese, M., and Stratmann, F. 2006. Calibration of LACIS as a CCN detector and its use in measuring activation and hygroscopic growth of atmospheric aerosol particles. *Atmos. Chem. Phys*., 6, 4519–4527.

Whitby, E. R., and McMurry, P. H. 1997. Modal aerosol dynamics modeling. *Aerosol Sci. Technol*, 27, 673-688.

Whitby, K. H. 1978. The physical characteristics of sulfur aerosols. *Atmos. Environ*. 12: 135–159.

Wiedensohler, A. 1988. An approximation of the bipolar charge distribution for particles in the submicron size range. *J. Aerosol Sci*., 19, 387-389.

Wiedensohler, A., Birmili, W., Nowak, A., et al. 2012. Mobility particle size spectrometers: harmonization of technical standards and data structure to

facilitate high quality long-term observations of atmospheric particle number size distributions. *Atmos. Meas. Tech*., 5, 657-685.

Wiedensohler, A., Hansson, H.-C., Orsini, D., Wendisch, M., Wagner, F. and co-authors. 1997. Night-time formation and occurrence of new particles associated with orographic clouds. *Atmos. Environ*., 31, 2545–2559.

Willeke, K., and Baron, P. A. 1993. Aerosol measurements: principles, techniques and applications, Van Nostrand Reinhold Publisgers, New York.

Wu, Z., Hu, M., Liu, S., et al. 2007. New particle formation in Beijing, China: Statistical analysis of a 1-year data set. *J. Geophys. Res*., 112, D09209.

Xue, H., Khalizov, A. F., Wang, L., Zheng, J., and Zhang, R. 2009b. Effects of Coating of Dicarboxylic Acids on the Mass-Mobility Relationship of Soot Particles. *Environ. Sci. Technol*., 43, 2787–2792.

Zhang, R., Wang, L., Khalizov, A. F., Zhao, J., Zheng, J., McGraw, R. L., and Molina, L. T. 2009. Formation of nano-sized particles of blue haze enhanced by anthropogenic pollution. *P. Natl. Acad. Sci*., 106, 17650–17654.

Zhou, J., Swietlicki, E., Hansson, H., and Artaxo, P. 2002. Sub-micrometer aerosol particle size distribution and hygroscopic growth measurements in the Amazonian rain forest during the wet season. *J. Geophys. Res*., 107, 8055.

ACKNOWLEDGEMENTS

The past four and a half years have been a great adventure. Like in a roller coaster I went up and down with many questions, some answers and a great fun. First of all I would like to thank many people from my host institute in Lithuania, where I have started this journey. I thank to dr. Vidmantas Ulevicius for introducing me to an aerosol science, supporting my research and providing me with valuable scientific discussions. I also thank to Professors Algimantas Undzenas and Vidmantas Remeikis for their support. Colleagues Kristina, Steigvilė, Narciza, Vadimas, Kęstas for their friendship. I also kindly thank to all institute personnel: administration for the help with various documentations, kitchen friends, institute labor for their kind help and many others whom I have met during my studies.

Extraordinary journey is only a desert walk without exceptional people we meet on our way. I greatly acknowledge the tremendous support by project "Promotion of Student Scientific Activities" (VP1-3.1-ŠMM-01-V-02-003) from the Research Council of Lithuania (the project is funded by the Republic of Lithuania and European Social Fund under the 2007-2013 Human Resources Development Operational Programme’s priority 3) which gave me an exceptional opportunity to visit TROPOS, Leipzig, Germany. Here I met the most extraordinary people who have left their fingerprints on me.

Foremost special thanks go to Prof. Alfred Wiedensohler for accepting me into his group. I cannot imagine better atmosphere he created and the experiences he brought me through. Ali, I have enjoyed every single moment of your friendship. Without your support and trust these pages would by just blank sheets of paper. Thank you, Ali, with all my heart.

My kindest words also go to dr. Wolfram Birmili. Your contagious laugh filled the corridors with the emotion which made the institute an unforgettable place. It is nearly impossible not to like your enthusiasm, vitality and easy going conversations. I greatly appreciate knowing you.

Two Tsingtao and gratitude go to dr. Thomas Tuch for his arrow-straight remarks, great ideas and a helpful hand when I needed it. Wide-open for the V-twin!

With all my respect, I thank Kay Weinhold for his amazing knowledge and expertise concerning everything where do aerosol particles flow. I wish I had more time to spend with you arguing how much actual zero is. Step by step, I believe, we would come to an agreement that 3 are small enough to be considered as a void.

I also want to acknowledge dr. Markus Hermann and dr. Birgit Wehner for their precise advices and non-idle talking.

Thanks to Anja for your kind help in the lab providing me all the tools I needed.

I will always remember our “TROPOSKI” team for their assistance, friendship and help during my stay in TROPOS. Thank you Johannes for introducing me to crazy Leipzig nightlife and those head ache mornings, late movie evenings and your friendship during my stay. Thanks to Shan for rhetorically asking the meaning of the life, Jia and Nan – for great evenings enjoying good food and warm conversations. Ying for positivity and help with MatLab, saving years of my life, MonyQ for all the tea I drunk and all the most tasty cakes I ate, Zhibin for the help taking care of instruments during my first stay in Xianghe and finally ShengLan for testing my patience and showing the beauty of China. It was my great pleasure to work and to know you. I only wish I had included you all more throughout my studies. I thank you all for valuable feedbacks, advices, and encouragement.